PLANT COVER, SOIL TEMPERATURE, FREEZE, WATER STRESS, AND EVAPOTRANSPIRATION CONDITIONS

Craig L. Wiegand, Principal Investigator
Co-Investigators: Paul R. Nixon
Harold W. Gausman
L. Neal Namken
Ross W. Leamer
Arthur J. Richardson

Science and Education Administration
U.S. Department of Agriculture
P. O. Box 267
Weslaco, TX 78596

(E81-10130) PLANT COVER, SOIL TEMPERATURE, FREEZE, WATER STRESS, AND EVAPOTRANSPIRATION CONDITIONS Final Report, 1 Dec. 1977 - Sep. 1980 (Science and Education Administration) 183 p HC A09/MF A01 CSCL 02C G3/43

N81-23543

Unclas
00130

February 1981

Type III Final Report
for period December 1, 1977 to September 1, 1980

Prepared for

GODDARD SPACE FLIGHT CENTER
Greenbelt, MD 20771

TECHNICAL REPORT STANDARD TITLE PAGE

1. Report No.	2. Government Accession No.	3. Recipient's Catalog No.

4. Title and Subtitle	5. Report Date
PLANT COVER, SOIL TEMPERATURE, FREEZE, WATER STRESS, AND EVAPOTRANSPIRATION CONDITIONS	February 1981
	6. Performing Organization Code
7. Author(s) Craig L. Wiegand, et al.	8. Performing Organization Report No.
9. Performing Organization Name and Address Science and Education Administration U. S. Department of Agriculture P. O. Box 267 Weslaco, TX 78596	10. Work Unit No.
	11. Contract or Grant No. S-40198B
	13. Type of Report and Period Covered TYPE III Final Report 12/1/77 to 9/1/80
12. Sponsoring Agency Name and Address GODDARD SPACE FLIGHT CENTER Greenbelt, MD 20771	14. Sponsoring Agency Code

15. Supplementary Notes

16. Abstract

Emissive (IR, 10.5 to 12.5μm) and reflective (VIS, .55 to 1.1μm) data for 10 day, and IR data for 6 night south Texas scenes, spanning the period 27 May 78 to 26 Feb. 79, were analyzed for the title objectives after procedures were developed for removing cloud-affected data. HCMM radiometric temperatures were: within 2C of dewpoint temperatures on nights when air temperature approached dewpoint temperature; significantly correlated with variables important in evapotranspiration (water depletion and days since rain or irrigation, ratio of actual to potential evapotranspiration the day of and the day prior to HCMM overpasses, vegetation greenness indexes, and insolation the hour and the day of HCMM overpasses); and, related to freeze severity and planting depth soil temperatures.

We conclude that: data sources for radiative transfer correction of emissive data are necessary; vegetation greenness indexes calculated from visible and reflective IR bands of NOAA-6 to -9 meteorological satellites will be useful in the AgRISTARS program for seasonal crop development, crop condition, and drought applications; radiometric nighttime temperature estimates planting depth and air temperature, and monitors synoptic surface temperature patterns and freezes; and the Earth's energy balance is strongly affected by plant cover and water availability for evapotranspiration.

17. Key Words (Selected by Author(s))	18. Distribution Statement
Soil Temperature, Freeze, Water Stress, Plant Cover, Canopy Temperature, Crop Stress, Evapotranspiration, HCMM, Clouds, Atmospheric absorption	

19. Security Classif. (of this report)	20. Security Classif. (of this page)	21. No. of Pages	22. Price*
UNCLASSIFIED	UNCLASSIFIED	159	

*For sale by the Clearinghouse for Federal Scientific and Technical Information, Springfield, Virginia 22151.

ACKNOWLEDGEMENTS

Many nonauthors contributed to the effort represented by this report. Richard Stonesifer, Contract Monitor, provided assistance in acquiring data from Goddard and answered questions promptly. John Price, HCMM Project Scientist, provided technical guidance and a radiative transfer model for correcting radiometric temperatures based on radiosonde data. The NWS-NOAA staff at Brownsville provided local weather and soil temperature data. Uvaldo Salinas operated a weather station specifically for this study at his Las Escobas Ranch. The Rio Grande Valley Sugar Growers Association prepared to compare sugarcane yields with HCMM freeze night temperatures. J. L. Jacobs, Soil Conservation Service, Harlingen consolidated soils information from the four test area counties to facilitate its use in this study, while B. J. Garner of the same office provided information about irrigation districts' boundaries. Joe Cuellar, Ben Goodier, and Wayne Swanson acquired, summarized, and analyzed field observations. Susan Caskey, Alex Garcia, Eddie Hernandez, and Kathy Solis programmed analyses, processed data, and prepared illustrations while Rey Riojas coordinated computer usage. Michael Johnson provided valuable statistical consultation. Finally, we thank Kathy Solis and our secretarial staff consisting of Louise Dalton, Rosa Almanza, and Alicia Cavazos who typed and collated the report.

TABLE OF CONTENTS

EXECUTIVE SUMMARY

Objectives

This contract dealt with the use of the emissive or thermal infrared band (10.5 to 12.5 μm) of the Heat Capacity Mapping Mission (HCMM) for specific agricultural applications: freeze damage assessment, planting date advisory, crop water stress, and temperature as affected by vegetative cover. More general or synoptic applications dealt with, for example, temperature gradients inland from the coast and the difference between HCMM indicated and screen height air temperature maxima (THCMM-Tmax, daytime scenes) or minima (THCMM-Tmin, nighttime scenes) across the 220-km wide test site in extreme south Texas. In addition, the 0.55 to 1.1 μm band, which we refer to as the reflective band[a/] was investigated as it helped edit clouds from the data, indicate major soil associations and as it related to vegetative cover.

Scope of Work

Computer compatible digital magnetic tapes (CCT) of 10 daytime emissive (IR) and reflective (VIS) scenes and six nighttime emissive scenes were obtained, preprocessed and analyzed. The CCT were retrospectively ordered after viewing hundreds of photo-products supplied to us on a standing order basis. The scenes obtained covered the time span 27 May 78 to 26 Feb 79.

The test site we used was encompassed by longitudes 97°00' to 99°30' W and latitudes 25°30' to 27°00' N. The generalized soil map of the area was digitized, and the soil association number for each 20-seconds of latitude and longitude was entered into computer memory. For more detailed analyses of smaller ground sites, 44 sites representing typical natural range plant communities, cities, water, and irrigated and dryland crop sites were chosen by reference to high altitude photography and Landsat images. Twenty-four weather station sites from which daily maximum and minimum air temperatures were reported during the winter months were used to relate HCMM indicated surface temperature to reported minimum temperature on cold nights. Ground truth was obtained weekly from 01 Jun to 15 Jul 78, for over 100 fields that constituted 22 intensive sites where soil water stress and ground cover were to be related to HCMM indicated surface temperature.

The "representative", weather station, and intensive sites mentioned above constituted 94 ground locations in the test site area that were located in the HCMM data by latitude and longitude of the center pixel. The temperature and albedo of the center pixel (1x1 matrix)--which represented 35-ha on the ground--as well as the temperature and albedo

---

[a/] This band includes a portion of the visible (0.4 to 0.7 μm) and reflective infrared (0.75 to 1.35 μm) bands. Therefore, it is more accurate to refer to it as the reflective band than a visible (VIS) band, as is done in the HCMM User's Guide.

of the 3x3, 5x5, 7x7 and 9x9 pixel matrices centered on it were determined. Standard deviations of temperatures and albedos and the dominant and the next most dominant soil association for the 3x3 and larger matrices were determined. On 15 Jun and 12 Jul 78, Landsat data were used to calculate vegetation indexes for most of the 94 sites. The vegetation greenness indexes were used in conjunction with ground truth, weather data, calculations of root zone soil water depletion and actual to potential evapotranspiration ratios from the USDA-ARS Irrigation Scheduling Program to relate HCMM radiometric temperatures to plant cover and crop water stress.

The above investigations were supported by three other facilities or efforts. One was a central weather station where numerous weather parameters were continuously monitored and their hourly integrated values were logged. Another was two 6-m square fallow plots, one of which was irrigated weekly and the other of which received only rainfall. In these plots, soil temperature was monitored at the 0.5, 5, 10, 20, 50, and 100-cm soil depths and recorded hourly on a strip chart recorder. These data helped to investigate the thermal response of the shallow soil layers to meteorological variables and the difference in thermal response of wet and dry soil. The third effort was daily maximum and minimum soil temperature at the 10-cm depth at four monitoring sites during the period 01 Jan through 31 Mar 79, which the NWS-NOAA used for planting advisories.

The above efforts provided the data for the contract objectives. In practice, however, we found that the HCMM scenes of our test site typically contained some clouds and that subvisible cirrus layers that affected the thermal data were also present over a part of some scenes. Consequently, considerable effort was expended in devising techniques for editing cloud-contaminated pixels from the data (see report section 2.2.1). We settled on what we called "modified cluster screening". In this procedure, scatter diagrams of the reflective and emissive pixel values were displayed by the printer-plotter. Clouds had random combinations of values in the two bands whereas land features and water had values that clustered. The analyst examined the scatter diagrams and subjectively positioned the line segments that separate cloud from noncloud pixels. The line segments were described mathematically and used to machine edit the data. It was found for eight summer overpasses that, on the average, each 10% cloud contamination reduced the radiometric temperature of land features by 0.9 C. Because temperature differences between surface features are small, cloud-contaminated data were edited out before most analyses were run. However, exemplary analyses are included that used data before and after cloud-contaminated pixels had been removed to illustrate the degradation in relationships observed.

Two other considerations in interpreting radiometric temperatures from HCMM were encountered. One was the low radiometric surface temperature determined (below ambient air temperature) under humid atmospheric conditions unless the radiative transfer model provided by Dr. John Price, HCMM Project Scientist, was used to make the "surface to satellite" temperature correction based on radiosonde observations

made by NWS-NOAA within the experiment test area (Brownsville). The correction for dry winter days (1 cm precipitable water in the atmosphere) was nil whereas it was up to 9 C for humid summer days with up to 4.4 cm precipitable water in the atmosphere (see Table 1.3). In this report, analyses involving temperature differences between dates or between the air and the surface usually have incorporated the radiative transfer model temperature correction whereas within date or among date regression analyses have not because the correction would be the same for all ground sites in the test area based on a single radiosonde observation.

The other consideration was number of HCMM pixels used to represent a given ground test site (field or larger area). In multiple regression analyses the multiple correlation coefficient, R, increased slightly as number of HCMM pixels in the sample increased from one (central pixel) to 81 (matrix of 9x9 pixels centered on the central one), but the improvement was not statistically significant at the p = 0.05 level (see report section 2.3.1.1). The standard deviation of the mean decreased but the value of the mean was not much affected. This was important in our study because the IFOV of HCMM is 36 ha--larger than all but a few percent of the crop fields.

Results and Significance

Synoptic analyses. A test site 220-km E to W and 80-km N to S at the southern tip of Texas was used for several synoptic thermal analyses. Isotherm lines at 2 C intervals adequately displayed the thermal patterns within the test site. The HCMM radiometric temperatures by soil associations from 10 daytime overpasses were typically highly correlated. Summer nighttime temperatures tended to be uniform across the test area and close to the dewpoint temperature which is reached each night. On winter nights with strong radiational cooling and dewpoints lower than the air reaches, there is a temperature gradient across the test site that is dominated by distance from the coast. Warm land areas adjacent to inland water bodies were observed in both summer and winter nighttime thermal data.

An "aridity index" defined as the difference between the daytime HCMM radiometric temperature and maximum air temperature for the day at the site of weather stations (THCMM - Tmax) increased with distance from the coast, except for a short time following general rains. The difference between the HCMM nighttime radiometric temperature and minimum air temperature (THCMM - Tmin) showed that THCMM was within 2 C of the dewpoint temperature on nights when the air reaches the dewpoint temperature.

The HCMM data contain useful direct synoptic information such as landscape temperatures during freezes, temperature gradients across scene areas and with respect to water bodies and estimates of minimum or dewpoint temperature. Day minus night radiometric temperatures, or radiometric and air temperature differences also appear to be useful aridity indexes. For the latter, the radiometric temperatures for the land surface need to be corrected for atmospheric path radiance.

Freeze hazard. Areas of least freeze hazard in our south Texas test area were identified by computer processing of HCMM data from cold nights. First a temperature frequency distribution was made of the pixels from 21 Oct 78 that comprised our test area, and identification was made of all pixel locations whose temperature was in the top third. The same procedure was used with the cold night data of 26 Feb 79 (Had usable data from other cold nights been available, they would have been processed to determine the locations of warmest pixels on those nights also.). Then the locations of warm pixels from both dates were superimposed to form a map showing the areas that had least freeze hazard. A bold symbol was used to identify locations that were warm on both dates. This approach offers promise as a useful method of classifying land areas according to freeze hazard. Because of variations in temperature patterns from date to date, information from several freeze or near freeze events should be combined in determining the safest areas to grow temperature-sensitive crops.

HCMM nighttime data from the serious freeze of 03 Jan 79 could not be validly analyzed for landscape temperatures because an absorbing--emitting atmospheric layer, probably subvisible cirrus (SCi), obscured surface emissions from view of the satellite. The SCi layer, which was not apparent to ground observers, retarded the loss of nocturnal terrestrial radiation to space and slowed the cooling of the landscape and air that night. The ability to detect an atmospheric layer that blocks the loss of terrestrial radiation should have important application in real-time freeze forecasting. Knowledge of the presence of such a blocking layer would be justification for raising upward the minimum temperature forecast for a cold night and could save growers from undertaking expensive freeze protection measures unnecessarily.

On the coldest SCi-free night for which we have HCMM data (26 Feb 79) the HCMM indicated surface temperatures surrounding weather stations approximated the minimum air temperatures observed at the stations. Since the HCMM overpass occurred at 0209 CST and the minimum air temperatures occurred about dawn, the HCMM radiometric temperatures were below air temperature at overpass time by an amount that approximately equaled the air temperature decline between overpass time and dawn. The results suggest that the satellite radiometric temperatures can be used to estimate minimum nighttime air temperature synoptically or at particular locations where air temperature is needed but ground observations are unavailable.

Planting advisory. HCMM radiometric temperatures on a clear night early in the 1979 planting season (26 Feb), when there was little atmospheric attenuation, were very close to minimum air temperature, 3.1 C. The radiometric temperature of the sandy upland was 1.4 C and differed from that of the loams and clays (3.3 C) that had the same centroid distance from the coast. Three environmental variables--average daily air temperature, insolation at ground level and extraterrestrial radiation--accounted for from 89 to 93% of the variation in maximum daily, minimum daily and average daily soil temperature at the 5-cm depth in dry plots and from 88 to 91% of the variation for wet plots. Standard errors of the estimate of maximum, minimum, and average daily soil temperatures from the three environmental variables ranged from 1.5 to 1.9 C.

Estimation of planting depth soil temperatures from radiometric temperatures appears feasible, provided the relation between planting depth and surface temperature is understood. The estimates should be superior to estimates currently made from air temperature observations.

Crop water stress. HCMM temperatures for sorghum, sugarcane and citrus crop sites were related to soil water depletion (DEPL) since the last rain or irrigation calculated from the USDA-ARS Irrigation Scheduling Program (ISP), to days since irrigation or rainfall (DSR) and to the ratio of estimated actual to potential evapotranspiration (ET/ETp) the day of and the day prior to HCMM overpasses. For a combined crops data set involving three HCMM overpasses, radiometric temperatures (means of 3x3 pixel arrays, T3) were highly significantly negatively correlated with ET/ETp ($r = -0.704^{**}$) and significantly positively correlated with DSR ($r = 0.484^{*}$). Temperatures were also highly significantly correlated with insolation on the day of the pass (IDOP) $r = 0.812^{**}$; the vegetation greenness index (PVI6) calculated from Landsat for the corresponding dates ($r = -0.642^{**}$) and maximum air temperature (Tmax) the day of the HCMM pass ($r = 0.619^{**}$). The linear correlation coefficients between HCMM radiometric surface temperature and variables important in evapotranspiration for seven dates (27 May through 08 Jul 78) consisting of 51 observations were: insolation the hour of the HCMM overpass (IHROP), $r = 0.668^{**}$; IDOP, $r = 0.660^{**}$; ET/ETp, $r = -0.581^{**}$; DSR, $r = -0.477^{**}$; Tmax, $r = 0.378^{**}$ and percent vegetation cover (PC), $r = -0.277^{**}$. For this data set, Tmax was highly significantly correlated with DSR, DEPL and ET/ETp.

The data demonstrate the strong correlation between variables related to evapotranspiration and HCMM surface temperatures, as well as the strong coupling of maximum daily air temperature to availability of water for evapotranspiration. In general, the findings indicate that surface temperatures observed by satellites, such as HCMM and the NOAA-6 to -9 series, are responding to shifts in the energy balance of the Earth's surface that are strongly affected by vegetative cover and availability of water for evapotranspiration. Such interpretations could have applications under the interagency AgRISTARS program as they relate to crop condition and yield assessments.

Plant cover. HCMM temperatures for five crops (sorghum, citrus, sugarcane, cotton and grass pastures) as one data set were significantly correlated with the vegetation indexes GVI, PVI and PVI6 calculated from Landsat multispectral scanner data acquired within four days of the HCMM overpasses but not with percent cover (PC) or plant height (PH). Weather (insolation, saturation deficit of the air and daily maximum air temperature on HCMM overpass dates), geographic (distance of sample sites from the coast) and time (days since irrigation or rainfall) variables influenced HCMM temperatures as much or more than vegetative conditions when crops that differed in stage of maturity, planting configuration and PC vs. PH relation were combined in one data set. For cotton and sugarcane which were increasing in ground cover during the observation period (27 May to 15 Aug 78), the cooling effect of increasing ground cover was about equally offset by the seasonal increase in ambient air

and agricultural landscape temperature. In general, the spread in HCMM temperatures among crops was narrow and the uncorrected temperatures were below ambient air temperatures at the time of the HCMM data acquisitions, 1400 to 1416 CST.

From these studies we anticipate that surface temperatures observed by the polar orbiting operational meteorological satellites (NOAA-6 to -9 series) will correlate with vegetation indexes calculated from their visible and near-infrared bands and be interpretable in the AgRISTARS program for synoptic seasonal crop development and drought occurrence applications.

Recommendations

Radiometric temperatures require interpretations along energy balance lines. Insolation (solar irradiance) needs to be known and available for the interpretations as does soil water availability for evapotranspiration. Therefore NASA should strongly support the efforts of NOAA to make insolation data available operationally from the GOES. Soil water balance models for the near surface soil layer and root zone are needed that can be readily implemented over a wide range of environmental conditions. It appears also that microwave data should be made more widely available for interpreting thermal data, and vice-versa.

Our experience in these studies is that radiometric temperatures from satellite altitudes need to be routinely adjusted for radiative transfer losses through the atmosphere when precipitable water in the atmosphere exceeds approximately 1-cm. The radiosonde data for such corrections are available only for a limited number of sites in the U. S. and those available were not taken at the time of HCMM overpasses. Consequently, provision of alternative sources of the data for such corrections is in order. For example, atmospheric sounders already orbiting may be able to supply the needed parameters. Or it may be that atmospheric sounders need to be placed on future earth observation satellites alongside the multispectral or pushbroom scanners.

Agriculturalists tend to associate specific observations with individual crop fields. However, IFOV's the size of those of HCMM (36-ha) or the NOAA-6 to -9 series of satellites (1-km^2) result in smoothing of the data across field boundaries so that it will be necessary to think in terms of larger sample sites on the ground that are representative of particular physiographic areas or ecological environments and less about individual cropped or fallow fields.

In these studies the vegetation indexes calculated from visible and reflective infrared bands of Landsat were significantly correlated with the thermal band data from HCMM. That is, the vegetation indexes provided useful vegetation cover and condition information for intepreting the thermal data. Therefore, in spite of the disappointing experience with the thermal band on Landsat-3, we recommend that NASA persevere in including thermal sensors on future earth observation systems.

LIST OF FIGURES

Page

LIST OF TABLES

ABBREVIATIONS AND SYMBOLS

AGL - above ground level

ARS - Agricultural Research Service

BP - barometric pressure, inches of mercury

BRT - Kauth's brightness index

CCT - computer compatible tape

CO - cotton

CT - citrus

D - day scene; obtained between 1342 and 1420 hours LST in this study

ΔT - day minus night temperature difference image, a NASA Goddard HCMM data product

ΔTI - thermal inertia difference image, a NASA Goddard HCMM data product

ΔTs - surface temperature difference between daytime maximum and nighttime minimum

DC - digital count

DEPL - soil water depletion since last rainfall or irrigation, mm

DIST - distance of each ground site from the Gulf coast, km

DSR - days since rainfall or irrigation

EDIS - Environmental Data Information Service

EPA - Environmental Protection Agency

EROS - Earth Resource Observation Satellite

ET - evapotranspiration, cm day^{-1} or mm day^{-1}

ETp - potential evapotranspiration, cm day^{-1} or mm day^{-1}

G - sensible heat flux to the soil

GR - grass

GT - ground truth

GVI - Kauth's green vegetation index (see section 7.3)

H - sensible heat flux to the air

HCMM - heat capacity mapping mission

ICDPD - average of current day's and previous day's insolation, Ly day^{-1}

IDOP - insolation the day of HCMM overpass, Ly day^{-1}

INSOL - insolation, Ly day^{-1} (same as current day's insolation in ICDPD)

IOA - insolation outside the atmosphere parallel to the earth's surface, Ly day^{-1}

I/W - ratio of insolation for current and previous day to wind movement current and previous day, Ly day^{-1}/km day^{-1}

IHROP - insolation the hour of the HCMM overpass, Ly

IPF - Information Processing Facility

ISP - irrigation scheduling program

IR - infrared -- in HCMM data the emissive band (10.5 to 12.5 μm)

JD - "Julian day" - actually the day of the year letting 01 Jan be JD 001 and 31 Dec be JD 365 in nonleap years

Ka - a soil moisture availability factor (see section 6.3)

Kc - a coefficient dependent on crop development and soil water conditions that relates ET to ETp (see section 6.3)

Kco - crop coefficient, dimensionless (see section 6.3)

Ks - a factor that lets evaporation directly from the soil contribute to ET when the soil surface is wet, dimensionless (see section 6.3)

Landsat - acronym for Earth Resources Technology Satellite with emphasis on land applications

LE - latent heat flux (evapotranspiration)

MDP - mean dew point, °C

N - nighttime scene; nighttime passes of HCMM occurred between 0205 and 0227 hours LST for this study

NASA - National Aeronautics and Space Administration

NEΔT - noise equivalent temperature difference

NOAA - National Oceanic and Atmospheric Administration

NWS - National Weather Service

OD - atmosphere's optical depth

PC - percent vegetation cover of the ground

PCN - percent cloud contamination, usually from 81 pixel sample

PFC - percent of field capacity

PLL - pressure at lowest atmospheric level of radiosonde observations, mb

PH - plant height, cm

PVI - perpendicular vegetation index derived from Landsat bands 5 and 7 (see section 7.3)

PVI6 - perpendicular vegetation index derived from Landsat bands 5 and 6 (see section 7.3)

PW - precipitable water in the atmosphere, cm

r - linear correlation coefficient

R - multiple correlation coefficient (R^2 = coefficient of determination)

R1, R3, R5, R7, R9 - albedo of central pixel and mean albedo of a sample 3x3, 5x5, 7x7, and 9x9 pixels in size, respectively (see section 7.3)

Rn - net radiation flux received at the Earth surface

Rs - incident solar radiation converted to equivalent depth of water evaporated, cm day

SC - sugarcane

SCi - subvisible cirrus (see section 2.2)

SCS - Soil Conservation Service

SDEF - saturation deficit of the air, mb (except in chapter 5.0 where units are inches of mercury)

SDW - saturation deficit times wind movement, inches Hg km day^{-1}

SR - sorghum

Ta - average daily air temperature, °C

TC - temperature correction, surface to satellite height, °C

THCMM - temperature derived from emissive band of HCMM, °C

TLL - temperature at the lowest atmospheric level of radiosonde observations, °K

Tm - mean daily air temperature, °F

Tmax - maximum daily air temperature, °C

Tmin - minimum daily air temperature, °C

T1, T3, T5, T7, T9 - Temperature of central pixel and mean temperature of sample 3x3, 5x5, 7x7, and 9x9 pixels in size, respectively, from IR band of HCMM, °C (one pixel = about 36-ha in ground area)

TW - air temperature (mean daily) times daily run of the wind, °C km day^{-1}

USDA - United States Department of Agriculture

USGS - United States Geological Survey

VIS - (from visible) in HCMM data, the reflective band (0.55 to 1.1 μm)

Xc - temperature of central pixel of a matrix of pixels (see section 2.2.1.6)

$\bar{X}w$ - mean temperature of a moving window of 9x9 pixels (see section 2.2.1.6)

WC - with clouds, i.e. pixels contaminated by clouds

WCAP - soil water holding capacity of the root zone, cm

WOC - without cloud contamination, i.e. pixels without clouds (pixels WOC)

1.0 INTRODUCTION

1.1 Objectives

The objectives of our HCMM investigation took advantage of the optimum day and night timing of the HCMM passes. Agriculturally related studies were conducted in the subtropical Lower Rio Grande Valley of south Texas. Rainfall decreases by 1-cm/4.5-km inland from the coast at the test site giving a natural gradient in plant species and soil water available for evapotranspiration. An important irrigated area of 260,000 ha provided fields that vary in irrigation date (degree of water stress), soil type (crop rooting depth), and crop species. In addition, freezes are a hazard to high value/ha citrus, sugarcane, and vegetables. Our research was organized for seasonal emphasis:

1. Synoptic studies (year around)
    a. Document surface temperature gradients inland from coast and around inland lakes
    b. Use HCMM to develop synoptic aridity index, THCMM - Tmax
    c. Relate nighttime HCMM temperatures to ambient air dew-point temperatures
    d. Relate HCMM surface temperatures to ground observed day and night air temperatures
2. Freeze hazard (Dec to Feb)
    a. Identify areas of least freeze hazard for growing temperature-sensitive crops
3. Planting date advisory (Jan to Apr)
    a. Relate nighttime soil temperatures to major soil texture variations over the Lower Rio Grande Valley
    b. Correlate HCMM soil surface temperatures with ground temperatures reported by NOAA in agricultural advisories, or with those directly measured at 5-cm planting depth
4. Plant cover (year around but primarily Mar to Jun)
    a. Document effect of percent ground cover on HCMM measured surface temperatures
    b. Identify bare fields
5. Crop water stress (Apr to Sep)
    a. Relate HCMM temperatures to soil water depletion and days since irrigation or rainfall

1.2 Data Sources

1.2.1 HCMM images and computer compatible tapes (CCT)

The 700-km wide swath of HCMM covered our test site (97°00' to 99°30'W longitude and 25°30' to 27°00'N latitude) partially or totally in the daytime on reference days 3, 8, and 14 whose NNW-bound orbits centered about over Brownsville, Laredo, and Houston, Texas, respectively. Nighttime overpasses, which occurred on the SSW-bound orbits of reference days 6, 11, and 1, had subsatellite cities, for relative positioning of the orbits, of McAllen, Houston, and Laredo (Falcon Lake), Texas. The dates of overpasses for the above reference days and ground identifying cities are summarized in Table 1.1.

Because we had a standing order with the Information Processing Facility (IPF), NASA, Goddard we received single 9x9-inch (230x230-mm) black and white prints of each coverage of our site as relayed to the Merritt Island, Florida, receiving station during the period May 78 through May 79. (Our site was on the very fringe of the range for both the Greenbelt, Maryland, and Goldstone, California stations; consequently they received little data for our site).

We received hundreds of prints to screen for data quality and cloud cover. From these, we selected 10 daytime emissive and reflective band scenes, and six nighttime emissive scenes for which we ordered 9 track 800 bpi CCT, single negative transparencies, and single positive prints for use in analyses and reporting. The dates of the overpasses, their ID, type of scenes (day or night), and average cloud cover over the test site are given in Table 1.2. For analyses purposes, the scenes are grouped chronologically as indicated in report section 1.1.

Because of our low latitude, consecutive day/night or night/day (12 hour difference) overpasses were not possible. However, day/night passes 36 and 60 hours apart were possible. We could retrospectively order day/night temperature difference (ΔT) and thermal inertia difference (ΔTI) products from Goddard. We did retrospectively order the ΔT and ΔTI processing of the 08 Jul 78 day and 06 Jul 78 night scenes.

1.2.2 Intensive test sites

For crop water stress and plant cover studies, 18 intensive test sites were selected using aircraft support photography, Landsat imagery, and visits to field sites that contained contiguous fields of the same crop or very large single fields--defined as land parcels managed alike (same crop species, planting date, cultivations, etc.) that were not dissected by field access roads, public roads, canals, fences, etc. The 18 segments were composed of 99 fields that were ground truthed. In four segments, large fields of two different crops occurred so that the data set consisted of 22 fields. The observed sites ranged in area from 1.08 km^2 (108 ha) to 12.40 km^2 (1240 ha). Representative fields ranged from 18 ha to 1240 ha and averaged 248 ha in size. These sizes were the basis of examining the HCMM temperature data for the center pixel of each site and the 3x3 pixel matrix (325 ha area) centered on the center pixel.

We waited until HCMM was launched and operational before we began weekly ground truthing individual fields (no ground truth data was obtained when muddy roads prevented field access) from 30 May to 13 Jul 78. The information obtained included crop species, plant height (PH), percent crop cover (PC), percent weed cover, stage of crop maturity, and date of irrigation. Notes were taken about plant condition (abnormal defoliation, leaf curling or rolling, color), soil condition (crusted, wet or dry soil surface, tillage in progress or recently completed, standing water), and obvious insect or disease incidence.

The data were summarized for each field and filed on discs for merging with data from other sources. The crop, longitude and latitude, and site number for each of these sites is given in Table 1.4 and their distribution in the test area is shown on the site map of Figure 1.1. The sites were concentrated in Hidalgo County to minimize the time and mileage to visit them.

1.2.3 Representative sites

Forty-eight ground locations were chosen within the test site that represented typical water, urban areas, irrigated and dryland cropped sites, native and improved rangeland, wildlife refuges, and special interest sites such as barren Padre Island (sand) and a native oak grove on deep sand. These sites were chosen for internal homogeneity by using high altitude photography, Landsat images, and various maps of the area. They ranged in latitude from 40-km off the coast to 160-km inland. They were intended for synoptic analyses and to be large enough so that HCMM data in up to 9x9 pixel matrices could be examined for these sites. These sites are listed by number, longitude and latitude, and a brief description of each is given in Table 1.5. A map showing their locations and distributions is Figure 1.2.

1.2.4 Supplementary Landsat data

The earth observation satellite, Landsat series, with its 4-band multispectral scanner (MSS) passed over the test site on two dates of low cloudiness, 15 Jun (Landsat-2) and 12 Jul 78 (Landsat-3), when the fields were being ground truthed. The CCT for these two dates were ordered from the EROS Data Center, Sioux Falls, South Dakota, and the digital count data for each Landsat band were extracted for subsamples of the 22 intensive sites as well as for many of the "representative" sites.

The digital samples were used to calculate Kauth transformations, greenness (GVI) and brightness (BRT) (Kauth and Thomas, 1976), and perpendicular vegetation indices (PVI, PVI6) (Richardson and Wiegand, 1977).

These vegetation indices were needed to corroborate ground truth, and to provide spectral indicators of vegetation greenness and ground cover for additional ground sites that were not ground truthed. These data were studied in relation to HCMM indicated earth surface and crop canopy temperatures.

1.2.5 Climate and weather

Supporting weather data were collected at a centrally located environmental station (Weslaco, Texas) where continuous measurements were made of solar radiation, total hemispherical radiation, wind movement, air temperature, and vapor pressure (dew point). These data were integrated for each hour of the day and archived as hourly means and daily totals.

Daily precipitation and daily maximum and minimum temperatures for 15 reporting stations within the HCMM test site area that are regularly reported and published (NOAA-EDIS, 1978 and 1979) were summarized. Also, specifically for the HCMM study, a recording thermograph station was installed in an unrepresented rangeland area. When needed for analyses, data from the reporting station nearest our individual test sites were used to estimate their precipitation and air temperature.

From Nov to Mar each year, NOAA-NWS uses volunteer observers to measure and report minimum daily temperature. Frequent observations are also made during periods of freezing or near freezing temperatures. These data were given to us by the NWS office at Brownsville, Texas. The data supplied had detailed air temperatures for interpreting results for 02 and 03 Jan 79, when a freeze occurred. The site number, coordinates, and names of such stations are given in Table 1.6, and their distribution over the test area is shown in Figure 1.3.

Radiosonde atmospheric soundings of temperature, pressure and humidity (dew point depression) made by NOAA-NWS at Brownsville on HCMM overpass days were used to correct the thermal satellite data by applying a radiative transfer model. Table 1.3 lists information from atmospheric soundings that were made nearest in time to the satellite data that we utilized.

1.2.6 Aircraft support flights

The contract proposal was submitted to NASA in Aug 75. At that time it was anticipated that HCMM would be launched in late 1976. We specified aircraft support flights on cold (the criterion used was that the predicted nighttime minimum be 5 C) clear calm nights in Jan and Feb 77, and in May, Jun, and Jul 77. Five flight lines were used for daytime flights that totaled 310 nautical miles (574-km).

Flights were requested at low (3,000-m AGL) and medium (9,100-m) altitudes with the C-130 aircraft that was equipped with a portable radiation thermometer (2°FOV), MSS, and aerial cameras. The low altitude data were needed to examine differences and gradients within the fields and the medium altitude data were needed to make comparisons among fields. High altitude (12,000 to 18,000-m AGL) data obtained with the RB57 airplane were needed for synoptic studies.

The C130 aircraft overflew three flight lines at night on 20 Jan 77 and part of the flight lines at 1,825-m and 7,900-m on 26 Jul 77. The photography was valuable to help select the representative and intensive test sites. No overflights occurred during the period when HCMM data were being supplied.

A locally-leased aircraft, equipped with a Zeiss RMK 9-inch camera, overflew the intensive test sites on 09 Jun 78. The photographs were used to locate the test sites and individual fields in the line printer gray maps of the Landsat data, determine the size of individual fields by planimetry, verify land uses within the sites, document variations in crop stands and vigor within individual fields, and document soil and topographic variations within test sites.

1.2.7 Ancillary information

Test fields and sites were located on USGS 7 1/2 minute quadrangle maps using aerial photographs and features displayed on the maps as aids. Once located on the topographic maps, the center coordinate of each site was assigned a latitude and longitude to the nearest ±.001 degree. This became the center pixel that was searched for in the HCMM data, and we later refer to it as the 1x1 pixel matrix for the site (one pixel in latitudinal and 1 pixel in longitudinal extent).

We carefully located the center pixel because each HCMM pixel represented about 36-ha on the ground which corresponds to a displacement of adjacent pixels by 20 seconds of latitude and longitude, or .006°. That is, we did not want site location specification to be less precise than the retrievability of the HCMM data from the CCT. (The HCMM data were registered to the ground scene to within about ±1 pixel--see report section 2.1.1 for HCMM data preprocessing procedures).

Soil association maps of the Lower Rio Grande Valley were provided in response to the HCMM study by the Soil Conservation Service (SCS) of the USDA. This information was digitized each 20 seconds of displacement to correspond to the HCMM pixel resolution. The identifying soil association number at every 20 seconds of the latitude and longitude grid was stored on disc for use in interpreting the HCMM data.

The SCS county soil surveys for Cameron and Starr Counties (Thompson et al., 1972; Williams et al., 1977) gave specific soil identifications for the intensive test sites in these counties. The soil data for test sites in Hidalgo and Willacy Counties were either obtained from unpublished work sheets in the Raymondville and Edinburg SCS field offices or from the generalized map.

1.2.8 Representative soil temperature, and experimental wet and dry plots

Daily maximum and minimum soil temperatures measured at the 10-cm depth for four locations within the test area were obtained from the NOAA-NWS office in Brownsville for the period 01 Jan 79 to 31 Mar 79. These data are useful indicators of soil temperature for planting advisories and for deriving relations among environmental variables and soil temperatures at the 10-cm depth.

To provide additional data for direct comparison with HCMM-indicated temperatures and for predicting soil temperature at various depths from meteorological parameters, two 6.1 m square continuously fallow plots were established. One plot received only rainfall while the other plot was also irrigated weekly. In each plot, thermocouples were installed at the 0.5, 5, 10, 20, and 100-cm soil depths, and their outputs were printed on a strip-chart recorder at hourly intervals. Data were recorded for the period 10 Aug to 29 Sep 78 and from 22 Nov 78 to the present. The data provided information for relating HCMM data to existing ground and environmental conditions at the time of its acquisition.

1.3 Literature cited

Kauth, R. J. and G. S. Thomas. 1976. The tasseled cap--A graphic description of the spectral-temporal development of agricultural crops as seen by Landsat. Proc. Machine Processing of Remotely Sensed Data, LARS, Purdue 6/29-7/02. Inst. Electron. and Electrical Engineers Cat. No. 76. Ch. 1103-1 MPRSD. New York, NY.

National Oceanic and Atmospheric Admin. (NOAA), Environ. Data and Inform. Ser. (EDIS). Climatological Data, Texas. Vols. 83 (1978) and 84 (1979), Numbers 1 through 12. National Climate Center, Asheville, NC.

Richardson, A. J. and C. L. Wiegand. 1977. Distinguishing vegetation from soil background information. Photog. Eng. and Rem. Sens. 43(12):1541-1552.

Thompson, C. M., R. R. Sanders, and D. Williams. 1972. Soil survey of Starr County, Texas. Supt. Doc., U.S. Govt. Printing Office, Washington DC. 62p + maps.

Williams, D., C. M. Thompson, and J. L. Jacobs. 1977. Soil survey of Cameron County, Texas. 1977. Supt. Doc., U.S. Govt. Printing Office, Washington DC. 62p + maps.

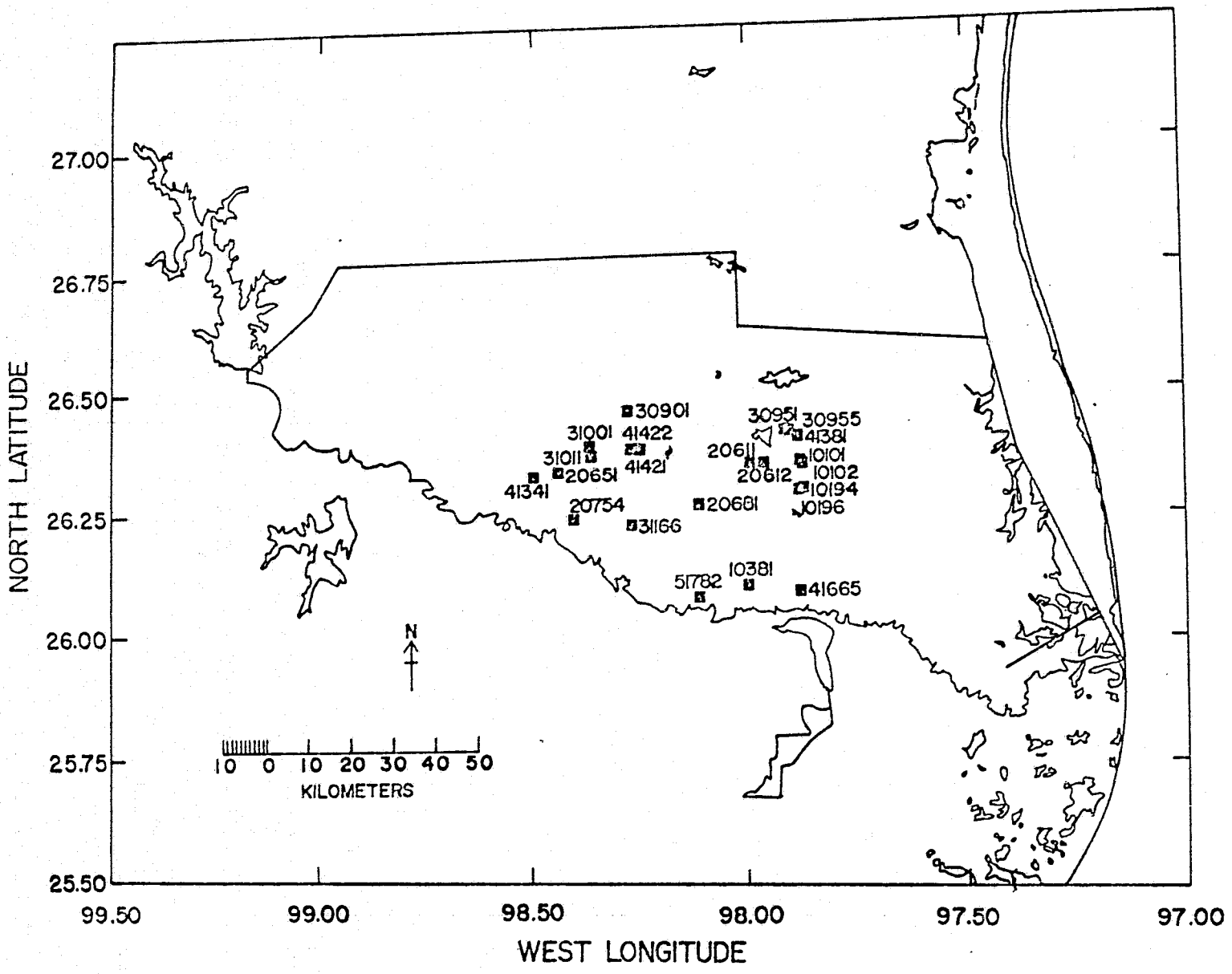

Figure 1.1 Distribution of 22 intensive sites for crop water stress and ground cover studies within the HCMM investigations test area.

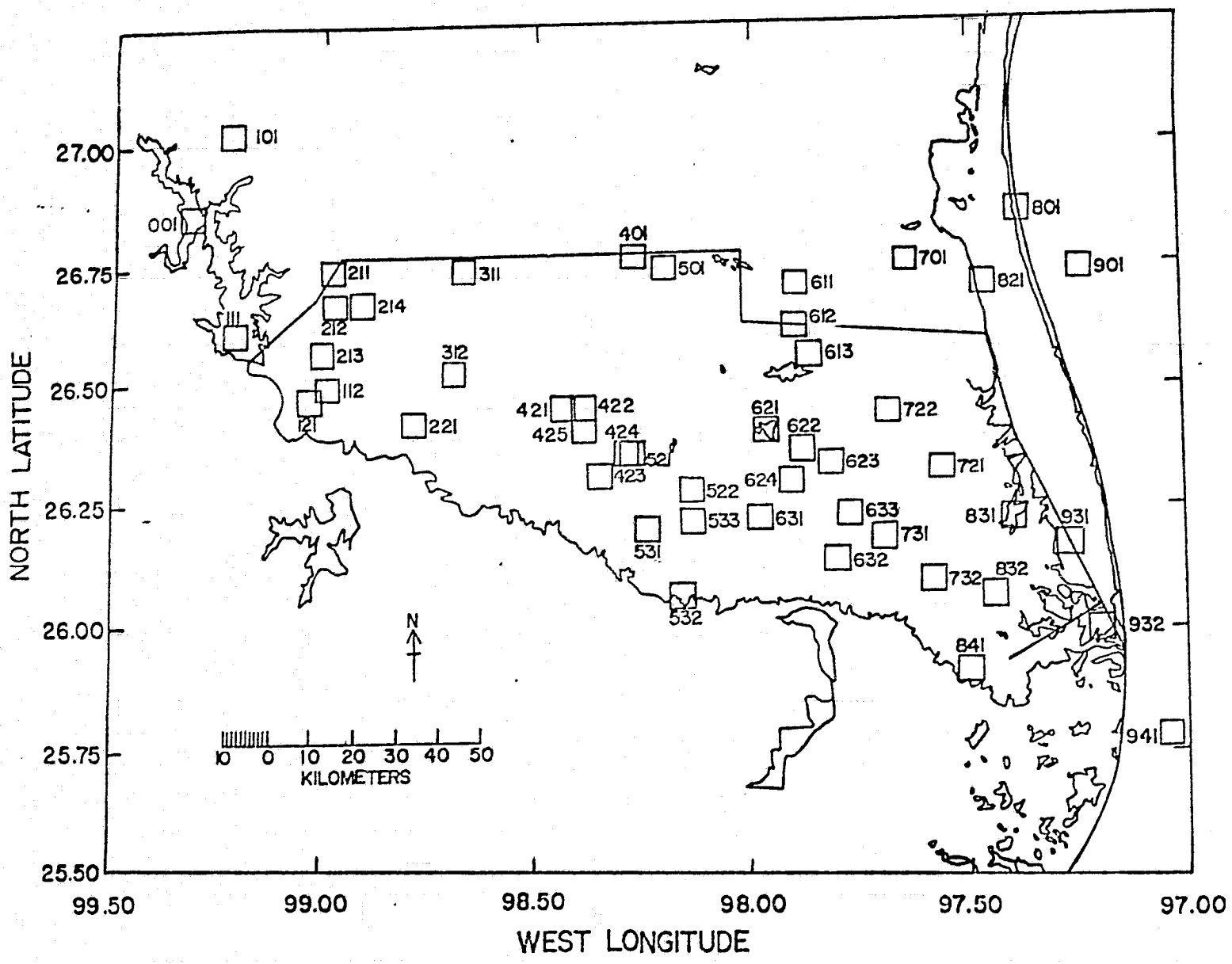

Figure 1.2 Distribution of 48 representative sites for synoptic analyses within the HCMM investigation test site.

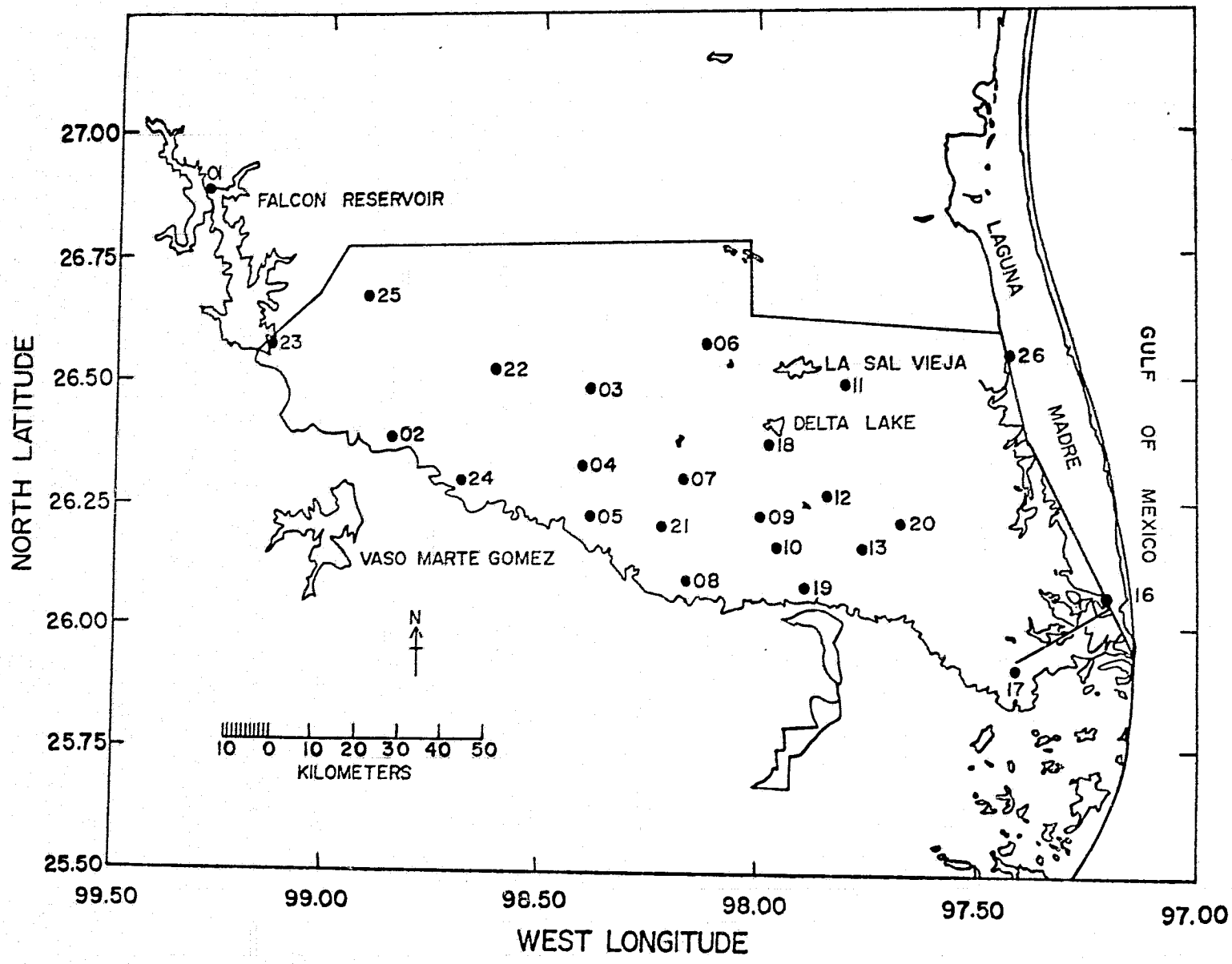

Figure 1.3 Distribution of 24 weather stations for air temperature reference within the HCMM investigation test site.

Table 1.1 Dates of HCMM overpasses by reference day orbits from launch through June 1979 that partially or totally covered our test site. A subsatellite city for relative positioning of the orbits is given in parentheses for each reference day orbit.

	Daytime			Nighttime		
	Ref. Day 3 (Brownsville)	Ref. Day 8 (Houston)	Ref. Day 14 (Laredo)	Ref. Day 1 (Laredo)	Ref. Day 6 (McAllen)	Ref. Day 11 (Houston)
1978	5/16	5/21	5/27	5/14	5/19	5/24
	6/01	6/06	6/12	5/30	6/04	6/09
	6/17	6/22	6/28	6/15	6/20	6/25
	7/03	7/08	7/14	7/01	7/06	7/11
	7/19	7/24	7/30	7/17	7/22	7/27
	8/04	8/09	8/15	8/02	8/07	8/12
	8/20	8/25	8/31	8/18	8/23	8/28
	9/05	9/10	9/16	9/03	9/08	9/13
	9/21	9/26	10/02	9/19	9/24	9/29
	10/07	10/12	10/18	10/05	10/10	10/15
	10/23	10/28	11/03	10/21	10/26	10/31
	11/08	11/13	11/19	11/06	11/11	11/16
	11/24	11/29	12/15	11/22	11/27	12/02
	12/10	12/15	12/21	12/08	12/13	12/18
	12/26	12/31		12/24	12/29	
1979			1/06			1/03
	1/11	1/16	1/22	1/09	1/14	1/19
	1/27	2/01	2/07	1/25	1/30	2/04
	2/12	2/17	2/23	2/10	2/15	2/20
	2/28	3/05	3/11	2/26	3/03	3/08
	3/16	3/21	3/27	3/14	3/19	3/24
	4/01	4/06	4/12	3/30	4/04	4/09
	4/17	4/22	4/28	4/15	4/20	4/25
	5/03	5/08	5/14	5/01	5/06	5/11
	5/19	5/24	5/30	5/17	5/22	5/27
	6/04	6/09	6/15	6/02	6/07	6/12
	6/20	6/25	7/01	6/18	6/23	6/28
	7/06			7/04	7/09	

Note: Orbit paths over Brownsville and McAllen came closest to being centered over our HCMM test site; however, passes over Houston and Laredo encompassed it because of the wide swath. Ref. Day 3 (daytime) and Ref. Day 1 (nighttime), and Ref. Day 8 (daytime) and Ref. Day 6 (nighttime) coverages, respectively, were 36-hours apart. Day and night coverages may occur each five (or six) days. The same orbit is repeated each 16 days.

Table 1.2 Overpass dates, scene identification numbers, day (D) or night (N) scene, and percentage of clouds over our test site for HCMM scenes investigated.

Overpass date	Julian date	Scene type	Scene ID	Percent clouds
27 May 1978	147	D-VIS[1]	A-A0031-20160-1	12.4
		IR[2]	A-A0031-20160-2	
6 Jun.1978	157	D-VIS	A-A0068-20060-1	19.6
		IR	A-A0068-20060-2	
12 Jun.1978	163	D-VIS	A-A0047-20150-1	
		IR	A-A0047-20150-2	11.3
17 Jun.1978	168	D-VIS	A-A0052-20080-1	
		IR	A-A0052-20080-2	25.8
23 Jun.1978	174	D-VIS	A-A0058-20200-1	
		IR	A-A0058-20200-2	25.2
3 Jul.1978	184	D-VIS	A-A0041-20040-1	18.8
		IR	A-A0041-20040-2	
8 Jul.1978	189	D-VIS	A-A0073-20000-1	3.4
		IR	A-A0073-20000-2	
15 Aug.1978	227	D-VIS	A-A0111-20040-1	3.6
		IR	A-A0111-20040-2	
8 Nov.1978	312	D-VIS	A-A0196-19440-1	
		IR	A-A0196-19440-2	0.1
7 Feb.1979	38	D-VIS	A-A0287-19420-1	0.2
		IR	A-A0287-19420-2	
30 Jun.1978	181	N-IR	A-A0065-08260-3	-
23 Aug.1978	235	N-IR	A-A0119-08270-3	-
10 Oct.1978	283	N-IR	A-A0167-08240-3	-
21 Oct.1978	294	N-IR	A-A0178-08270-3	-
3 Jan.1979	003	N-IR	A-A0252-08050-3	-
26 Feb.1979	057	N-IR	A-A0306-08090-3	-

[1] 0.55 to 1.1 μm, or reflective band

[2] 10.5 to 12.5 μm, or emissive band

Table 1.3 Lowest level temperature (TLL), lowest level pressure (PLL), precipitable water (PW), atmospheric optical depth (OD), and surface to satellite temperature correction (TC) as determined by a radiative transfer model for the HCMM scene dates investigated using morning (6am) and evening (6pm) radiosonde data.

	6am					6pm				
	TLL (°K)	PLL (mb)	PW (cm)	OD (--)	TC (°C)	TLL (°K)	PLL (mb)	PW (cm)	OD (--)	TC (°C)
27 May 78	297.5	1012	4.12	1.221	3.5	304.2	1101	3.60	0.914	6.45
06 Jun. 78	299.8	1008	4.53	1.414	5.6	304.2	1005	4.35	1.217	6.83
12 Jun. 78	299.2	1014	3.83	1.103	3.79	305.3	1016	3.88	1.065	7.21
17 Jun. 78	297.0	1015	3.91	1.059	3.97	305.9	1014	3.94	0.985	8.66
23 Jun. 78	295.9	1014	3.63	0.891	2.14	306.4	1014	4.45	1.186	9.77
03 Jul. 78	299.2	1010	4.46	1.174	5.87	306.4	1009	3.41	0.691	5.85
08 Jul. 78	299.2	1015	3.65	0.955	3.99					
15 Aug. 78	299.2	1014	4.32	1.180	4.45	307.0	1014	3.84	0.941	7.73
08 Nov. 78						290.9	1017	0.88	0.133	0.68
07 Feb. 79	282.5	1016	0.96	0.125	0.29	286.4	1020	0.99	0.166	0.92
30 Jun. 78	295.9	1016	4.31	1.108	3.61					
23 Aug. 78	295.9	1014	3.63	0.891	2.14					
10 Oct. 78	293.1	1015	2.93	0.795	1.14					
21 Oct. 78	290.3	1015	2.26	0.560	0.26					
26 Feb. 79	278.1	1025	0.81	0.092	-0.21	292.5	1026	0.71	0.080	0.76

Table 1.4 Site number, coordinates, and crops at 22 intensive test sites used in the HCMM investigations.

Site No.	Longitude	Latitude	Crop
	- - - - Degrees - - - -		
10101	97.870	26.368	Sorghum
30901	98.245	26.460	Sorghum
31001	98.358	26.404	Sorghum
31011	98.354	26.382	Sorghum
41341	98.500	26.333	Sorghum
41381	97.865	26.419	Sorghum
41421	98.245	26.372	Sorghum
10194	97.885	26.308	Sugarcane
10196	97.875	26.306	Sugarcane
30951	97.902	26.425	Sugarcane
41422	98.250	26.373	Sugarcane
41665	97.884	26.087	Sugarcane
51782	98.120	26.080	Sugarcane
10102	97.872	26.058	Cotton
10381	97.920	26.096	Cotton
20611	97.984	26.352	Cotton
30955	97.898	26.416	Cotton
20681	98.134	26.276	Citrus
20754	98.402	26.244	Citrus
31166	98.262	26.230	Citrus
20611	97.970	26.351	Bermudagrass
20651	98.428	26.321	Buffelgrass

Table 1.5 Site number, coordinates, and a brief description of each land use at 48 representative sites used in the HCMM investigations.

Site No.	Longitude	Latitude	Site Description
	- - - Degrees - - - -		
001	99.301	26.854	Falcon Lake (Inflow)
101	99.226	26.969	Rangeland, Zapaia
111	99.199	26.610	Falcon Lake (Main Storage)
112	99.010	26.513	Native Brushland, Nonsaline
121	99.034	26.475	Buffelgrass, Sandy Loam
211	98.972	26.744	Grain Sorghum (Dryland)
212	98.968	26.659	Saline Rangeland
213	99.000	26.569	Buffelgrass, Some Brush Reinfestation
214	98.901	26.667	Rangeland, Las Escobas Ranch
221	98.769	26.415	Rangeland, Ricaby Oil Field
311	98.674	26.741	Rangeland, LaGloria
312	98.688	26.516	Rangeland, Rincon
401	98.279	26.777	Rangeland (Red Soil)
421	98.435	26.453	Grain Sorghum (High Reflectance Soil)
422	98.384	26.443	Grain Sorghum (Low Reflectance Soil)
423	98.340	26.334	Mixed Crops, Mainly Citrus
424	98.268	26.368	Monte Christo Citrus Area
425	93.386	26.405	Citrus, Topographic Drain
501	98.194	26.760	Rangeland (Natural)
521	98.250	26.366	Sugarcane
522	98.136	26.261	Edinburg Citrus Area
531	98.231	26.200	City of McAllen
532	98.147	26.075	Santa Ana Wildlife Refuge
533	98.134	26.219	Mixed Crops, San Juan
611	97.879	26.705	Rangeland (Soil Coloration)
612	97.880	26.604	Rangeland (Numerous Swales)
613	97.855	26.555	Rangeland
621	97.947	26.413	Delta Lake (Irrigation Reservoir)
622	97.860	26.376	Mixed Cotton and Sorghum (Raymondville)
623	97.809	26.356	Mixed Cotton and Sorghum (Willacy-Raymondville)
624	97.881	26.302	Sugarcane
631	97.676	26.212	Mid-Valley Mixed Crops
632	97.789	26.151	Adams Gardens Citrus Area
633	97.775	26.239	Mixed Crops, Primera
701	97.623	26.767	Oak Trees (Extensive Grove)
721	97.555	26.322	Mixed Cotton and Sorghum (Willacy-Ramondville)
722	97.671	26.466	Sorghum and Cotton, Reflective Soil
731	97.699	26.169	City of Harlingen
732	97.572	26.108	"Homogeneous" Area
801	97.368	26.827	Padre Island Sand
821	97.441	26.721	Laguna Madre (Shallow water)
831	97.388	26.233	Laguna Atascosa
832	97.418	26.067	Grassland (High Water Table)
841	97.498	25.905	City of Brownsville
901	97.217	26.750	Gulf of Mexico - 12 km. E. of Padre Island
931	97.247	26.169	Laguna Madre (Deep Water)
932	97.201	26.006	Mud Flat
941	97.037	25.787	Gulf of Mexico - 12 km. E. of Washington

Table 1.6 Site number, coordinates, and station names of 24 weather station sites used in the HCMM investigations.

Site No.	Longitude	Latitude	Station Site Name
	- - - Degrees - - -		
1	99.284	26.868	Zapata
2	98.865	26.382	Rio Grande City
3	98.386	26.486	McCook
4	98.408	26.331	Texan Gardens
5	98.396	26.220	Bates Power
6	98.117	26.566	San Manuel
7	98.158	26.298	Edinburg
8	98.159	26.090	Schuster Farm
9	97.988	26.223	Research Farm
10	97.962	26.157	Weslaco
11	97.791	26.487	Raymondville
12	97.869	26.265	Santa Rosa
13	97.777	26.158	Adams Gardens
16	97.211	26.075	Port Isabel
17	97.425	25.913	Brownsville Airport
18	97.968	26.378	Monte Alto
19	97.892	26.064	Mercedes
20	97.681	26.209	Harlingen
21	98.218	26.202	McAllen
22	98.604	26.521	Rincon
23	99.131	26.566	Falcon Dam
24	98.686	26.311	Garciasville
25	98.901	26.667	Las Escobas Ranch
26	97.430	26.558	Port Mansfield

2.0 METHODS, PROBLEMS, AND SOURCES OF VARIATION

2.1 Data preparation and organization

2.1.1 HCMM whole test site (~100,000 pixels)

Once HCMM scenes (see Table 1.2 for a listing) were received from NASA Goddard, they were processed for analyses as follows where the name of the Weslaco USDA computer program is given in parentheses:

a. Locate test site in magnetic tape, by referring to transparencies and/or Dicomed display (DSPLY).

b. Determine digital count range of the test site (DIGN5).

c. Prepare IR gray map on line printer-invert daytime data to match nighttime record sequence (because of opposite direction of satellite travel) (GRYN5, DAYN5).

d. Find georeference sites on IR data and produce location equations that relate pixel line and column to latitude and longitude. Cut and try to obtain minimum error of fit by discarding poorly identified georeference sites as indicated by computer analysis (W1101).

d1. Print IR gray map with georeference sites to check regression equation coefficients that relate pixel line and column numbers to latitude and longitude. If this check is good then processing proceeds on to NTWK1. If not regression equation will need to be reworked (LATN5).

e. Assign the IR value of the nearest pixel to each coordinate cell (20-seconds latitude x 20-seconds longitude). Store these data on disc (NTWK1).

f. Repeat steps a through e with VIS data.

g. Graphically represent six parallel IR (and VIS) transects that cross the test site (PROFL).

h. Select and apply "threshold" values to the IR data so as to exclude all cloud contaminated data from further analysis. Determine threshold value by plot of individual IR pixel values vs corresponding VIS pixel values, and by examination of IR (and VIS) transect graphs (SOPFL, RATDF, TEMP3, TEMP4).

i. Prepare IR gray map of test site using only retained, non-contaminated data (DISC2).

j. Print out mini-maps of thermal environment surrounding all sites (Intensive, Representative, and Weather Sta. sites). Identify which pixels in the 9x9 cell scene were cloud contaminated (TEMP3, TEMP4).

k. Calculate mean temperature and standard deviation of the 9x9 pixel area surrounding (or comprising) the site. Include only cloud-free pixels in the calculations (TEMP3, TEMP4).

l. Prepare histogram of temperatures in the 9x9 pixel areas, excluding cloud contaminated pixels (FREQ5, FREQ1).

m. Prepare summary table of surface temperatures and albedos at all sites for 1x1, 3x3, 5x5, 7x7, and 9x9 pixel areas. Tabulate mean values and number of cloud-free pixels in each size area (TEMP3, TEMP4).

n. Compare surface temperatures with air temperatures measured at the weather stations (TEMP3, TEMP4).

o. Determine the mean temperatures and standard deviations for the 34 soil associations of the test area (exclude cloud-contaminated data from analyses) (SOIL2, SOIL3).

p. (Required to be done only once) Determine the centroid of the area of each soil association. Information was used in analyzing for effect of proximity to the coast (CENTR).

q. Determine histograms of agricultural area and rangeland area (FREQ2).

r. Using the frequency distribution of the agricultural area (excluding cloudy pixels), determine the temperature limits for Cold, Medium, and Warm areas, such that one-third of the area falls in each classification (FREQ2).

s. Prepare map of test site showing areas of Warm, Medium, and Cold classification (FREQ2).

t. Overlay selected nighttime IR maps of test site that display the occurrence of pixels in the Warm category--of step r, above--by a dark print symbol, pixels in the Medium category by a dot, and pixels in the Cold category by a blank space (CLDWM).

u. Using selected pairs of day/night IR scenes prepare a disc file of temperature differences, cell by cell. Process these "difference" data according to the procedures of steps g, i, j, k, l, m, n, q, r, and s (DIFF).

These processing steps are extensive but are necessary to derive the data to meet the various objectives of the contract.

2.1.2 HCMM temperature, albedo, and dominant soil by 1x1, 3x3, 5x5, 7x7, and 9x9 pixel cells for 94 ground sites

The data were produced by the above processing steps j, k, l, and m. The central point for each ground site of interest was identified on USGS 7½-minute quadrangle maps, and assigned latitude and longitude positions to the nearest 0.001 degree. Once this pixel was identified in the ground registered digital data, surrounding pixels were assigned to build the pixel configuration up to 3x3, 5x5, 7x7, and 9x9 pixel cells.

The dominant soils could be determined because we digitized the generalized soil map of the four LRGV counties supplied by the SCS-USDA at 20-second intervals (0.006°) of latitude and longitude. Thus each HCMM pixel could be associated with the soil at that pixel location.

2.1.3 Ground truth for 22 intensive sites

The intensive test sites are described in section 1.2.2. A total of 99 fields were ground truthed weekly. The information recorded included Julian day and year of observation; sample stratum, segment, field and division within the field; crop; percent crop cover; percent weed cover; stage of crop development or maturity; plant height; unusual plant condition (defoliation, discoloration, etc.); soil surface condition (wet or dry, cloddy, freshly cultivated or tilled, etc.); visible apparent disease or insect infestation; irrigation or rainfall amount (when determined); and, date.

Aerial photographs of some of the sites were obtained with a locally based aircraft on 09 Jun, while photographs of the others were available from previous investigations dating back to 1972. The photographs were planimetered to determine the hectarage of each field. The 09 Jun photography was valuable for helping to locate fields of interest in the gray map printouts of Landsat data (see section 1.2.3) from which vegetation indexes were derived. The photography also verified within field variation in crop appearance and differences in maturity of adjacent fields.

A coding system for the ground truth was devised and the data were filed on discs for ready merger with data from other sources.

2.1.4 Weather data

Weather data described in section 1.2.5 were obtained from the central environmental station, 15 reporting stations in the test site area (NOAA-EDIS, 1978 and 1979), and NOAA-NWS volunteer observer reports of minimum daily temperature (from Nov to Mar). Twenty-four of the ground sites chosen for analyses of HCMM data were locations of NWS weather stations or volunteer observers (see Table 1.5), so that there would be a close correspondence between reported air temperature and precipitation, and temperature deduced from HCMM data. Air temperature for the remainder of the 94 ground sites was taken from the nearest

reporting station. The temperature, rainfall, and other weather data were assembled for the HCMM overpass dates and times of interest, and were placed on disc files for ready access (WATST).

Late in the investigation period, radiosonde data from Brownsville, Texas, was acquired for selected dates from Asheville, North Carolina, for use with a radiative transfer model provided by the HCMM Project Scientist. The objective was to find out the magnitude and direction of the temperature corrections it calculated for the HCMM data.

2.1.5 Landsat data (15 Jun and 12 Jul 78)

Landsat with its 4-band MSS passed over the test site on two dates of low cloudiness, 15 Jun (Landsat-2) and 12 Jul (Landsat-3). The 15 Jun Landsat data were paired with the HCMM measured temperatures and albedos for the HCMM's 12 and 17 Jun 78, overpasses and the 12 Jul Landsat data were paired with the 08 Jul HCMM data.

The Landsat scenes acquired from the EROS Data Center, Sioux Falls, South Dakota, were rectified to the ground scenes. The segments of the scenes, identified by latitude and longitude, over the ground sites of interest were extracted. These scene segments were used to produce gray map products of MSS 5 and 7. Use of USGS 7½-minute quadrangle maps and aerial photographs enabled the recognition of individual fields in the gray map printouts. Since the ground resolution of Landsat data is 0.45 ha, samples of from 40 to 120 Landsat pixels from each band were used to represent a given ground site. Usually samples were from a single field that was representative of the larger area sensed by HCMM (36 ha/pixel or 325 ha/3x3 matrix of HCMM pixels).

The Landsat digital samples were used to calculate the Kauth transformation (GVI) and brightness (BRT) (Kauth and Thomas, 1976), and the perpendicular vegetation indexes (PVI, PVI6) (Richardson and Wiegand, 1977) (See chapter 7, section 7.3 for the equations that define the vegetation indexes.).

The Landsat data were identified by ground site, field within site, crop, and date and placed on disc file for use with HCMM data.

2.2 Special problems

2.2.1 Coping with cumulus cloud contamination

2.2.1.1 Daytime scenes

Two of the 10 daytime HCMM scenes that we studied were clear. The test area in the other scenes was covered by from 3 to 26% clouds. These clouds were mainly of the "popcorn" cumulus type. If they were not densely aggregated we analyzed the scenes. To avoid erroneous conclusions from analyzing cloud contaminated data, it was necessary to develop methods of machine screening for clouds. The descriptions that follow enumerate the methods that we tried in our attempt to remove from analyses all pixels that were cloud contaminated. The problem of coping with contamination by subvisible cirrus (SCi) layers not apparent in the

VIS images is discussed in section 2.2.2 (In this respect, we distinguish between true clouds (mostly cumulus) that are apparent in both the VIS and IR images, and SCi layers that are apparent only in the IR.).

2.2.1.2 Reflective (VIS) screening

Screening reflective (VIS) data above a threshold value removed many of the clouds but there were areas of uncertainty. If the threshold was set low enough to detect thin clouds and pixels partly contaminated by clouds, the more reflective land areas such as fallow and dune areas were excluded. Also, the reflective criterion did not remove cloud shadows.

2.2.1.3 Emissive (IR) screening

Screening solely on the basis of emission was not feasible because water and cloud temperatures tended to overlap.

2.2.1.4 Reflective/emissive ratio screening

The ratioing of reflective (VIS) to emissive (IR) pixel values was tried for screening daytime clouds. This required that the data from the two wavelengths be registered so they could be overlaid and ratioed pixel by pixel. This was done by initially geometrically rectifying all HCMM data to map coordinates as discussed in section 2.1.1 of this chapter.

Screening for clouds by the reflective to emissive ratio was superior to either reflective or emissive screening alone. The ratio is useful because clouds are the brightest (highest digital count (DC)) scene component in the reflective channel and clouds are usually colder (lower digital count) than land features in the emissive data. Thus, the ratios, VIS/IR or IR/VIS, contrasted clouds very well versus other scene features for a given overpass date.

A weakness of the ratio method is that the division between clouds and terrestial features is not a fixed ratio but varies from scene to scene and with season.

2.2.1.5 Standard deviation screening

Tarpley (1979) described a process for eliminating cloud contaminated observations from GOES VISSR thermal data using standard deviations. His reasoning was that the standard deviations for cloud-contaminated data would be more variable than noncloud contaminated data. However, data for water body-land interfaces such as for Falcon Reservoir, the Gulf of Mexico, and the bay (Laguna Madre), also have high standard deviations; thus Tarpley's scheme would incorrectly classify these water body-land interface areas as clouds. Also, the subvisible cirrus contaminated area does not yield a high standard deviation; thus, Tarpley's scheme would incorrectly identify the SCi contaminated areas as clear.

It is possible that the Great Plains area, where Tarpley's scheme was applied, had a dry enough atmosphere and a dearth of water bodies so that neither was a problem. However, there are many other places in the world where this may be a problem.

2.2.1.6 Moving-window screening

A cloud detection scheme was applied to emissive scenes that uses the ratio of the center pixel value (X_c) to the average pixel value ($\bar{X}_w$) of a moving nxn pixel size window (Figure 2.1). Variations in X_c due to clouds are treated as high frequency image detail that is partially blocked by the low pass filter, $\bar{X}_w$ data. Ratio values less than $X_c/\bar{X}_w=0.92$ we found experimentally to be due to a partial cloud and the corresponding center pixel values were censored. The value 0.92 appears to be set by sensor NEΔT and the other noises.

This approach appears to distinguish between cloud values and surface and water body values satisfactorily. It does not censor vapor contamination. Unfortunately, it causes many individual pixels to be discarded in the vicinity of cloud edges because it is subject to the relative number of cloud-free and cloud-contaminated pixels in the nxn pixel window used as a filter. This may not be ojectionable where generalized results are desired.

The same $X_c/\bar{X}_w=0.92$ ratio value was applied to all test-site data for cloud detection. Figure 2.2 shows the effect of the 0.92 ratio value for partly cloudy 27 May and 12 Jun 78 HCMM overpass dates, and clear days 21 Oct 78 and 07 Feb 79 on east-west temperature transects across the test site. Note the small variability on the right side of all scenes, the Gulf of Mexico.

2.2.1.7 Cluster screening

In another cloud screening method, we took advantage of the fact that clouds are individualistic in scatter diagrams of reflective and emissive pixel values. Clouds have few locations where pixel values of both wavebands are the same as for the other scene features. That is, in two-dimensional spectral space, clouds do not cluster. Conversely, pixel values from the Earth's surface tend to have numerous locations where both pixel values are the same as other locations. Thus, clusters are formed. The scatter in cloud data and the clustering of clear areas were used to separate data with clouds from data for noncloudy areas. The scatter diagrams of Figure 2.3 show the clustering tendency of the data from land and water areas and the disperse nature of cloud data.

Gray maps were prepared after discarding all reflective-emissive combinations that did not recur at least 17 times in the test area of approximately 100,000 pixels. Combinations that recurred at least 17 times are identified by $ in the figures.

Close examination of the gray maps prepared by the clustering criterion showed that some cloud shadows remained in the scene and certain land and water areas had been discarded.

2.2.1.8 Modified cluster screening

Of the above methods of screening for clouds, clustering was the best. Most of the HCMM data discussed in this report were processed with a modification of the cluster method.

The modification was applied by examining a scatter diagram of reflective and emissive pixel values (such as the samples in Figure 2.3). The analyst draws a subjectively positioned line (not necessarily straight) on the scatter diagram so as to separate cloud pixels from noncloud pixels. The line is then described mathematically and applied in machine processing of the data. All pixels having reflective-emissive combinations that fall on the cloud side of the line are discarded.

A gray map prepared from the retained data was examined for undesirable data (such as cloud shadows) or inappropriate exclusion of valid features (such as highly reflective land areas). If the gray map was unsatisfactory, the line separating the clouds from valid data on the scatter diagram was adjusted and the procedure repeated. Table 2.1 lists the screening equations used in processing HCMM data.

2.2.1.9 Nighttime scenes

Consecutive day-night HCMM overpasses for thermal inertia analysis are not possible at our test site latitude, although pairs of scenes separated by several days have been examined. Thus, our main interest in nighttime emissive data has been confined to relationships with dew points and minimum air temperatures, and with cold-night surface temperature distributions. For these purposes, only clear night scenes have been analyzed, except that the freeze night of 02-03 Jan 79 was studied because of its economic importance, even though a subvisible cirrus layer was present.

2.2.2 Coping with subvisible cirrus contamination

A phenomenon observed in some HCMM scenes was illustrated in the emissive (IR) and reflective (VIS) wavelengths images for 08 Jul and 15 Aug 78 (Figure 2.4). Visual comparison shows that cumulus clouds had the same pattern and extent in both wavelengths. However, there were additional patterns in the emissive scenes that had no counterparts in the reflective images. The more pronounced patterns seen in the emissive images were often observed in the reflective images, but the edges were very diffuse and effects were too subtle to be readily detected in automated processing of the digital reflective data. We attributed the patterns readily discernable in the emissive images, but not in the reflective images, to a subvisible cirrus (SCi) layer.

Portions of the test area were under SCi layers on six of the 10 daytime HCMM scenes considered in this report. These atmospheric layers occurred in the summer time. The 08 Nov 78 and 07 Feb 79 scenes seemed to be free of SCi layers.

Identification of surface areas that were obscured from the satellite sensor by a SCi layer was possible by simultaneously viewing the HCMM emissive (IR) scene and a location map on a zoom transfer scope. The SCi layers were clearly distinguishable from typical cumulus clouds because of their uniform and usually extensive nature. These characteristics contrast with the "popcorn" type cumulus clouds common in our test area.

2.3 Sources of variation

2.3.1 Small test sites (weather stations, representative sites, and intensive fields)

We anticipated that many variables would affect the apparent Earth surface (agricultural landscape) temperatures and albedos as recorded by the emissive and reflective sensors of the HCMM. We designed a number of these (vegetative cover, plant water stress, ambient air temperature, distance from the coast, soil type, nighttime dewpoint temperature) into our objectives. Other variables also influenced our results, and it is the objective of this section to present an overview of some of these sources of variation.

The data used were pooled from the representative sites that were chosen especially for synoptic analyses (Chapter 3), weather station sites that were needed for freeze hazard analyses (Chapter 4), and intensive sites where ground truth were taken by individual fields for the water stress (Chapter 6) and plant cover (Chapter 7) studies.

From the 94 possible sites for each HCMM overpass date, we deleted any that were urban (nonagricultural), those that contained water, and all sites on a given overpass date that contained any cloud or subvisible cirrus-contaminated pixels in the 9x9 matrix for the site. Consequently, if the 9x9 matrix was deleted so was the 7x7, 5x5, 3x3, and 1x1 matrix for that site and date. Eight summer dates, 27 May through 15 Aug 78, were included. The restrictions put on the data resulted in 168 observations for each of the following variables: HCMM temperatures (T1...T9) and albedo (R1...R9), respectively, for ground areas consisting of 1x1, 3x3, 5x5, 7x7, and 9x9 pixels; saturation deficit of the air (SDEF,mb) measured at the central environmental station between 1300 and 1400 hr CST; distance of each site from the Gulf coast (DIST,km); insolation the day of the pass (IDOP,ly day^{-1}) and hour of the pass (IHROP,ly); water holding capacity (WCAP) of the rootzone of the dominant soil type; maximum air temperature (TMAX,°C) the day of the HCMM overpass; time since rainfall or irrigation (DSR,days); and square root of days since rainfall or irrigation $(DSR)^{\frac{1}{2}}$. Temperature was used as the dependent variable in step-wise multiple regression analyses. (A ridge regression analysis would have been better but that analysis capability was unavailable.)

2.3.1.1 Ground sample size

Figure 2.5 summarizes the percent of the sum of squares (R^2x100 where R is the multiple correlation coefficient and R^2 is the coefficient of determination) accounted for as the HCMM ground sample increased from the single central pixel (36 ha) to a sample of 81 pixels (9x9 pixel sample=2900 ha=29 km^2). The regression coefficients for the first five terms in the regression model were significantly different from zero (t-test) but coefficients for additional terms were not. To learn whether the R values were different as the sample size increased, we compared the R value for five variables in the regression, for the 81 pixel sample (0.936) with the R value for the central pixel sample (R=0.906). The test used was

$$t = \frac{z_1 - z_2}{\sqrt{\frac{1}{n_1 - 3} + \frac{1}{n_2 - 3}}}$$

where $z=\frac{1}{2}\ln(\frac{1+R}{1-R})$

and z_1 identifies R for the 9x9 pixel sample,

z_2 identifies R for the 1x1 pixel sample, and

n_1 and n_2 each equaled 164.

Calculated t was significant at the 10% probability level. Thus, the same relationships seem to be discerned regardless of the HCMM sample size that was used.

The values of IDOP, IHROP, SDEF, DIST, DSR, $(DSR)^{\frac{1}{2}}$, Tmax, and WCAP were common for all ground sample sizes. The means and standard deviations (S.D.) for these variables were:

	Variables			
	IDOP	IHROP	SDEF	DIST
	ly day^{-1}	ly	mb	km
Mean	408.6	74.3	28.8	101.5
S.D.	46.6	24.0	7.1	33.1
	DSR	$(DSR)^{\frac{1}{2}}$	TMAX	WCAP
	days	$(days)^{\frac{1}{2}}$	°C	cm
Mean	17.9	3.74	36.4	16.2
S.D.	17.5	1.96	2.1	1.4

The means and standard deviations of HCMM temperature and albedo for the various size samples were:

	Sample size				
Pixel configuration:	1x1	3x3	5x5	7x7	9x9
Number of pixels:	1	9	25	49	81
Mean (°C):	33.00	32.95	32.90	32.87	32.84
S.D. (°C):	4.60	4.48	4.41	4.38	4.37
Mean R (%):	17.29	17.30	17.33	17.31	17.28
S.D. R(%):	2.21	2.01	1.90	1.84	1.78

The means and standard deviations presented showed that mean temperature and its standard deviation decreased slightly but steadily as number of pixels in the ground sample increased from 1, to 9, to 25,... to 81. The albedos went through a maximum for a sample of 25 pixels, but the standard deviation decreased slightly but steadily as the sample size increased. The decrease in standard deviations as sample size increased seems to explain why the R^2 values in Figure 2.5 increase as sample size increases.

These results seem to indicate that a single HCMM pixel can represent ground conditions almost as well as a larger sample, and that the observed HCMM temperatures are influenced by variables such as insolation and air temperature to such an extent that these synoptic variables may be as strongly related to the observed temperatures as field to field variations in ground cover and water conditions. In Chapters 6 and 7 we used ground samples of 1 (central pixel) and 9 pixels because the ground truth and vegetation indexes represented individual fields or adjacent fields and we wanted the closest correspondence between sample sizes we could get in data from different observation sources. Inclusions of variables such as ground cover or vegetation greenness and evapotranspiration rates in the analyses consistently raised the proportion of the sums of squares accounted for in the regressions by about 15%.

2.3.1.2 Saturation deficit, distance from the coast, insolation, and soil type

The first five variables included in the multiple regressions were SDEF, DIST, IHROP, IDOP, and WCAP. Saturation deficit of the air and the two insolation variables are weather related, distance from the coast is geographic, and water holding capacity is a soil property. The four variables not included were Tmax, R, DSR, and $(DSR)^{\frac{1}{2}}$.

Table 2.2 presents the linear correlation coefficients between HCMM observed temperatures for each ground sample size and each of the variables. The simple correlation between Tmax and HCMM temperatures was highly significant ($r=0.686^{**}$ to 0.738^{**} for the various ground sample sizes). However, Tmax was highly significantly correlated with SDEF, DIST, and IHROP, and they rather than Tmax were included in the multiple regressions. Days since rainfall, DSR, and $(DSR)^{\frac{1}{2}}$, were most highly correlated with SDEF and Tmax. The albedos (R) from HCMM were highly significantly correlated with insolation and distance from the coast, as well as the HCMM temperatures.

2.3.1.3 Cloud contamination

To determine the effect of percent cloud contamination (PCN) on the observed HCMM temperatures, we added the observations that contained clouds and vapor contamination to the cloud-free data of sections 2.3.1.1 and 2.3.1.2 above for the 9x9 pixel samples. Numerical values of cloud contamination were obtained by counting the number of pixels that were determined to be cloud-affected using man-machine interactive procedures, dividing that number by 81, and multiplying by 100 to express the proportion as a percentage. Then we analyzed the data for each of the 8 summertime dates for which we had data.

The regression equations established for each of the dates, the number of observations, and the r^2 values are summarized in Table 2.3. The average regression coefficent for the 8 linear equations is -0.093 which indicates that each 10% increase in cloud contamination lowered the observed HCMM temperatures by 0.9 C.

The distribution of data points for two of the dates (17 Jun and 03 Jul) is illustrated in Figure 2.6. The temperature variability for the data points with low cloud cover was real and was associated with differences in surface cover, land use, distance from the coast, and days since rainfall included in the data set. Labeling of data points for the 27 May data by land use showed, e.g., that most high temperatures represented rangeland sites; these had low vegetative cover and were very dry.

Generally, the cloud contamination effect on HCMM temperatures indicated that the weaker effects we were interested in would be found only by using noncontaminated pixels. Consequently, in later chapters only pixels judged to be unaffected by cumulus or cirrus clouds are included in the analyses.

2.4 Literature cited

National Oceanic and Atmospheric Admin. (NOAA), Environ. Data and Infor. Ser. (EDIS). Climatological Data, Texas. Vols. 83 (1978) and 84 (1979), Numbers 1 through 12. National Climatic Center, Asheville, N.C.

Kauth, R. J. and G. S. Thomas. 1976. The tasseled cap--A graphic description of the spectral-temporal development of agricultural crops as seen by LANDSAT. Proc. Sympos. Machine Proc. of Remote Sensing Data. (LARS, Purdue Univ.) IEEE Cat. No. 76, Ch. 1103-1 MPRSD.

Tarpley, J. D. 1979. Estimating incident solar radiation at the surface from geostationary satellite data. Jour. Applied Meteor. 18:1172-1181.

Richardson, A. J. and C. L. Wiegand. 1977. Distinguishing vegetation from soil background information. Photogram. Engin. and Remote Sensing. 43:1541-1552.

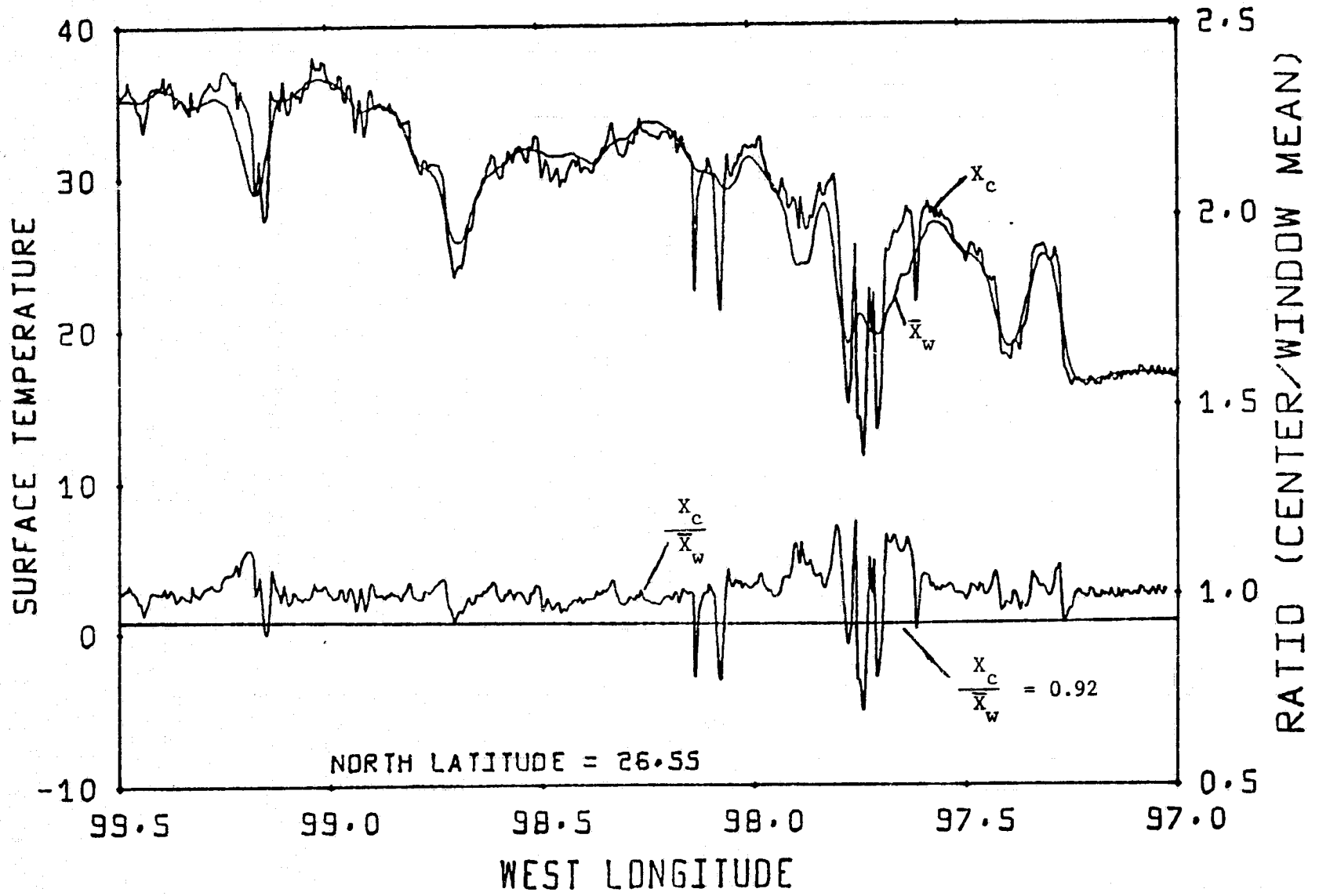

Figure 2.1 Upper curves show unfiltered (X_c) and filtered ($\bar{X}_w$) temperature profiles of an east-west transect across the LRGV test sites on latitude 26.55 N. during a relatively clear day, 15 August 1978. The lower curve ($X_c/\bar{X}_w$) shows the ratio of the temperature of the center pixel to the mean temperature of a 9 pixel by 9 pixel moving window. Areas falling below the 0.92 ratio line ($X_c/\bar{X}_w = 0.92$) are considered to be cloud contaminated.

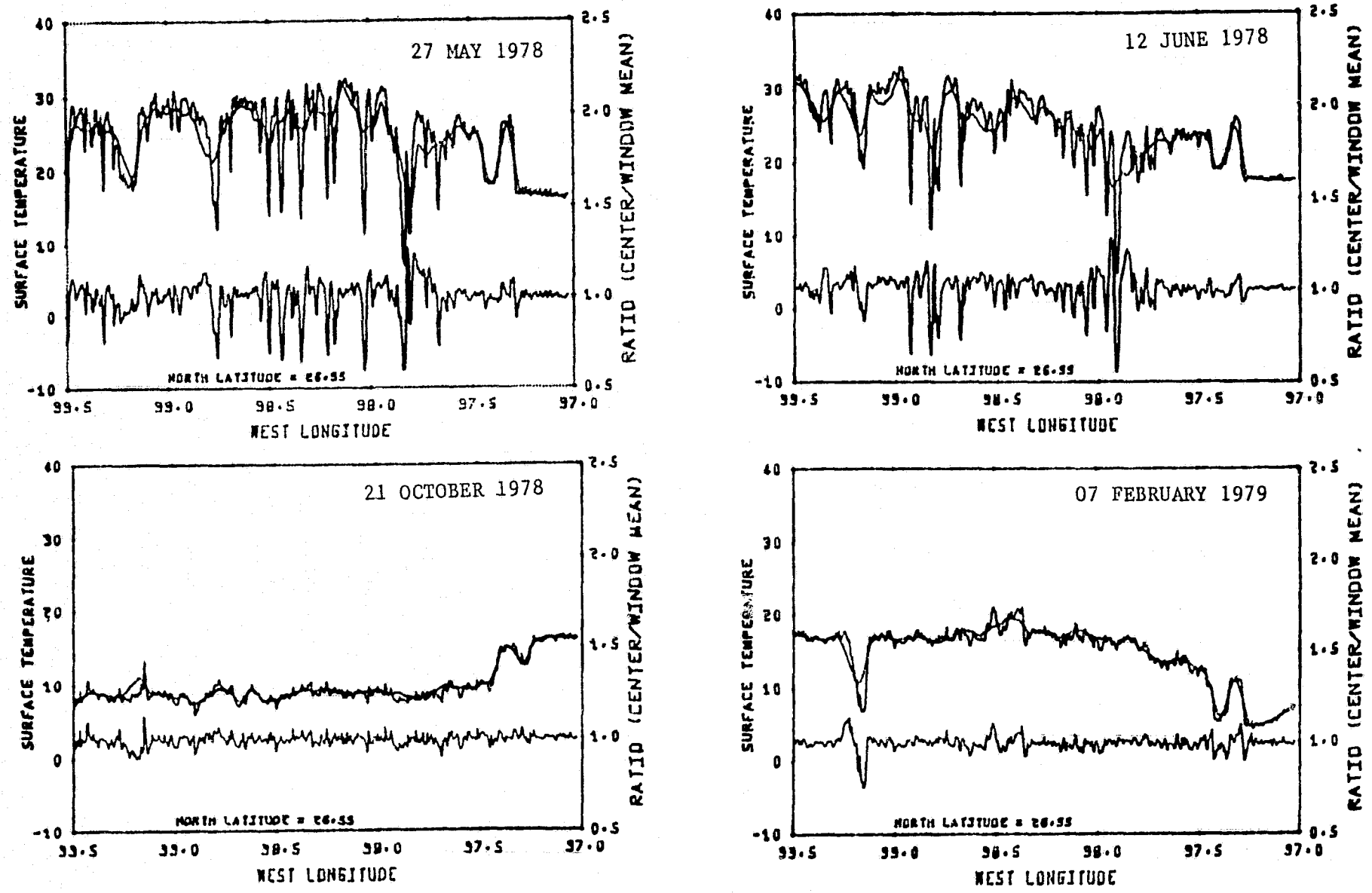

Figure 2.2 The upper curves of each graph show the unfiltered and filtered daytime temperature profiles of east-west transects across the test site on latitude 26.55°N. Two partly cloudy and two clear dates are illustrated. The lower curve of each graph shows the ratio of the temperature of the center pixel to the mean temperature of a 9 pixel by 9 pixel moving window.

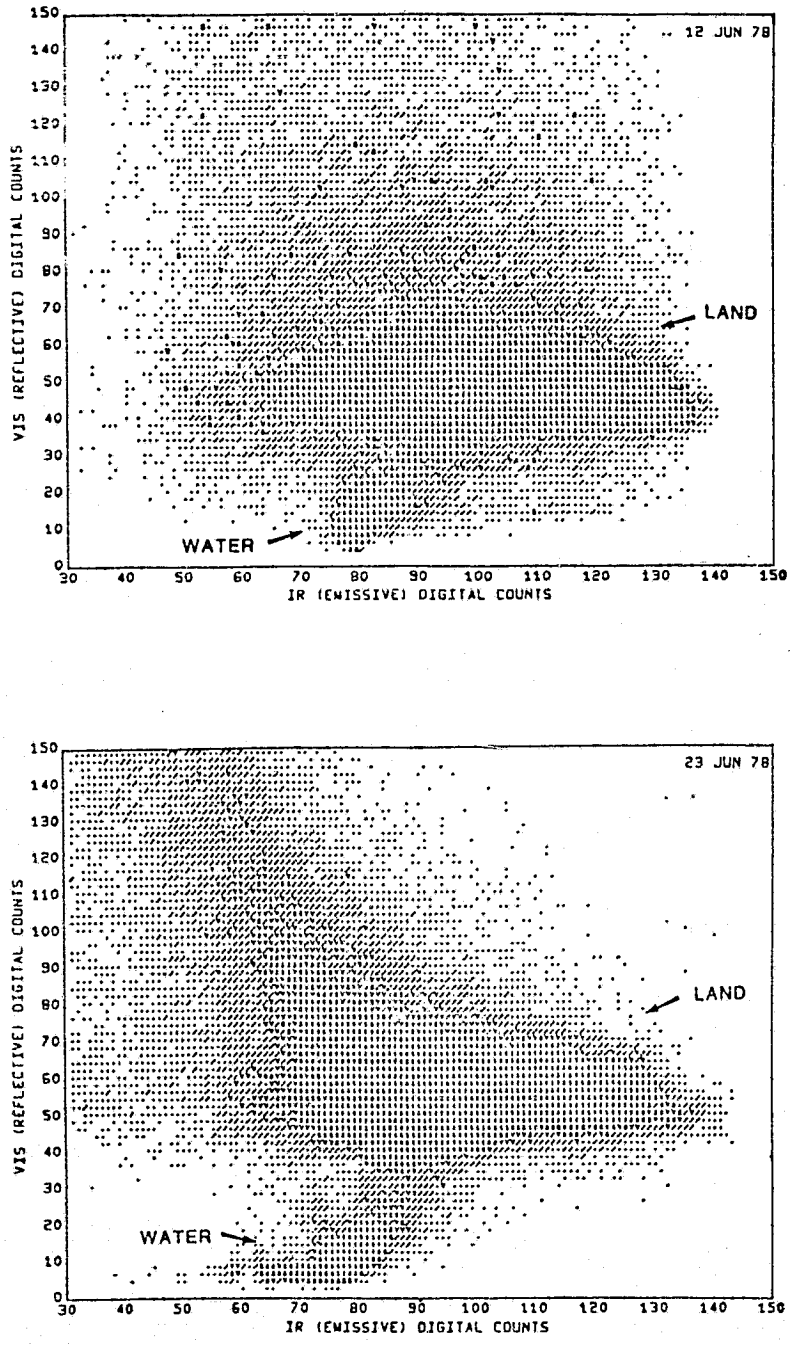

Figure 2.3 Scatter diagrams of reflective(VIS) vs emissive(IR) pixel values on 12 June 78 and 23 June 78. The wide scatter is attributable to the individualistic nature of clouds. Clustering over cloud-free land and water areas is shown by the $ symbols representing reflective/emissive combinations that recurred at least 17 times in the 100,000 pixel test area.

15 Aug 78 Day-VIS

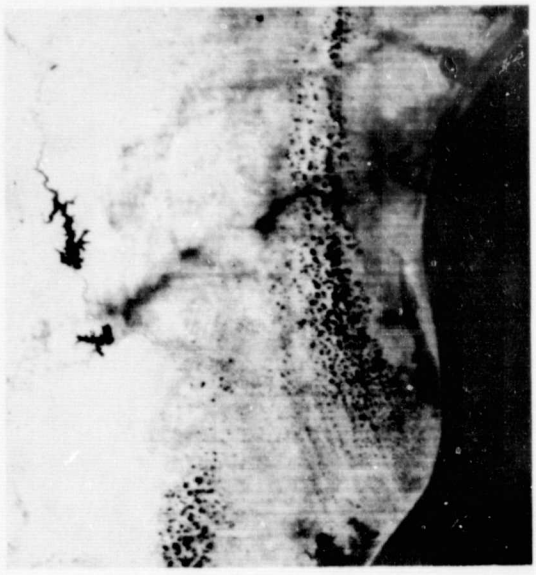

15 Aug 78 Day-IR

03 Jul 78 Day-VIS

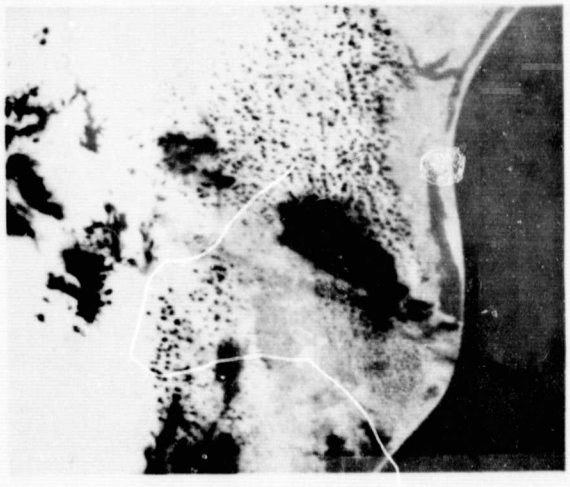

03 Jul 78 Day-IR

Figure 2.4 HCMM daytime scenes of the test site on 15 Aug 78 (upper) and 03 Jul 78 (lower). In the 15 Aug scene, scattered cumulus clouds paralleling the coast (right and lower center) are apparent in both VIS and IR images while an atmospheric absorbing-emitting layer (wispy dark areas left center to upper right) are apparent only in the IR band scene. In 03 Jul scene, the dark globs and striations in the IR scene are clouds that are more apparent than in the VIS scene.

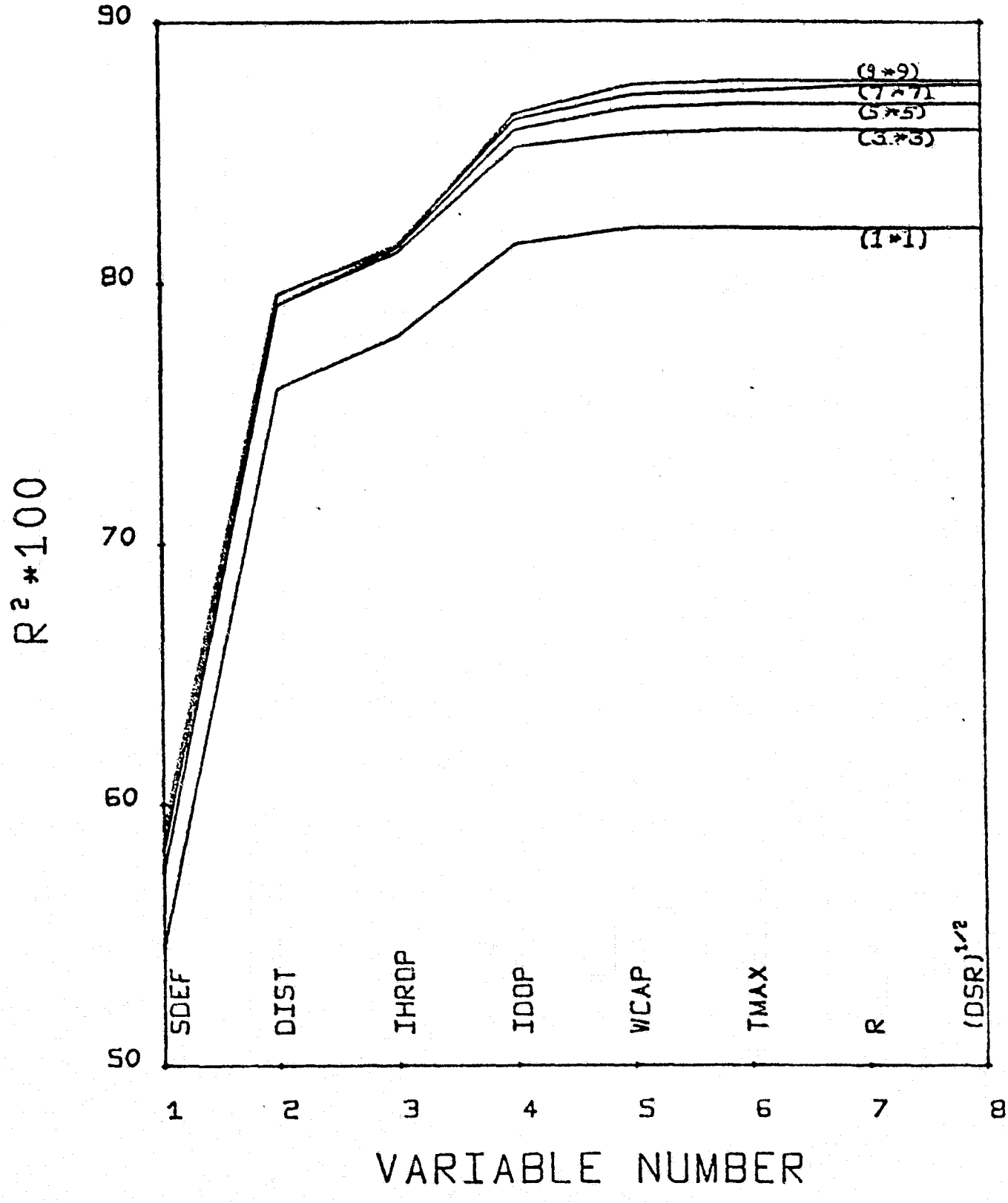

Figure 2.5 Percent of sum of squares (R^2x100) accounted for as variables were added to multiple regression analyses for ground samples of 1, 9, 25, 49 and 81 HCMM pixels.

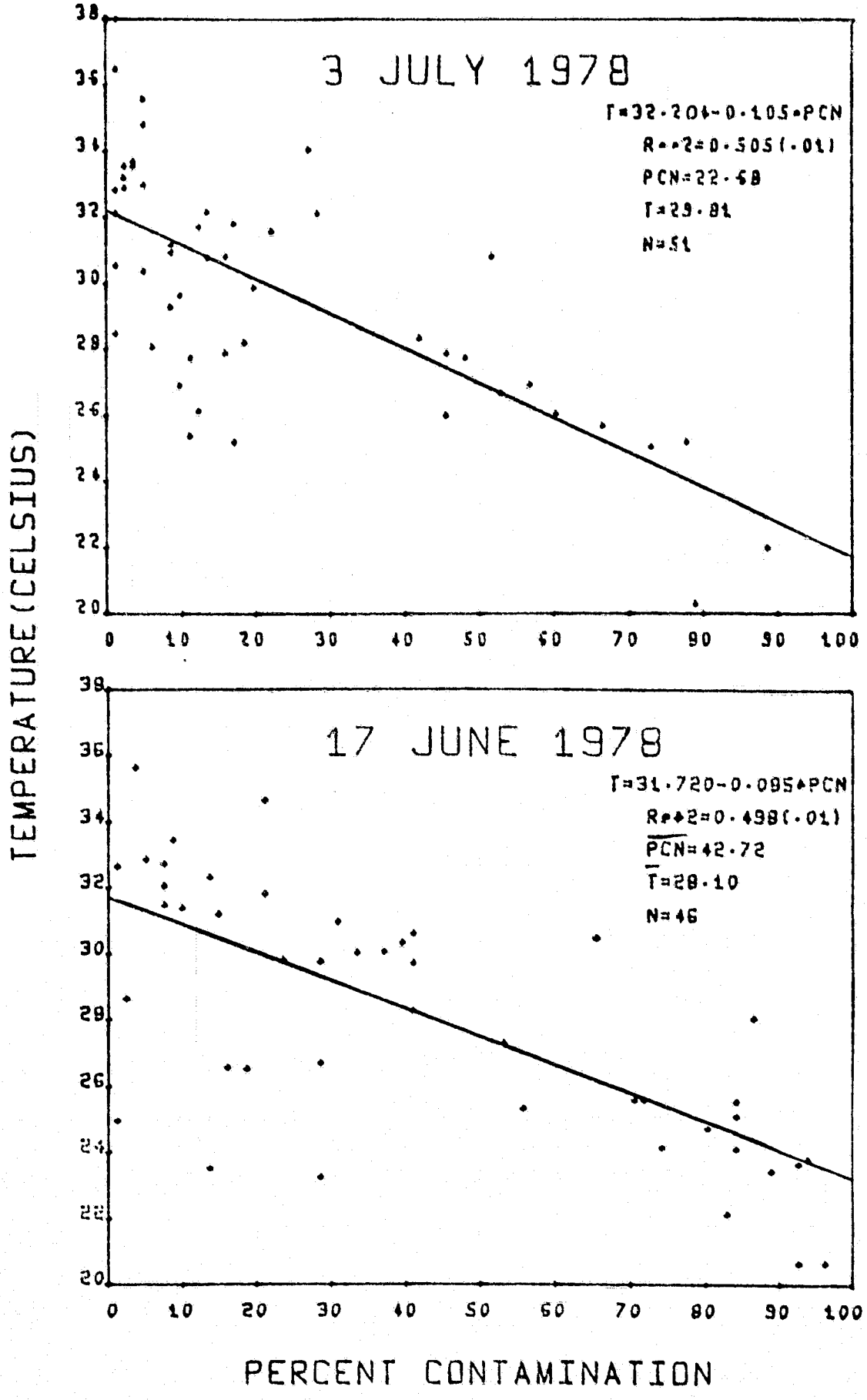

Figure 2.6 Temperature dependence on percent cloud contamination (PCN) for two dates.

Table 2.1 Equations applied to reflective (VIS) and emissive (IR) digital counts to specify which data should be discarded as cloud contaminated.

Overpass Date	Equations
27 May 78	If IR$\leq$68, or VIS$\geq$13.9 + 0.518 IR
06 Jun 78	If IR$\leq$75, or VIS$\geq$14.4 to 0.552 IR
12 Jun 78	If IR$\leq$63, or VIS$\geq$37.9 + 0.304 IR
17 Jun 78	If IR$\leq$70, or VIS$\geq$-5.0 + 0.768 IR
23 Jun 78	If IR$\leq$77, or VIS$\geq$44.2 + 0.360 IR
03 Jul 78	If IR$\leq$66, or IR$\leq$97 and VIS$\geq$31.56 + 0.248 IR, or IR$\geq$97 and VIS$\geq$-20.28 + 0.776 IR
08 Jul 78	If IR$\leq$41, or VIS$\geq$16.52 + 0.416 IR
15 Aug 78	If IR$\leq$69, or VIS$\geq$-177.80 + 2.645 IR
08 Nov 78	If VIS$\geq$-52.174 + 1.304 IR
07 Feb 78	If IR$\leq$50 and VIS$\geq$-84.94 + 2.359 IR, or IR$\geq$50 and VIS$\geq$23.76 + 0.208 IR

Table 2.2 Linear correlation coefficients between temperature and climatic, soil, geographic and time variables for HCMM sample sizes of 1, 9, 25, 49 and 81 pixels(T1, T3, T5, T7, T9).

Variable	T1	T3	T5	T7	T9
	r				
SDEF	.738**	.758**	.763**	.765**	.768**
DIST	.721**	.729**	.725**	.725**	.721**
IHROP	.600**	.613**	.616**	.614**	.610**
IDOP	.128	.126	.115	.109	.101
WCAP	-.170*	-.171*	-.180*	-.194*	-.205**
TMAX	.686**	.712**	.721**	.732**	.738**
R[a]	.180*	.276**	.296**	.276**	.245**
DSR	.472**	.481**	.485**	.492**	.500**
$(DSR)^{\frac{1}{2}}$	.453**	.486**	.490**	.498**	.507**

[a] was determined from same number of pixels as T, so that R's are R1 . . . R9 across the table.

n=168 r(.05)=0.152 r(.01)=0.199

* denotes significance at the 0.05 level
** denotes significance at the 0.01 level

Table 2.3 Equations expressing temperature (T9) dependence observed by HCMM on percent cloud-contaminated pixels (PCN) for eight dates.

Date	Equation	No. of Observations	r^2
27 May	T9=31.45-0.073(PCN)	60	.214
06 June	T9=28.40-0.064(PCN)	54	.496**
12 June	T9=30.21-0.105(PCN)	64	.536**
	T9=31.39-0.226(PCN)+0.002$(PCN)^2$	64	.622**
17 June	T9=31.72-0.085(PCN)	46	.498**
23 June	T9=30.86-0.082(PCN)	73	.371**
03 July	T9=32.20-0.105(PCN)	51	.505**
08 July	T9=28.05-0.139(PCN)	24	.229
15 August	T9=33.50-0.101(PCN)	30	.406*

3.0 SYNOPTIC ANALYSES

3.1 Abstract

A test area 240-km across and 130-km N to S at the southern tip of Texas was used for various synoptic thermal investigations. Isotherm lines at 2 C intervals adequately displayed the thermal patterns within the test area. The temperature range -11 to +40 C generally encompassed the temperature range encountered for land features, water bodies and clouds.

Digitization of the soil association map for a four county area each 20-seconds of latitude and longitude corresponding to the pixel resolution of HCMM enabled stratification of HCMM albedo and temperature data by soil associations. Soil association temperatures from 10 daytime overpasses were typically highly correlated. Summer nighttime temperatures tended to be uniform across the test area and close to the dewpoint temperature which is reached each night. On winter nights with strong radiational cooling and dew points lower than the air reaches, there was a temperature gradient across the area that was dominated by distance from the coast. Soil type and land use had much weaker influences. Warm areas adjacent to inland water bodies were observed in both summer and winter nighttime thermal data.

The gradient of rainfall across the test area, that averages 1 cm/4.5 km annually, prompted us to calculate an "aridity index" defined as the difference between daytime HCMM temperature and maximum air temperature for the day at the site of the weather stations. The aridity index for 10 dates increased with distance from the coast. The difference between the HCMM-indicated nighttime surface temperature and the minimum air temperature showed that HCMM-indicated temperatures were within 2 C of dewpoint temperatures on nights when the air reaches the dewpoint temperature.

The day temperature transect across the test area for 07 Feb 79 and the night temperature transect for 26 Feb 79 were nearly mirror images of each other, and showed that ground sites that warmed most in the daytime also cooled the most at night. No rain fell between observation dates, vegetation growth was controlled by low temperatures, and the atmosphere was dry on observation dates. The data indicated that when test area and atmospheric attenuation conditions were similar, day minus night temperature data separated in time by 2 weeks or more was meaningful.

Overall, these studies demonstrated that data with approximately 1-km ground resolution such as that from the NOAA-6...9 series of satellites contain useful information about synoptic thermal conditions. They can be used directly to measure thermal responses such as freezes, but they must be interpreted along with other relevant data for inferences about near surface soil water conditions, evapotranspiration, and crop condition.

3.2 Introduction and objectives

The energy balance at the earth's surface is:

$$Rn = H + LE + G$$

where Rn = net radiation flux received by the surface
H = sensible heat flux to the air
LE = latent heat flux (evapotranspiration)
G = sensible heat flux to the soil

Since the equation expresses the principle of conservation of energy, it is clear that sensible heat (H) becomes an increasingly important product of the transformation of radiant energy at the earth's surface (Rn) when soil water depletion limits latent heat production (LE). In the south Texas study area daytime air temperatures increase inland in relation to increasing aridity (annual rainfall decreases going inland at about 1 cm/4.5 km over a large portion of the study area). The prevailing wind is from the Gulf of Mexico toward the mainland and evidently helps moderate the inland surface and air temperatures. One objective of the synoptic analyses was to document the daytime increase of radiometric surface temperature with distance inland.

Increased surface temperatures is the mechanism by which reportioning of transformed energy takes place. Under the influence of midday insolation the surface is the warmest feature and heat moves from the soil surface into the soil by conduction and into the air by convection and radiative transfer. Stressed vegetation, which is above air temperature, also contributes to heating of the air. Because of vertical mixing with cooler air above, the air temperature lags surface temperature temporally and in amount. At midday the surface of dry soil is typically 20 C above air temperature. Thus the drier the landscape condition, the greater is the expected difference between surface temperature and bulk air temperature.

The question to be investigated was: Can the degree of aridity be represented on a synoptic scale by comparing Weather Service air temperature measurements (daily maximum) with HCMM indicated daytime surface temperatures in the vicinity of the weather stations? This was investigated in the climatic gradient that exists between the Gulf of Mexico and weather station locations up to 170-km inland. We coined the term "aridity index" for THCMM-Tmax.

Another objective was to relate nighttime HCMM temperatures to ambient air dew point temperatures at the Weslaco Environmental Station and to minimum air temperatures at 14 weather stations located from the Gulf of Mexico to 170-km inland. Hygrothermographs usually maintained at weather stations are not very accurate so there would be measurement error in humidity and temperature values taken from their charts.

Dew is important in agriculture because it provides a wet surface on which pathogens can develop and because it delays the onset of transpiration after sunrise. Our study area conditions are often favorable for nighttime dew formation (high humidity, light wind, clear sky) except during the winter months when the air is sometimes very dry. On nights of dew formation the landscape surface will usually be a few degrees colder than air temperature at shelter height. This temperature inversion results from reduced air temperature near the surface associated with radiation heat loss and the lower dew point temperature near the surface caused by removal of moisture from the air by condensation.

The minimum air temperature (usually at dawn) may be closely correlated with surface temperature at HCMM overpass time. This was investigated for a summer night with data collected at the Weslaco environmental station. The high moisture content of Gulf of Mexico air (vapor pressure of approximately 28-mb during half the year) limits the air temperature decline during dew formation in the late nocturnal hours (relatively great amount of dew formation, with attendant heat release as the ambient air temperature approaches the dewpoint temperature).

There were other minor objectives including the determination of thermal islands in the vicinity of inland water bodies and cities, and comparisons of day and night temperature transects across the test area.

3.3 Methods

Procedures described in steps a through s of section 2.1.1 were applied in meeting the objectives of this chapter. The HCMM indicated surface temperatures were corrected by a radiative transfer model (J. C. Price, personal communication, 1980; Barnes and Price, 1980). Radiosonde data from Brownsville, Texas (0600 CST or 1800 CST as appropriate) were used in determining the corrections which were applied uniformly to the entire test area. It is recognized that ideally the corrections would be determined at overpass time at several locations and interpolated over the area.

Surface temperature gradients from the coast to 240-km inland were determined for the ten daytime HCMM scenes. The profiles were prepared from parallel east-west transects 20-km apart.

To study the aridity index the maximum air temperatures measured at 14 weather stations on the dates of HCMM overpasses were paired with radiometric surface temperatures derived from the HCMM emissive band for various HCMM ground sample sizes, ranging from 0.3 to 29-km^2, centered on weather station coordinates.

For nighttime HCMM scenes the HCMM radiometric temperatures were compared with ambient air dewpoint temperature recorded at weather stations and on one night with the minimum air temperature recorded at the central environmental station.

3.4 Results and discussion

3.4.1 Thermal contouring

One of our objectives was to determine if there are locations in the LRGV that have consistently different temperatures from surrounding areas. One possibility of detecting areas that are consistently different from surrounding areas is to produce and examine temperature contour maps.

Each of 10 scenes of the LRGV was stored on a computer disc registered as described in 1.2.7. A computer program was modified to permit drawing of contour lines over any portion of the slightly more than 100,000 pixels in each scene. Due to memory limitations of our computer, individual pixel data were contoured by breaking the scene into sections 32 pixels by 64 pixels, contouring that section, then matching adjacent sections until the LRGV was covered. Lesser detail was obtained by averaging groups of pixels in the array.

We found that isotherm lines drawn at 2 C intervals gave adequate detail to show the temperature patterns in the Valley. We used three colors of ink in the plotter pen to distinguish one isotherm from another. Temperatures from -11 to 40 C were contoured where present. Isotherms representing temperature multiples of 5 C were cross-hatched to assist in reading the maps. Most scenes had more than a six degree range of temperatures so isotherms drawn by any color could represent temperatures six degrees apart. Cross-hatching of the isotherm multiples of five, and the sequence of colors made it possible to identify the temperature represented by each isotherm.

Temperature isotherms, especially at the single pixel scale, showed the location of clouds. Cloud tops were cooler than surface temperatures. Large cloudy areas were also evident in maps of blocks of pixels, but the temperature gradients were not as steep as for the individual pixel contours; the steepness of the gradient depended upon the size and arrangement of the clouds within the block of pixels.

The VIS channel data were also contoured. Rather than converting the VIS digital counts to the engineering unit, albedo, the contour lines were drawn with a digital count interval of eight between adjacent contours, or 24 counts between contours of the same color. Again the contours that were multiples of five were cross-hatched to simplify reading the resulting maps. Because of the difficulty and expense of reproducing colored maps, they are not included in this report.

3.4.2 Soil association temperatures

A soil association map, based on Soil Conservation Service soil surveys (section 1.2.7) was digitized and stored on computer disc file so that each area corresponding to a satellite pixel was given a symbol representing the predominant soil in the pixel. This soil map was registered with the HCMM data so there was a soil association symbol for each pixel location of the reflective and emissive data. Table 3.1 summarizes the information for the soil association map of the LRGV area.

Because the two sets of data (satellite and soil association) were registered on a pixel by pixel basis, it was possible to determine the albedo and the surface temperature of each soil association pixel. The number of pixels of each temperature from each soil association was counted and a histogram developed. The temperature histograms of the clear scenes showed a sharp peak for each soil association. The temperature at the peak of the temperature histogram was used to represent the temperature of the soil association. For clear scenes this value contained the median temperature for each soil association. The term median temperature was used to refer to the temperature at the peak of the temperature histogram for each soil association; only in a few cloudy scenes was the true median temperature not in the histogram cell at the peak of the histogram.

Clouds over a scene gave combinations in a scatter diagram of reflective and emissive data such that few pixels fell in the same scatter diagram cell. Data from ground surface, on the other hand, yielded a high frequency of occurence of reflective and emissive data pairs in a tight cluster (section 2.2.1.7).

Figure 3.1 and 3.2 are scatter diagrams of reflective and emissive data for a clear and a cloudy scene, respectively. This characteristic of clouds and ground surface to group, or to be scattered, was used to separate cloud-covered pixels from pixels with a clear view of the ground surface. Any pixel falling in a scatter diagram cell containing 17 or more pixels was considered to be cloud-free; fewer than 17 data pairs in a cell indicated cloud-contaminated pixels. Table 3.2 lists the number of cloud-free pixels in each of 36 soil associations for the ten dates. According to this criterion 27 May, 8 Jul, and 15 Aug 78 were cloud-free.

Because clouds are not uniform in either surface temperature or brightness, temperature histograms for cloudy soil association pixels peaked at essentially the same temperature as did the cloud-free pixels. Table 3.3 shows the minor differences from calculating soil association temperatures using only cloud-free pixels and using all pixels. The three dates included in Table 3.3 were the three with the fewest cloud-free pixels in Table 3.2. The small differences in these three dates indicated that other dates with fewer cloudy pixels would have less temperature differences from using all pixels or excluding the cloudy pixels.

The clustering method of distinguishing between cloudy and cloud-free pixels requires that data from both reflective and emissive channels be available. This limits the procedure to daytime passes of the satellite. The median temperature for each soil association can be determined from the emissive data from either a daytime or a nighttime pass. Because the histogram peak temperature was found to be very similar using both all pixels or only cloud-free pixels, the temperature histogram procedure can be used when only emissive data are available.

Temperatures determined by the histogram peak method for the 36 soil associations on the 10 daytime dates are given in Table 3.4. Linear correlation coefficients for all combinations of soil association temperatures for the 10 dates (n=10) showed that most temperatures were significantly correlated statistically. The fact that surface vegetation affected emissive measurements may have masked possible differences in soil associations.

Soil temperatures at the nightime HCMM overpass tended to be uniform across the test area in summer (Table 3.5). This is illustrated by Figures 3.3 and 3.4 which show the mean temperature of all pixels within each of the soil associations. The standard deviations related to them are indicated by dots in the Figures. The symbols representing the soil associations in the figures are identified in Table 3.5. The W's represent water temperatures of the Gulf of Mexico, Laguna Madre, and Delta Lake.

In the LRGV dew frequently forms on vegetation at night, and instrument shelter air temperatures approach the dew point within a degree or two. The liberation of heat in dew formation tends to retard further temperature decline and results in relatively uniform air and surface temperatures through the area. This is indicated for most dates listed in Table 3.5 and is illustrated for the night 30 Jun 78 by Figure 3.3.

The mean temperatures and standard deviations of HCMM pixels falling in the grouped associations on the 30 Jun 78 night are illustrated by Figure 3.4. The grouped loamy upland soil associations (identified as 3, consisting of C, D, E, F, G, H, I, J, and K of Figure 3.3), and saline clays and loams (identified as 5, consisting of U, X, and Y) were about half a degree warmer than the other soils.

Variable amounts of soil visible to the satellite, climate characteristics typical of the various soil associations, and their different thermal inertias were among conditions causing these results. However, the overriding factor appears to have been nighttime dew formation over the entire test area.

Figure 3.5 shows the soil association temperature means and standard deviations for cool season conditions of 21 Oct 78. There was a pronounced decline of temperature with distance inland from the Gulf of Mexico. There was no dew on this night, however, because the dew point was much below ambient temperature.

3.4.3 Daytime temperature increase from the coast

3.4.3.1 Transects

Surface temperature transects were made across the test area (Figure 1.3) using HCMM data for all 10 daytime dates studied. An example of summer daytime conditions is shown in Figure 3.6, representing 15 Aug 78. The east ends of the transects originated in the Gulf of Mexico (right side of figure) and traversed inland to west longitude 99.5° (left side of figure). These parallel east-west transects were separated from each other in north-south direction by 0.2° latitude. Each transect is identified (right margin) by the north latitude which it represents.

Figure 3.6 shows that the surface temperature of the Gulf of Mexico was uniform with little change from pixel to pixel, or for the entire length of the transect across the water on 15 Aug 78. (The temperature transect representations of the five latitudes have been offset from one another in the figure by 10 C temperature increments to facilitate examination of the individual traces. The temperature scale on the left side of the graph applies to the temperature trace made at 26.01° north latitude.).

A trend of increasing temperatures with distance inland, from right to left, was apparent in all daytime traces that we prepared except for 27 May 78 and 06 Jun 78, when there was little overall change across the test area.

In Figure 3.6, the relatively cool temperatures at 99.00° W near the western (left) end of the 26.21° N transect were caused by the water in the Marte Gomez reservoir in Mexico (Figure 1.3). This water was at about the same temperature as the Gulf of Mexico.

Cloudy conditions bounded by 97.7° N to 98.0° N resulted in the irregular traces on transects 26.41, 26.61 and 26.81° N. Areas of data removed from analyses by automatic cloud screening were "bridged across" by the computer in making these traces. The temperature dip at 97.95° W on transect 26.41° N was real and represented the water temperature of Delta Lake (Figure 1.3). Similarly, the cooler temperatures on transects 26.61 and 26.81° N between 99.2 and 99.4° W were caused by Falcon Reservoir (Figure 1.3).

The surface temperature transects of a clear winter day are illustrated in Figure 3.7. These temperatures are 15 to 20 C cooler than the summertime temperatures discussed above. On this date, 07 Feb 79, the Gulf of Mexico's temperature illustrated by the rightmost portion of each trace was colder near shore (Padre Island) than farther out. This contrasts with summertime traces which showed rather uniform Gulf temperatures.

The two southernmost transects (26.01 and 26.21° N) showed increasing surface temperature with distance inland (right to left). The transects through the middle and northern part of the test area showed a positive temperature gradient immediately inland from the coast, but generally constant or even declining temperatures in the western half or two-thirds of the land area represented.

As in the summertime, water bodies were cooler than daytime temperatures of land areas. The water bodies (Gulf of Mexico, Delta Lake, Marte Gomez, and Falcon Reservoir) (Figure 1.3) are apparent in the temperature traces.

3.4.3.2 Ground sites

The data set used is the same one as analyzed in section 2.3.1.2. For this purpose, however, the linear regression equation for each of 8 dates that related the temperature observed by HCMM for 9x9 pixel sites on the ground (T9, °C) to distance from the coast (DIST, km) was determined. The results given in Table 3.6 showed that r^2 was significant for 5 of the 8 dates. In general, the proportion of the variation in temperature accounted for by site distance from the coastline was poor for the early sampling dates, went through a maximum for 23 June, and then declined--although remaining highly significant--through 15 Aug.

The 27 May data were taken near the end of a long rainless period, whereas the 06 Jun data were taken following rains on Jun 03-05 that should have left the soil surface wet at all sites. Another long, essentially rainless period lasted through the 15 Aug observation date. If the same sites had been used on all dates, a continuously increasing temperature with time after 06 Jun would be expected. However, only sites left after cloud-contaminated data were deleted were used so that number of observations and their distance from the coast was unique for each set.

The intercepts of the regression equations of Table 3.6 are the estimated temperatures at the coastline and the coefficients in front of DIST give the rate, °C km^{-1}, at which temperature increased with distance from the coast. The average coefficient for the 8 dates was 0.05 so that there was an average 5 C temperature difference between the coast and the mean distance inland of the sites (100 km). The coefficients increased steadily from 06 Jun to 03 Jul as soil water was depleted and seasonal evaporative demand increased.

Based on the expected steady increase in temperature expected after 06 Jun, the 17 Jun and 03 Jul intercepts or coastline temperatures are notably low (Inland sites have reasonabe temperatures for 03 Jul because of the large regression coefficient, 0.09 C km^{-1}.). The coastline temperature on these two dates was too low to be accounted for by inclusion of a disproportionate number of irrigated sites in the sample (the temperature difference between means of irrigated and dryland sites was not that large; see Table 7.3). Precipitable water in the atmosphere that attenuated the emissions, lower temperatures due to shadowing of the sites by cumulus clouds just preceding the HCMM overpass, and undetected cirrus clouds are also possible explanations for the low coastline temperatures.

The lower part of Table 3.6 provides information on the mean temperature and distance from the coast for each date and their standard deviations. The mean distance from the coast for sites sampled on 17 Jun was only 56.8 km as compared with an average of 107 km for the other seven dates. The temperature standard deviation generally increased as the distance from the coast increased, probably because the sites farthest from the coast were dry rangeland sites with highest temperatures.

Figures 3.8 and 3.9 show mean and standard deviations of surface temperatures at "representative sites" that consisted of 3x3 pixels. The letters designate the type of land use at the sites as follows (cropland may be fallow except in summer):

A	Sand
C	Cotton
G	Grass
K	Sugarcane
M	Mixed crops
R	Rangeland
S	Grain sorghum
T	Citrus
U	Urban and industrial
W	Water
Z	Wildlife refuge

The positive and negative standard deviations are noted by dots above and below the letters representing the sites. All of the 94 HCMM study sites that were not cloud covered are shown in the Figures.

Figure 3.8 shows the situation on 17 Jun 78, a day characterized by a moderate inland climatic gradient and more than the usual spread of values. Figure 3.9 represents 08 Jul 78 when a strong climatic effect resulted in a more marked temperature gradient from the ocean.

It had been 9 days since rainfall in the test area on 17 June and 10 days on 08 Jul. Factors which may have contributed to the varying results were the presence of 26% cloud cover over the test area at HCMM overpass on 17 Jun compared with 3% on 08 Jul, and daily atmospheric transmissivities (fraction of solar radiation which survives passage through the atmosphere to the earth's surface) measured at the Weslaco Experimental Station of 0.53 and 0.68 on the respective dates. Also, the mean saturation deficits were 12.0 and 15.8 mb, and the calculated potential evapotranspiration (Kincaid and Heermann, 1974) were 7.0 and 9.1 mm/day on the respective days.

Striking temperature differences betweer land uses are absent although some land uses did maintain their relative relationships with one another. For example, sugarcane (K) tended to be below average temperature, and rangeland (R) was generally warmer than cropland.

Examples of winter temperatures at the representative sites are given in section 3.4.7.

3.4.4. Nighttime thermal islands in the vicinity of water bodies

Nighttime surface temperatures in the vicinity of Delta Lake, La Sal Vieja and Sal del Rey are shown in Figure 3.10 for 26 Feb 79. The first two lakes are located and identified by name in Figure 1.3. Sal del Rey is the small lake in the upper left of Figure 3.10. The area represented in this surface temperature map measures about 40 by 40 km. The scale distortion is caused by the line and character spacing of the line printer that made the illustration.

The nighttime surface temperatures shown in the figure were made to fall into three classes: warm, medium, and cold. Each class contains approximately one-third of the total pixels as determined from a frequency distribution of temperatures. In this case, the warm designation (darkest symbol) represents 3.44 C or warmer, cold (lightest symbol) is 2.23 C or colder, and medium is the range in between. Although the water bodies were the warmest features of the scene their areas have been left blank to facilitate identifying their locations.

The heat island effect surrounding the lakes on this winter night was apparent in Figure 3.10. This was the coldest clear night (free of sub-visible cirrus clouds) for which we have HCMM data. The warm areas some distance to the southeast of the lakes (lower right) are probably unrelated to the water bodies. They may have resulted from a high proportion of fallow land and possibly high water tables. Bare soil, especially if moist, has warmer nighttime temperatures than low growing vegetation (Geiger, 1965; Monteith and Szeicz, 1962; and Nixon and Hales, 1975). The nighttime temperature decline was not impeded by dew formation on this night; when HCMM overpassed, the average dew point depression at 1.5 m above the ground was 6.7 C at the Weslaco Environmental Station (Station 9, Figure 1.3).

The uniformly cold northern (upper) portion of the illustration is rangeland, outside of the irrigated area. A dry vegetated area would be expected to be the coldest part of the landscape in contrast with fallow soil (especially if moist) or irrigated crops. The area is level to gently rolling so topographic relief was not a major factor in establishing nocturnal temperature patterns resulting from air drainage.

The heat island effect was also apparent in Figure 3.11 where HCMM surface temperature patterns of two cold nights (21 Oct 78 and 26 Feb 79) are combined. The area represented by Figure 3.10 is located in the upper middle portion of the figure. The outlines of the three lakes help identify the area.

The heat island effect was also apparent during a summer night, 30 Jun 78, illustated for the three lake area by Figure 3.12. The darkest symbol represents temperatures of 20.54 C and warmer, the lightest symbol 19.50 C and colder, and the medium toned symbol the range in between. There was a relatively uniform distribution of temperature across the scene, except in the vicinity of the lakes. Dew had probably formed in

most of the area by the time of the HCMM overpass, and it probably caused the uniform temperatures. The dew point depression measured at the Weslaco Environmental Station (Section 9, Figure 1.3) during the hour in which HCMM overpassed was 0.9 C at 1.5 m above the ground. This is indicative of dew conditions (Jensen, 1974).

3.4.5 Synoptic aridity index

Even at midday, canopy temperature of a fully transpiring crop is close to air temperature, unless a strongly advective situation prevails. However, as soil water becomes limiting and evapotranspiration is impeded, the balance of energy transformation is changed. Sensible heat becomes important and is associated with surface temperatures that are significantly above air temperature. This is especially true at the soil surface (at midday dry soil is typically 20 C above air temperature). Thus, the drier the condition, the greater is the difference between bulk air temperature and surface temperature. The question investigated was: Can the degree of aridity be represented on a synoptic scale by comparing Weather Service air temperature measurements (daily maximum) with HCMM indicated daytime surface temperatures in the vicinity of the weather stations?

Figures 3.13, 3.14, and 3.15 are given to examine this question. They show the difference between the daytime surface temperatures (°C) of 9x9 pixel footprints surrounding the weather stations and the maximum air temperatures (°C) recorded on the day of the HCMM overpass. We call this an aridity index (THCMM-Tmax).

The symbols showing the aridity index in the figures are identified in Table 3.7 as to their weather station locations. The table also gives identifying numbers that show geographic locations in Figure 1.3.

The HCMM data used in this section have been corrected by a radiative transfer model (J. C. Price, personal communication) using 1800 CST radiosonde data from Brownsville, Texas, applied to the entire test area. The temperature correction for each date is noted in Table 3.8.

Figure 3.13 gives the aridity index on 27 May 78 following a 34-day dry period. It shows that the aridity index increased with distance inland from the coast, as land use changed from irrigated agriculture to rangeland, and went from an area of coastal showers to a more arid interior. Annual rainfall decreases at about 10 mm/4.5km from the coast over a large portion of our test area. The predominant land uses within the HCMM 9x9 pixel footprints surrounding the weather stations are given in Table 3.7.

The meteorological conditions for the dates represented by Figures 3.13, 3.14, and 3.15 were:

Date	Percent clouds at overpass	Solar radiation, ly/day	Daily atmos. trans-mission	Mean saturation deficit, mb	Potential evapotranspira-tion, mm/day
27 May 78	12	661	0.70	11.0	8.6
06 Jun 78	20	628	0.66	8.4	7.7
23 Jun 78	25	616	0.64	12.4	8.4

The percent cloud cover at HCMM daytime overpass was determined by analysis of the VIS (reflective) coverage of the test area in conjunction with the IR (emissive) data. The percentages do not include areas, if any, that were covered by subvisible cirrus clouds (SCi). The daily solar radiation and the other entries were measured at the Weslaco Environmental Station (station 9, Figure 1.3). The daily atmospheric transmission is the ratio of measured daily solar radiation (horizontal surface) to the theoretical extraterrestrial radiation on the day under consideration. The mean saturation deficit is the integrated daily difference between the actual vapor pressure and the saturation vapor pressure at the existing temperature. Daily potential evapotranspiration was calculated from meteorological records using the Penman (1963) method as applied by Kincaid and Heermann (1974).

The condition on 06 Jun 78 is shown in Figure 3.14. Rain had occurred at all locations during one to four of the preceding five days, averaging 33 mm, but ranging from a minimum of 4 mm at Port Isabel (H in Figure 3.14 and station 16 in Figure 1.3) to 73 mm at Raymondville (G and 11 in the figures) and Zapata (A and 1) (Point "A" for Zapata is missing from these figures because the northwest corner of the test area was truncated in processing the scene.). Potential evapotranspiration on these three dates was above normal (Nixon and Smithey, 1979) for their respective times of the year. Recent rainfall was apparently the cause of the small aridity index on 06 Jun 78.

Aridity indexes for 23 Jun 78 (Figures 3.15) resulted from 14 essentially rainless days (A few light showers occurred at stations nearest the coast between 17 and 21 Jun, with the maximum cumulative amount of 12 mm recorded at Raymondville (G and 11). The high aridity indexes in the inland portions of the test area can be attributed to soil moisture deficits that accumulated as a result of successive days of high evaporative demand without moisture replenishment. The steepness of the best fit line of Figure 3.15, compared with Figure 3.13, showed that more arid conditions prevailed inland on the June date than 27 days earlier in May. The best fit lines (dashed) were determined using only land-bound weather stations. Stations A, H, L, and N were excluded from regression calculation on this and other dates because of nearby water (Laguna Madre and Falcon Lake; see description of station surroundings in Table 3.7). The water surfaces in the 9x9 pixel footprints surrounding the stations could distort the land representations.

Table 3.8 lists the equations of the aridity index best fit lines with respect to distance inland (km) for all daytime HCMM data processed. On one date, 08 Jul 78, the radiative transfer model was not used because of missing radiosonde data. Of necessity, the correction for that overpass was estimated and applied to the intercept.

The regression coefficients of aridity indexes listed in Table 3.8 reflect the influence of decreasing available soil moisture with time in the interior rangeland, and the increased evaporative demand from spring to summer. In general, the coefficients increased from May to a maximum on 08 Jul. The relatively small regression coefficient calculated for 15 Aug was likely caused by subvisible cirrus cloud contamination of data, as discussed in Chapter 2 of this report.

The positive regression coefficients in Table 3.8 showed that the aridity indexes were frequently greatest in the interior rangeland. This is expected considering the decline of rainfall from the coast (annually 10 mm/4.5 km inland), and the fact that irrigated surroundings predominated within 90 km of the coast.

The standard deviations of aridity indexes from the best fit lines, listed in Table 3.8, averaged 2.88 C for the 10 dates. The standard deviations are in °C because the aridity index is calculated by subtracting air temperature, °C, from satellite indicated surface temperature, °C. The lowest values occurred on 06 Jun 78 following a rainy period and on 07 Feb 79 a cool winter day (9.7 C mean). By comparison the standard deviations of aridity indexes from best fit average were 2.35 C for nights of unimpeded radiational cooling (21 Oct 78 and 26 Feb 79) and 0.90 C for nights of dew formation (30 Jun 78, 23 Aug 78, and 10 Oct 78).

The deviation of daytime aridity indexes from the best fit line with respect to distance inland is given in Table 3.7 for individual weather station locations. Some locations had consistently high aridity indexes while others tended to be below the trend. This is indicated in the Table's right column where the number of negative to positive occurrences are given.

Locations that usually had positive aridity index deviations were McCook (C), Mission (D), and McAllen (K). These values above the best fit line may have resulted from either unusually hot surface temperatures in the 9x9 pixel footprint, or cold air temperatures. The urban surroundings of McAllen would contribute to a positive deviation (White, et al. 1978).

Negative aridity index deviations were observed at Raymondville (G) and Las Escobas Ranch (M). These could have been caused by unusually cold surface or hot air temperatures.

Other causes of either positive or negative aridity index deviations could be an inaccurate thermometer, a poorly located instrument shelter, or a nonrepresentative microclimate. We recognize, however, that the aridity index we calculate is not the true temperature difference between the air at instrument shelter height and the land surface at the time of the satellite overpass.

Analysis was made of 365 consecutive days (10 May 78 through 09 May 79) of thermograph records from the Weslaco environmental station (station 10, Figure 1.3, representative of the irrigated area) and Las Escobas Ranch (station 25, Figure 1.3, representative of rangeland). In both the surroundings, the maximum air temperature was usually warmer than at nominal HCMM overpass time; within 1 C over half the time, and within 3 C during 90% of the time.

The HCMM data do not measure landscape surface temperature precisely; they need correction for atmospheric effects and surface emissivity. We corrected the daytime HCMM data used in this section by applying a radiative transfer model (J. C. Price, personal communication) with radiosonde measurements from Brownsville, Texas (station 17, Figure 1.3). To represent actual conditions the corrections listed in Table 3.8 should have been higher because the air temperatures were higher (resulting in more correction) at satellite overpass than at 1800 CST when the observations we used were obtained. Also, we applied the Brownsville radiative transfer corrections to the entire test area, but in reality the corrections should have varied with distance inland due to increasing air temperatures and decreasing humidity in the lower atmosphere.

Our HCMM data have not been corrected for emissivity. During the summer much of the irrigated area (eastern portion of test area) was covered by adequately watered vegetation. The rangeland (inland western portion of test area) had vegetation that sparcely covered the soil in many locations, and the soil surface was generally dry. Thus, the temperature corrections for emissivity would have been greatest in the rangeland (Fuchs and Tanner 1966, 1968; Sutherland and Bartholic, 1977). A change in emissivity of 0.01 corresponds to a temperature change of about 0.7 C (Phinney and Arp, 1975).

The factors discussed above (higher actual surface temperature and lower actual air temperature at satellite overpass) gave greater differences than expresssed by our aridity index. Also, the differences between surface and air temperatures would increase more with distance inland if emissivity corrections were made. Even though the aridity index does not exactly represent the difference between surface temperature and air temperature at satellite overpass, it deserves further examination.

3.4.6 Nighttime HCMM temperatures vs ambient dewpoint temperatures

Examples of nighttime surface temperatures in the presence of dew on 30 Jun 78 have been presented in the discussion of soil association temperatures (Figure 3.3) and thermal islands in the vicinity of water bodies (Figure 3.12). Those illustrations show that generally uniform surface temperatures prevailed under dew conditions. The dew point depression averaged 0.9 C at 1.5 m above the ground at the Weslaco environmental station during the night hour in which HCMM overpassed on 30 Jun 78.

The differences between HCMM indicated nighttime surface temperatures surrounding weather stations (average of 9x9 pixels) and the minimum air temperatures recorded at the weather stations are illustrated in Figure 3.16 for 30 Jun 78. This representation of THCMM-Tmin was computed in the same manner as the aridity index described in section 3.4.5. The HCMM temperatures of the test area used here were adjusted by the radiative transfer model results obtained with 0600 CST radiosonde data from Brownsville, Texas.

Figure 3.16 shows that THCMM-Tmin was positive at most stations, and it tended to increase with distance inland. The weather station identifications corresponding to the letters in the Figure are given in Table 3.7.

Several factors are involved in the THCMM-Tmin results. Nocturnal cooling under a clear sky causes surface temperatures that are below air temperature because of heat loss by radiation. Hence, if it were not for other factors, THCMM-Tmin would be negative. Because landscape emissivities range from 0.95 to 0.99 (bare soil to full canopy), the equivalent black body temperatures seen by the satellite are lower than actual surface temperatures, a further cause of negative THCMM-Tmin.

Negative tendencies may be counteracted by the fact that minimum air temperature is used in calculating THCMM-Tmin, instead of the usually warmer air temperature at HCMM overpass time. Analysis of 365 consecutive days of thermograph records (10 May 78 through 09 May 79) from the Weslaco environmental station (irrigated area) and Las Escobas Ranch (rangeland) showed that during 85% of the nights, air temperatures at overpass time were within 3 C of the minimum for the night.

Even though a radiative transfer model was used, the radiosonde data were obtained several hours after overpass, hence adjustments were not exact. Furthermore, even if the adjustments were exact at one location (perfect model and atmospheric data obtained at overpass time), they would not precisely apply to all pixels of the large test area.

The radiative adjustment of 3.61 C applied to the 30 Jun 78 nighttime HCMM data appeared to be too large at the Weslaco Research Farm environmental station in an irrigated area. Weather information from the hour in which HCMM overpassed and HCMM surface temperature data from 9x9 pixel footprints surrounding the weather stations are listed below:

	Environ. Station	Las Escobas	Avg. All Stations
Dewpoint at overpass, °C	22.11	-	-
Air temperature at overpass,°C	23.01	24.64	-
Minimum air temperature, °C	22.67	23.19	22.11
THCMM, unadjusted, °C	19.68	20.20	19.86
THCMM, adjusted, °C	23.29	23.81	23.47
Std. Deviation (9x9 THCMM),°C	0.91	0.81	0.78
Std. Error (9x9 THCMM), °C	0.10	0.09	0.09

The situation shown for the Weslaco environmental station (first data column) is unlikely in that the adjusted THCMM exceeded air temperature at the nighttime overpass, 23.29 C vs 23.01 C. The humidity at this time was 94% at shelter height. The minimum air temperature of 22.67 C (hourly average) occurred between 0300 and 0400 CST. The THCMM-Tmin at the environmental station was 0.62 (23.29-22.67).

The situation shown for Las Escobas Ranch in the rangeland area (second data column) is reasonable. The adjusted surface temperature was 0.83 C below air temperature.

At the inland location of Las Escobas Ranch (station 25, Figure 1.3) a slightly lower dew point might be expected than at the Weslaco environmental station. The similarity of nighttime minimum air temperatures in summer in the central and western portions of the test area is in agreement with widespread nocturnal dew formation. The narrow range in dewpoint temperatures, in turn, resulted in a rather uniform distribution of HCMM nighttime surface temperatures. By inference the dew point (not measured) at Las Escobas was less than a degree below the minimum air temperature of 23.19 C (Geiger, 1965; Jensen, 1974) and the adjustment made to the HCMM surface temperature was within 0.5 degree of being correct.

The last two lines of the above information give an idea of the thermal variability of the nighttime scene. The standard deviation and standard error relate to the 81 pixel (9x9) HCMM footprint surrounding the weather station. The mean is the THCMM value.

Averages of values obtained at all test area weather station locations are presented in the right column, except that stations are excluded whose 9x9 HCMM footprint contained water of Laguna Madre or Falcon Reservoir. These data substantiated the earlier statement that surface temperatures are quite uniform over the entire test area when dew is present.

The use of temperature data to the second decimal place is unrealistic considering the magnitude of the measurement errors that were involved. However, decimal fractions of degrees are important to the usefulness of HCMM data, especially where differences among surface temperatures rather than absolute amounts are considered.

The mean daily maximum and minimum air temperatures, °C, for five summer months for the period 1931-1962 (Orton et al., 1967) are given in Table 3.9 for stations representing coastal, intermediate, and interior locations (see Figure 1.3 for station locations corresponding to the identification numbers in the table). Note the similarity of minimum air temperatures at Weslaco and Rio Grande City. The table shows that the large inland diurnal temperature range is due to higher inland maximum temperatures. The wintertime diurnal temperature ranges are also greatest at inland locations, but they result mainly from lower minimums (Table 3.9) made possible by low dew points characteristic of that time of year.

3.4.7 Day and night temperature transects for 07 Feb 79 and 26 Feb 79

For our LRGV test area, it was not possible to obtain day/night HCMM coverage 12 hours apart, nor was it possible to obtain cloud-free 36-hour day/night coverage. We did receive a day-IR scene for 07 Feb 79 and a night-IR scene for 26 Feb 79. These two were clear winter scenes with weak atmospheric absorption, characteristic of that time of year. The data in these two profiles were smoothed with a 3x3 moving window ($\bar{X}$). Air temperatures averaged 6 C and 21 C for the night and day scene, respectively.

Figure 3.17 shows that the 07 Feb 79 day scene and the 26 Feb 79 night scene unadjusted temperature profiles across the LRGV at latitude 26.2° N were almost mirror images; that is, high day land surface temperatures on 07 Feb 79, were generally mirrored by the low night land surface temperatures on 26 Feb 79. The temperatures of water in Falcon Reservoir and the Gulf of Mexico are almost identical on both dates, as expected for these deep water bodies. If 12-hour or even 36-hour day minus night HCMM coverage were available, the temperature difference between day and night land surface temperature profiles may

have been more pronounced. The Figure indicates, however, that day/night overpasses need not be that frequent if vegetative cover remains essentially static and little or no rain has fallen in the intervening period.

The clear and weak atmospheric absorption characteristics of the 07 Feb 79 and 26 Feb 79 day/night scene pair means that the temperature profiles shown are probably due to near surface soil water content and to vegetative cover. Surface temperature adjustment calculated by a radiative transfer model using Brownsville, Texas radiosonde data for 1800 CST, 07 Feb 79 was 0.92 C and for 0600 CST, 26 Feb 79 it was -0.21 C.

3.5 Literature cited

Barnes, W. L. and Price, J. C. 1980. Calibration of a satellite infrared radiometer. Applied Optics. 19:2153-2161.

Fuchs, M. and Tanner, C. B. 1966. Infrared thermometry of vegetation. Agron. J. 58:597-601.

Fuchs, M. and Tanner, C. B. 1968. Surface temperature measurement of bare soils. J. Applied Meteorol. 7(2):303-305.

Geiger, R. 1965. The climate near the ground. Harvard University Press. 611 pp.

Jensen, M. S. (Ed.). 1974. Consumptive use of water and irrigation water requirements. Report of Tech. Com. on Irrig. Water Requirements. American Society of Civil Engineers. 215 pp.

Kincaid, D. C. and D. F. Heermann. 1974. Scheduling irrigations using a programmable calculator. Agricultural Research Service, USDA Technical Report ARS-NC-12. 55 pp.

Monteith, J. L. and G. Szeicz. 1962. Radiative temperature in the heat balance of natural surfaces. Quart. J. Roy. Meteorol. Soc. 88:496-507.

Nixon, P. R. and T. A. Hales. 1975. Observing cold-night temperatures of agricultural landscapes with an airplane-mounted radiation thermometer. J. Applied Meteorol. 14(4):498-505.

Nixon, P. R. and R. E. Smithey. 1979. Potential evapotranspiration in the Lower Rio Grande Valley. J. Rio Grande Valley Hort. Soc. 33:91-100.

Orten, R., D. J. Haddock, E. G. Bice, and A. C. Webb. 1967. Climatic Guide--The Lower Rio Grande Valley of Texas. MP-341. Texas Agric. Expt. Station. College Station. 103 pp.

Penman, H. L. 1963. Vegetation and Hydrology. Tech. Communication No. 53, Commonwealth Bur. of Soils, Harpenden, England. 125 pp.

Phinney, D. E. and G. K. Arp. 1975. The measurement and interpretation of thermal infrared emissivities. Report LEC-5621. Lockheed Electronics Co., Inc., Houston, Texas.

Sutherland, R. A. and J. F. Bartholic. 1977. Significance of vegetation in interpreting thermal radiation from a terrestrial surface. J. Applied Meteorol. 16(8):759-763.

White, J. M., F. D. Eaton, and A. H. Auer, Jr. 1978. The net radiation budget of the St. Louis metropolitan area. J. Applied Meteorol. 17:593-599.

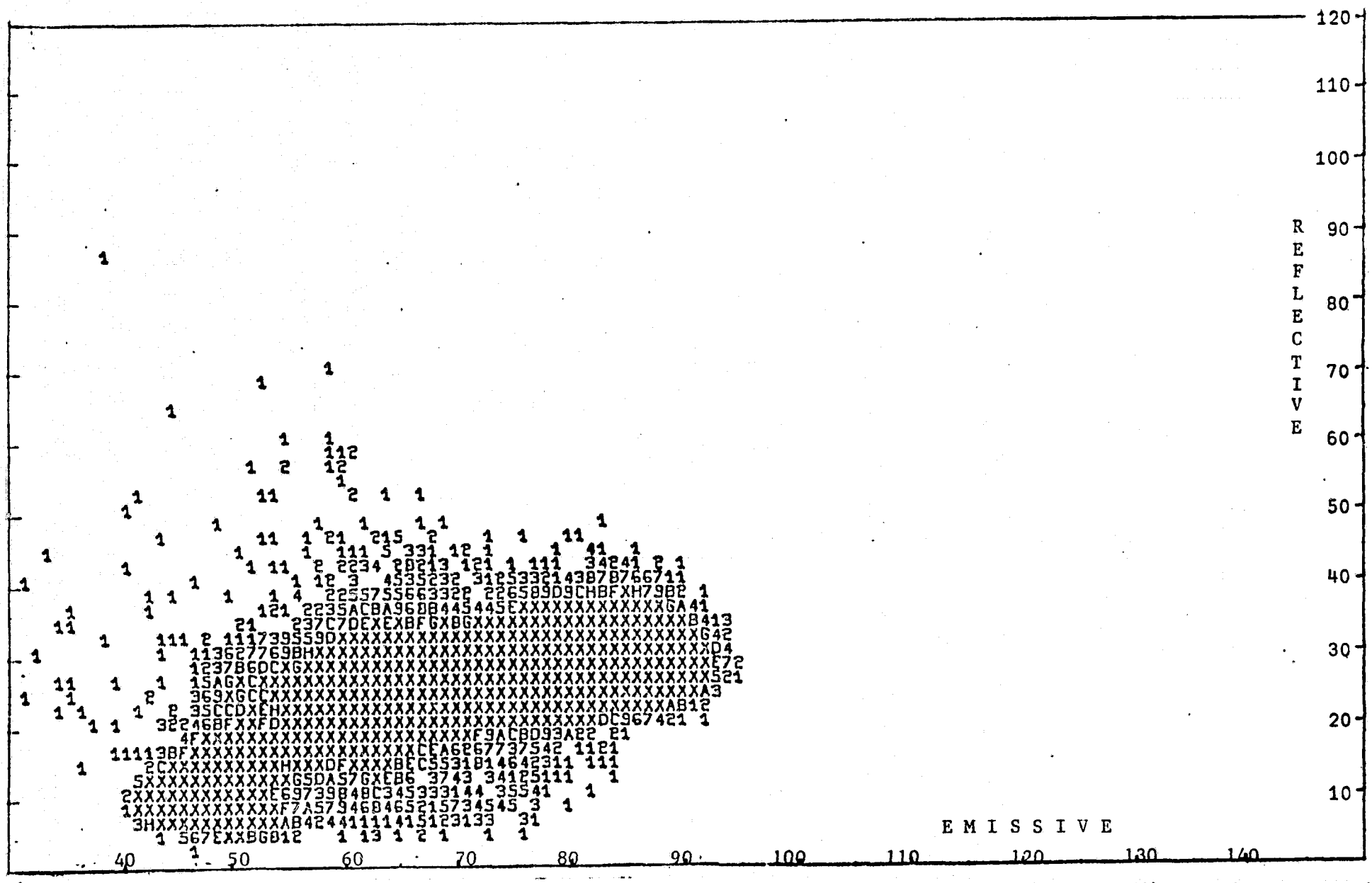

Figure 3.1 Scatter diagram of emissive (X-axis) and reflective (Y-axis) pixels of clear (07 Feb. 79) satellite pass. The numbers represent the count of pixels falling in each cell of the diagram. Counts of 10 to 16 are coded A to G; counts above 16 are designated by X.

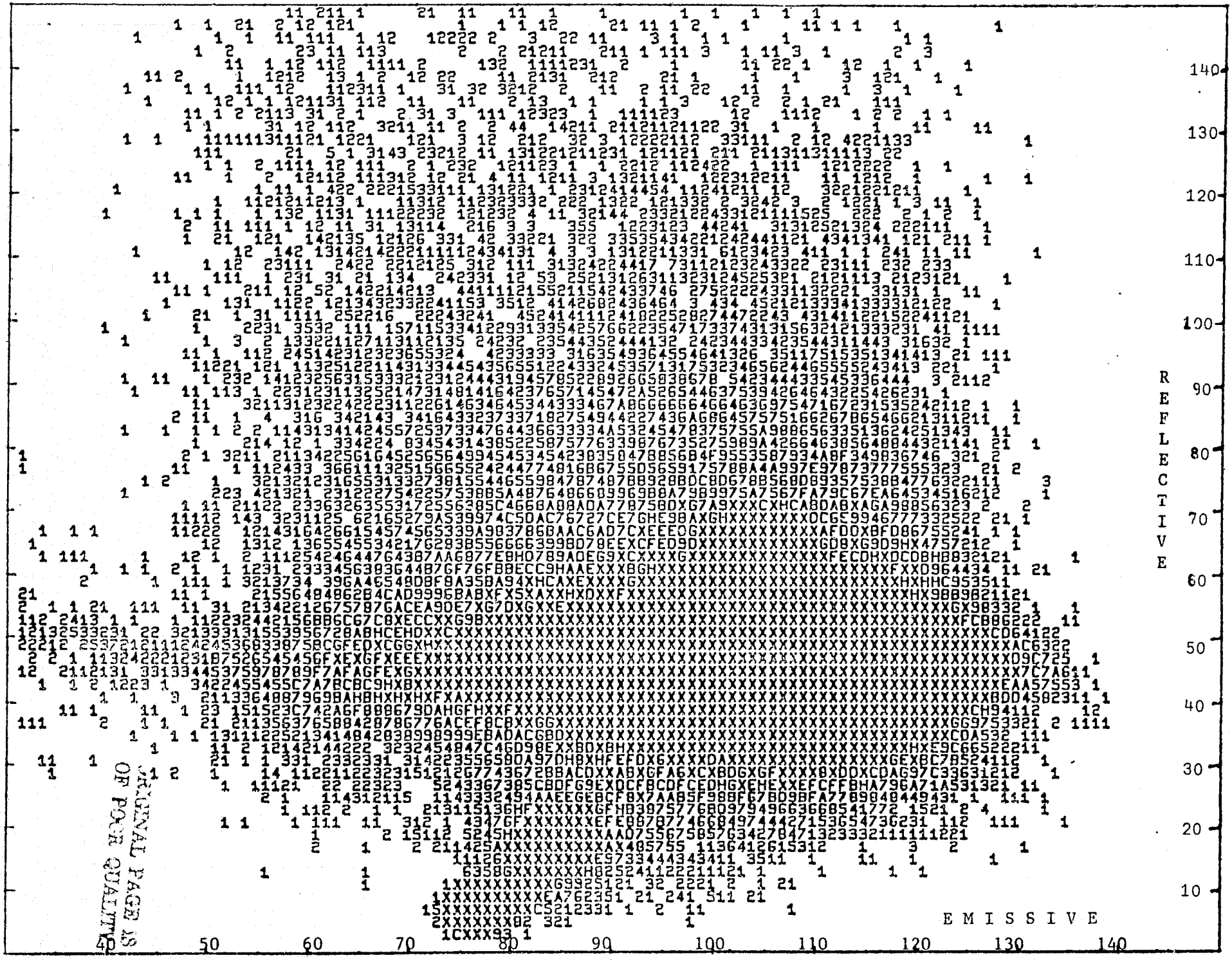

Figure 3.2 Scatter diagram of emissive (X-axis) and reflective (Y-axis) pixels of cloudy (27 May 78) satellite pass. The numbers represent the count of pixels falling in each cell of the diagram. Counts of 10 to 16 are coded A to G; counts above 16 are designated by X.

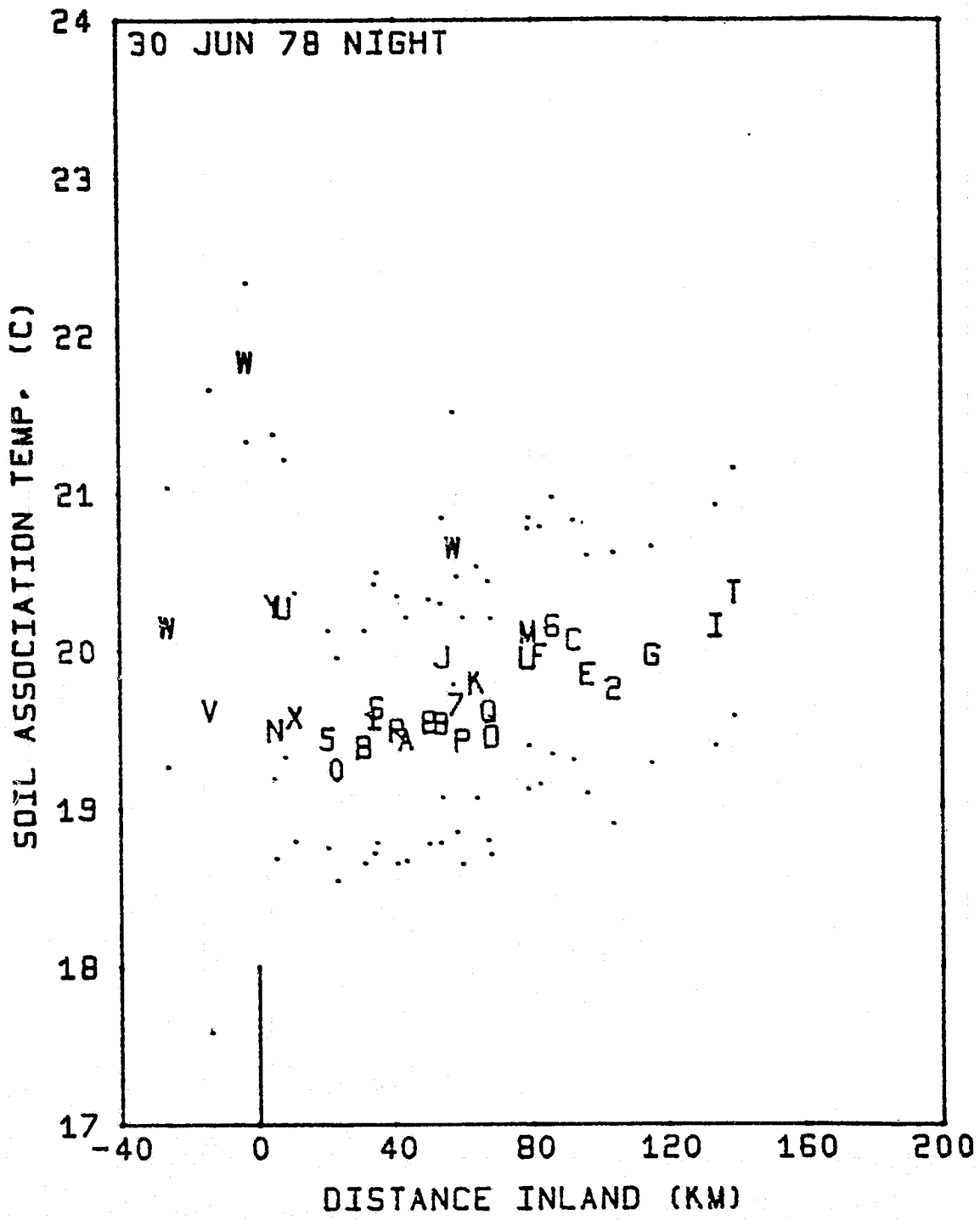

Figure 3.3 Soil association temperatures versus distance inland from the coast for the night of 30 Jun 78 (Standard deviations of temperature are indicated by dots above and below each soil association symbol).

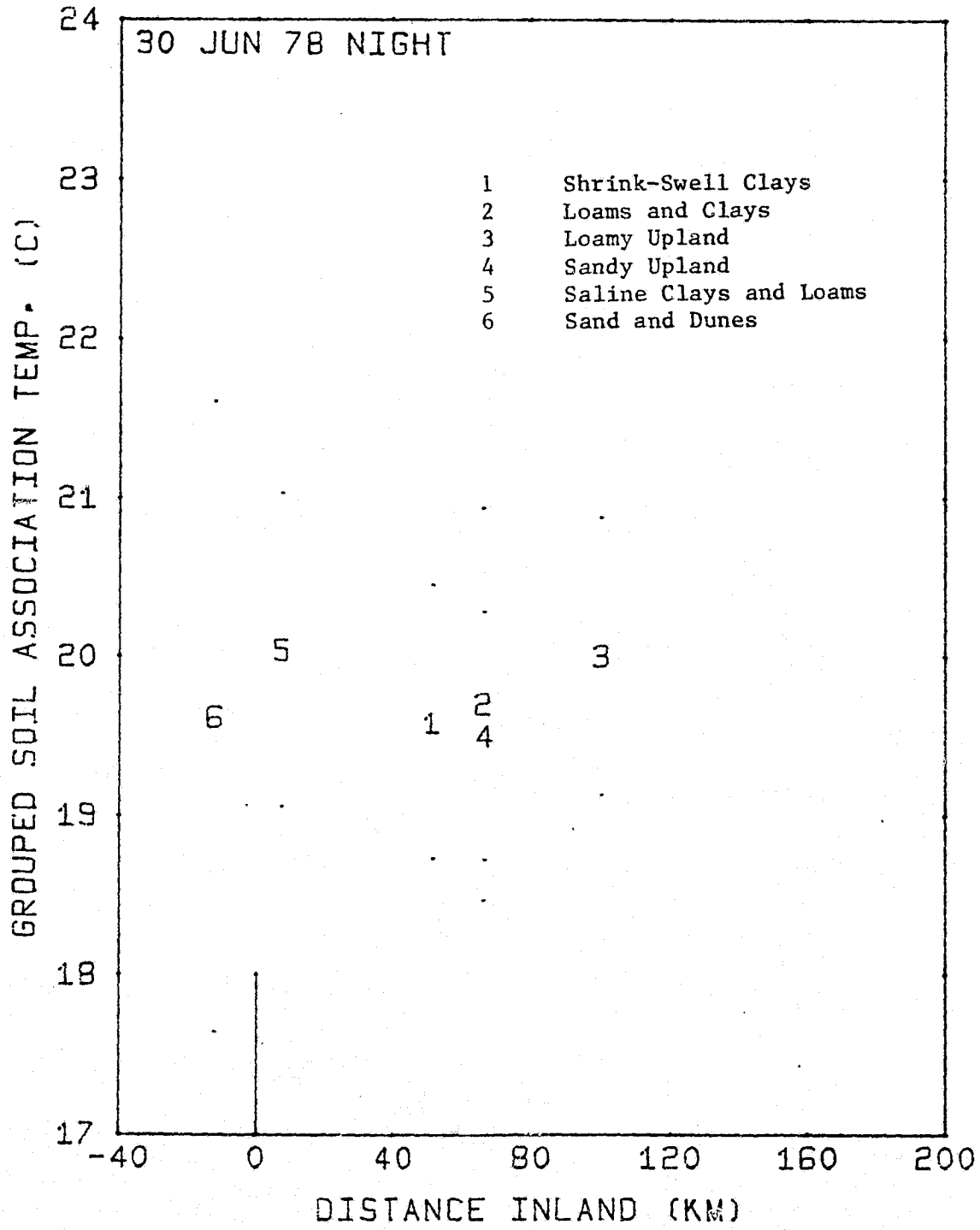

Figure 3.4 HCMM temperatures versus distance inland from the coast for six groups of soil associations with similar properties for the night of 30 June 78.

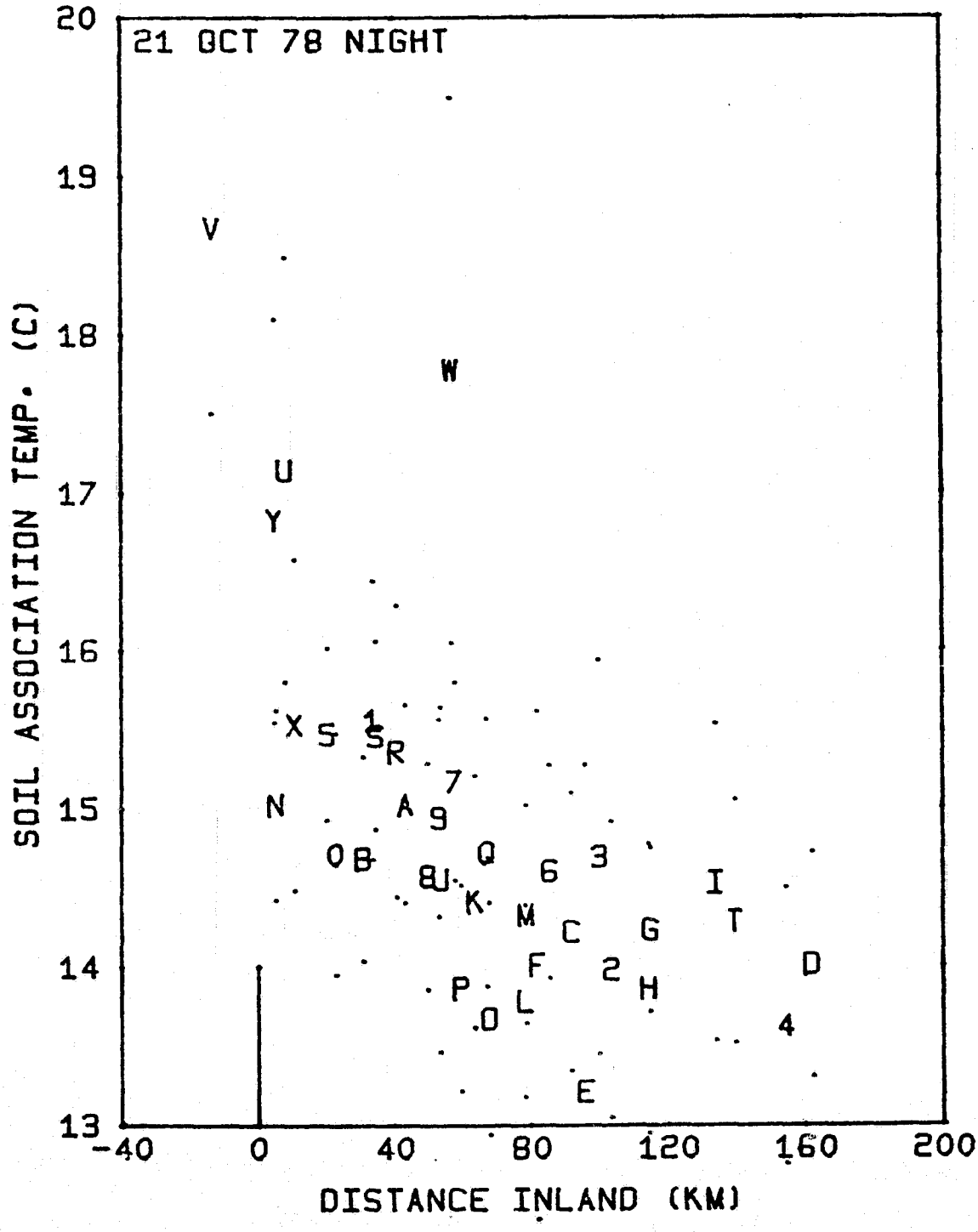

Figure 3.5 Soil association temperatures from HCMM versus distance from the coast for the night of 21 Oct. 78. (Standard deviations of temperature are indicated by dots above and below each soil association symbol.)

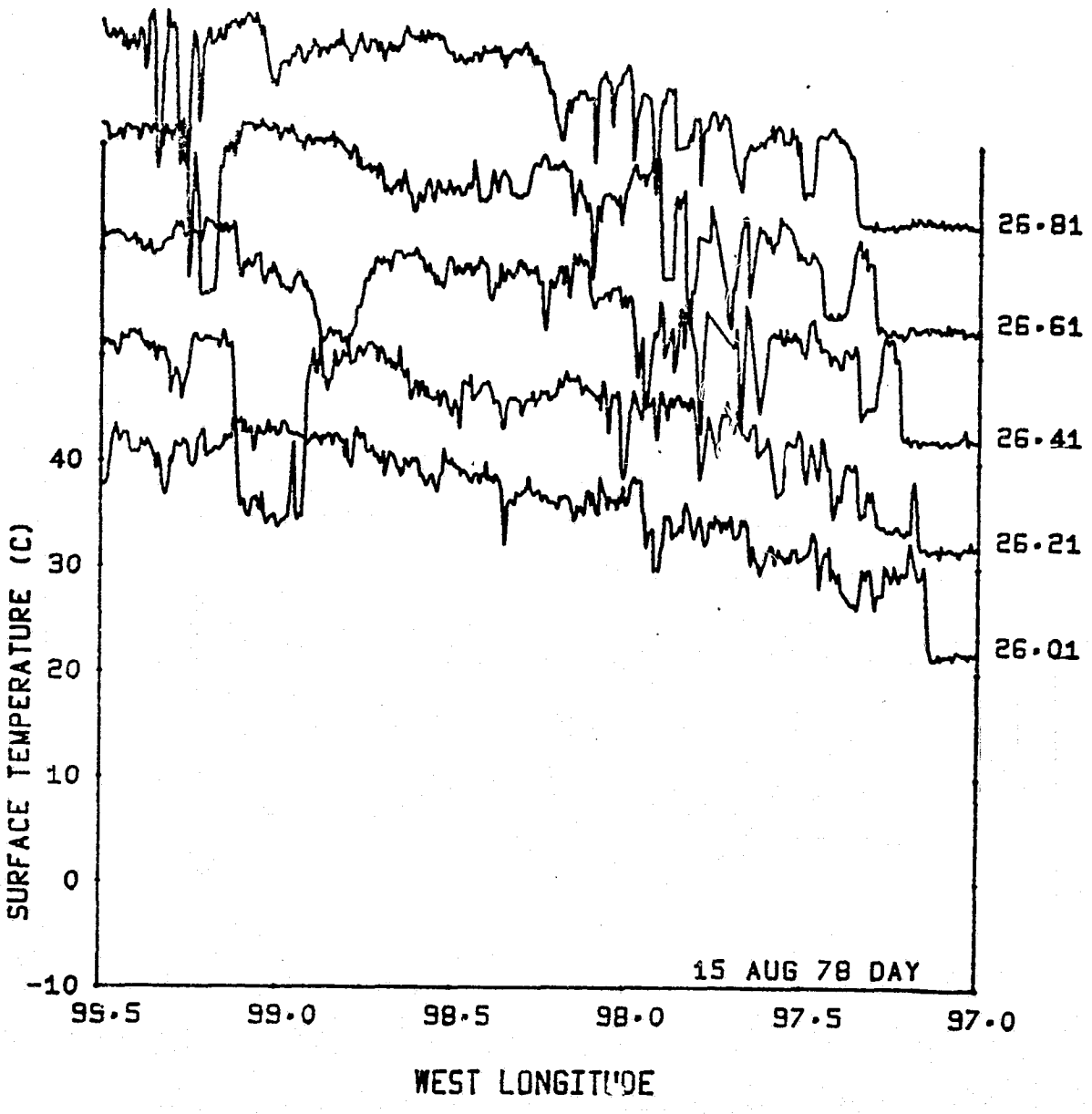

Figure 3.6 Surface temperature transects across the test site at each of five latitudes for the daytime overpass on 15 Aug. 78.

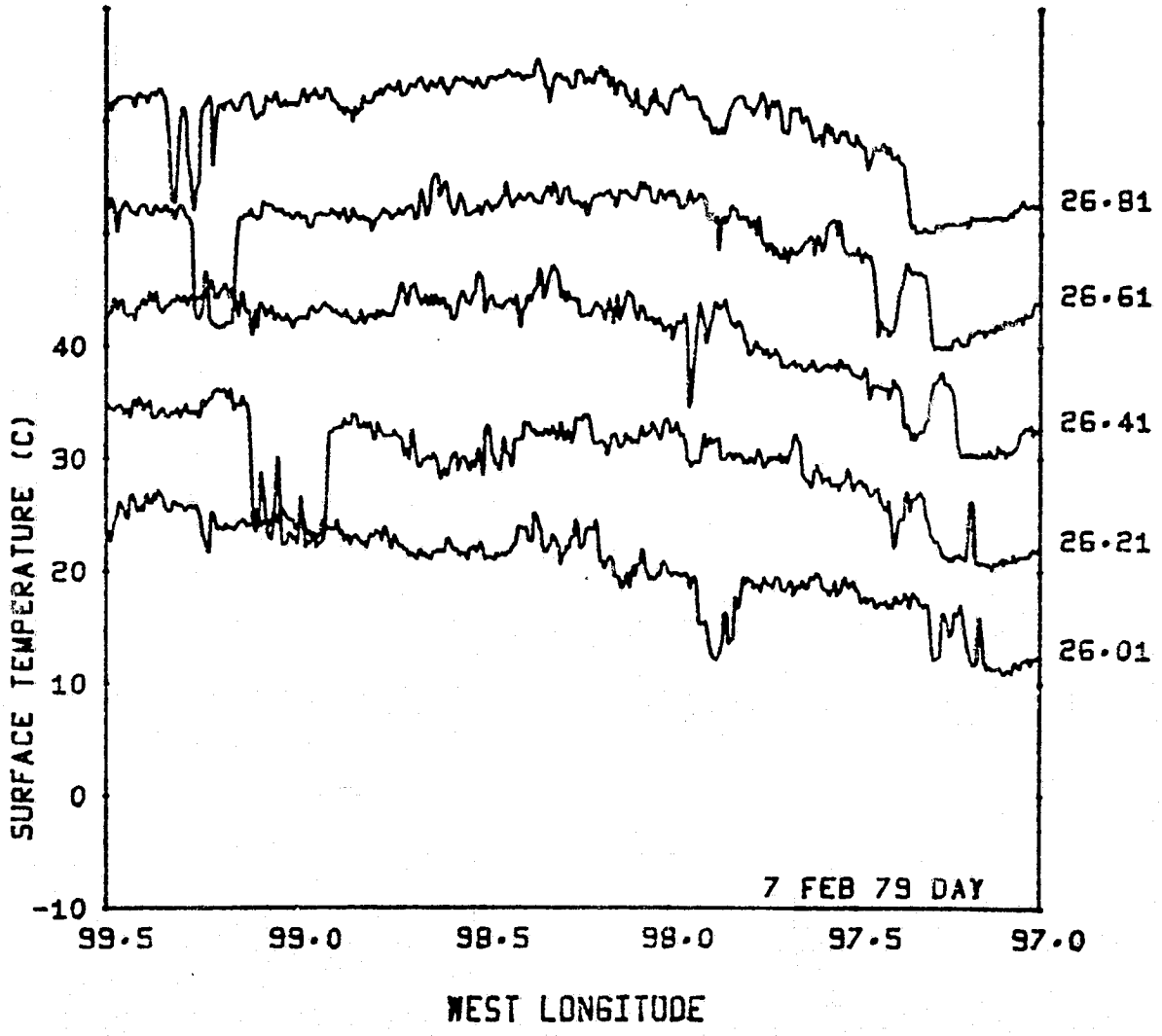

Figure 3.7 Surface temperature transects across the test site at each of five latitudes for the daytime overpass on 07 Feb. 79.

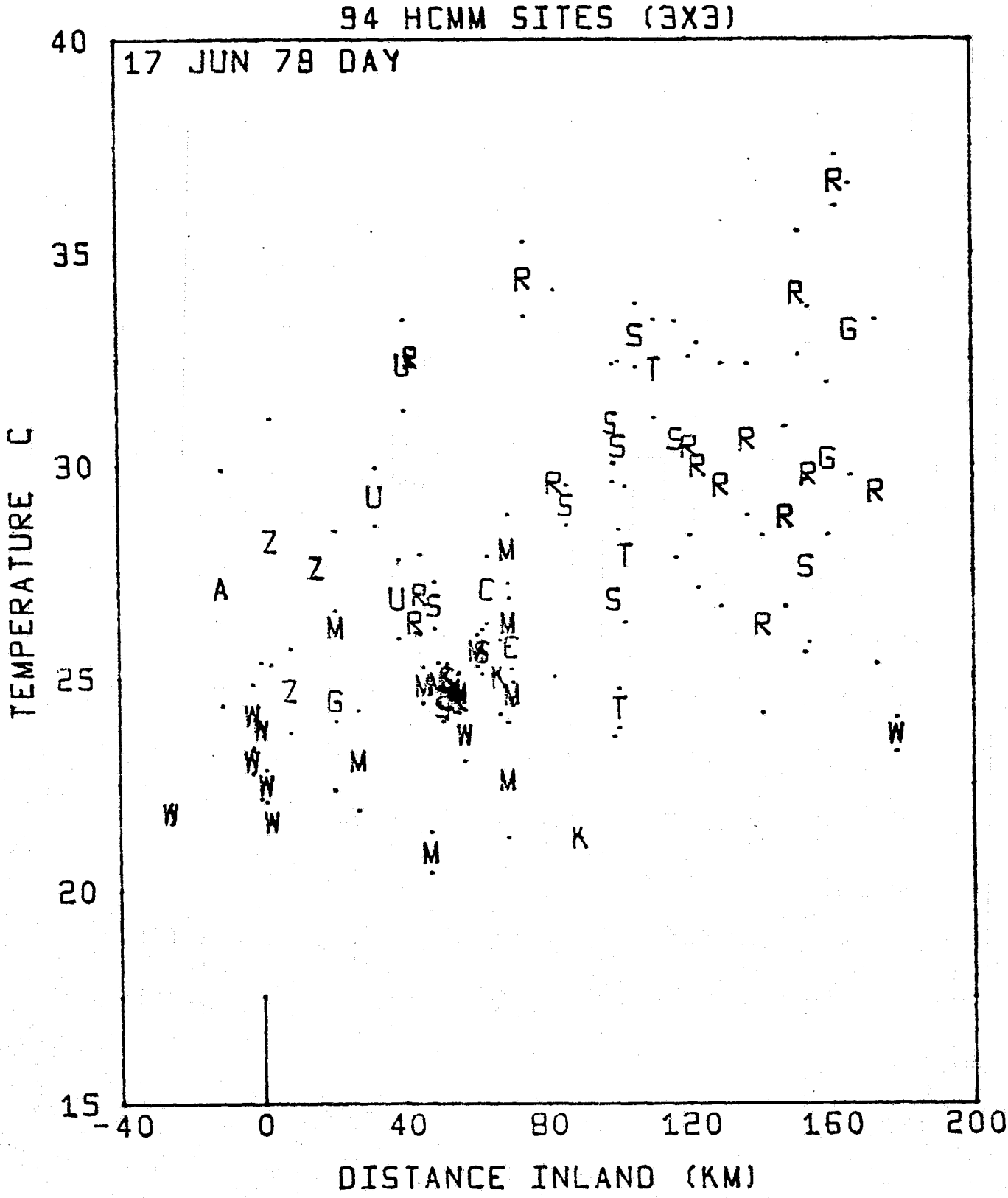

Figure 3.8 Surface temperature (3x3 pixel means and standard deviations) by 11 land use categories at 94 sites versus distance inland from the coast for the daytime overpass on 17 June 78.

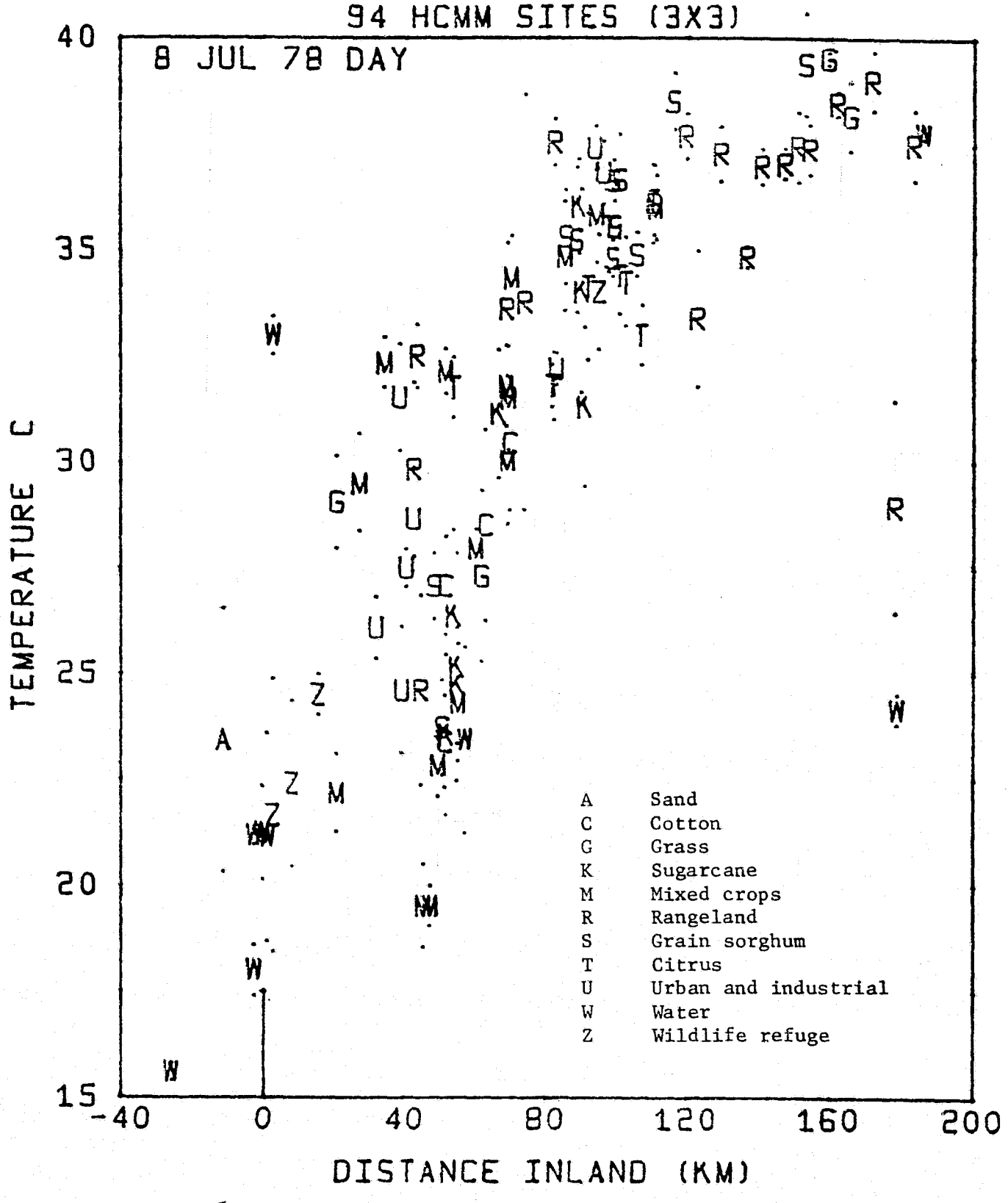

Figure 3.9 Midsummer gradient of temperature inland from the coast by land use codes (identified by letter). Standard deviations of temperature are indicated by dots above and below each land use symbol.

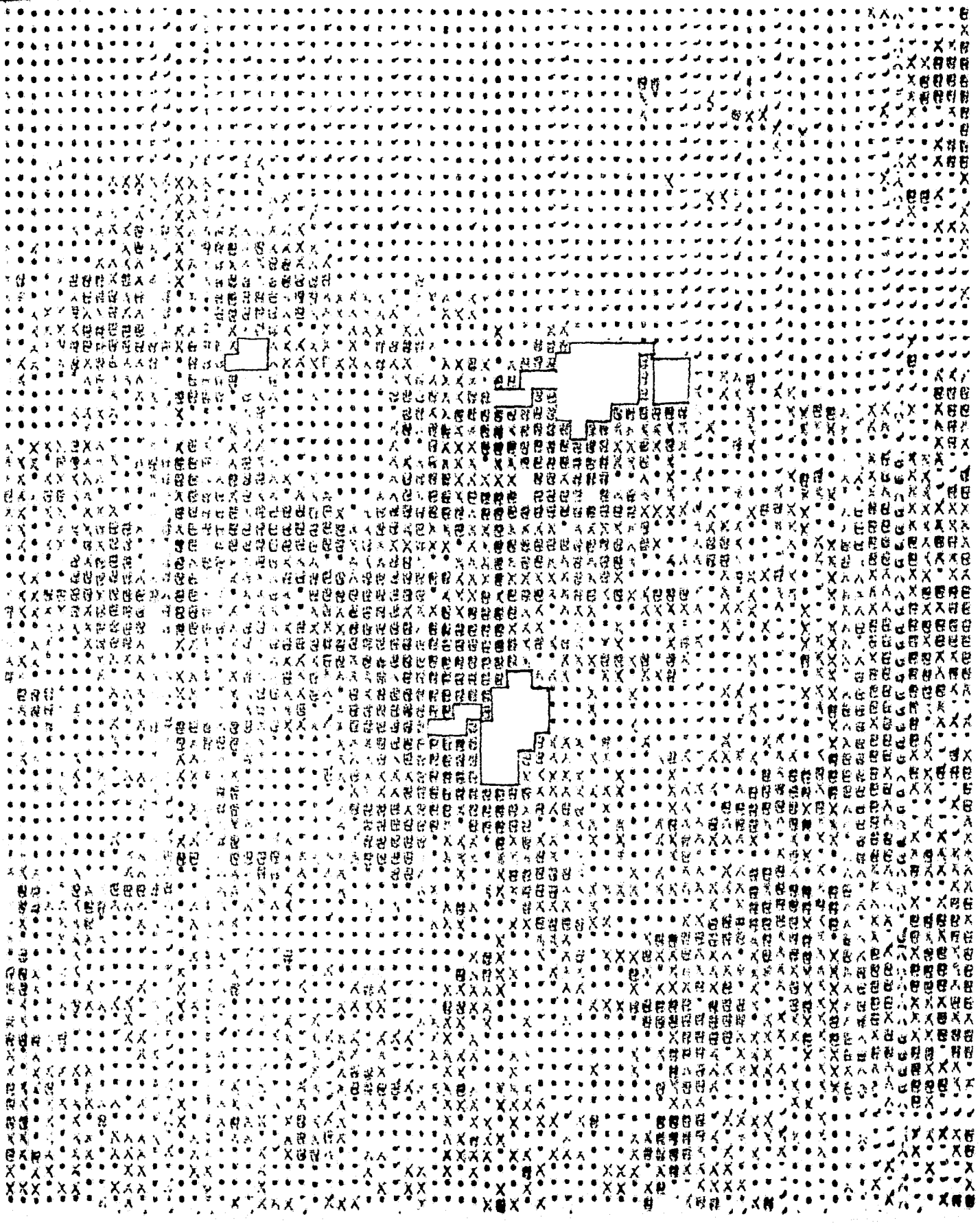

Figure 3.10 Nighttime surface temperature on 26 Feb. 79 displayed by pixel as 1/3 warmest (≥3.44 C, darkest symbol), 1/3 coldest (≥2.23 C, light symbol) and 1/3 intermediate (2.23-3.44 C, intermediate symbol) for a portion of the test site. Water bodies left blank and outlined.

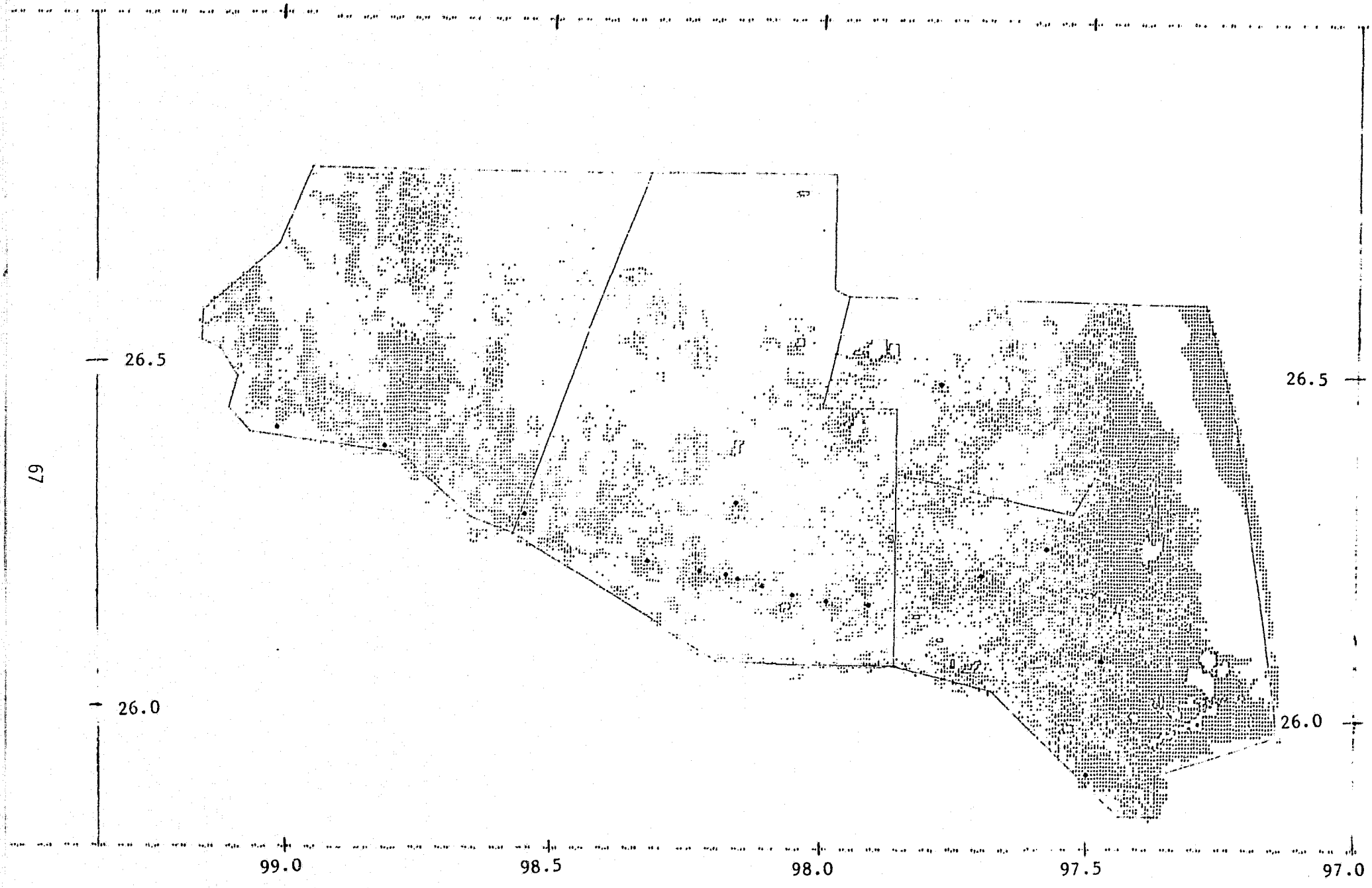

Figure 3.11 Areas of greatest emissions during nighttime overpass on 21 Oct. 78 and 26 Feb. 79. Inland water bodies are outlined, and the centers of cities and towns are identified by dots.

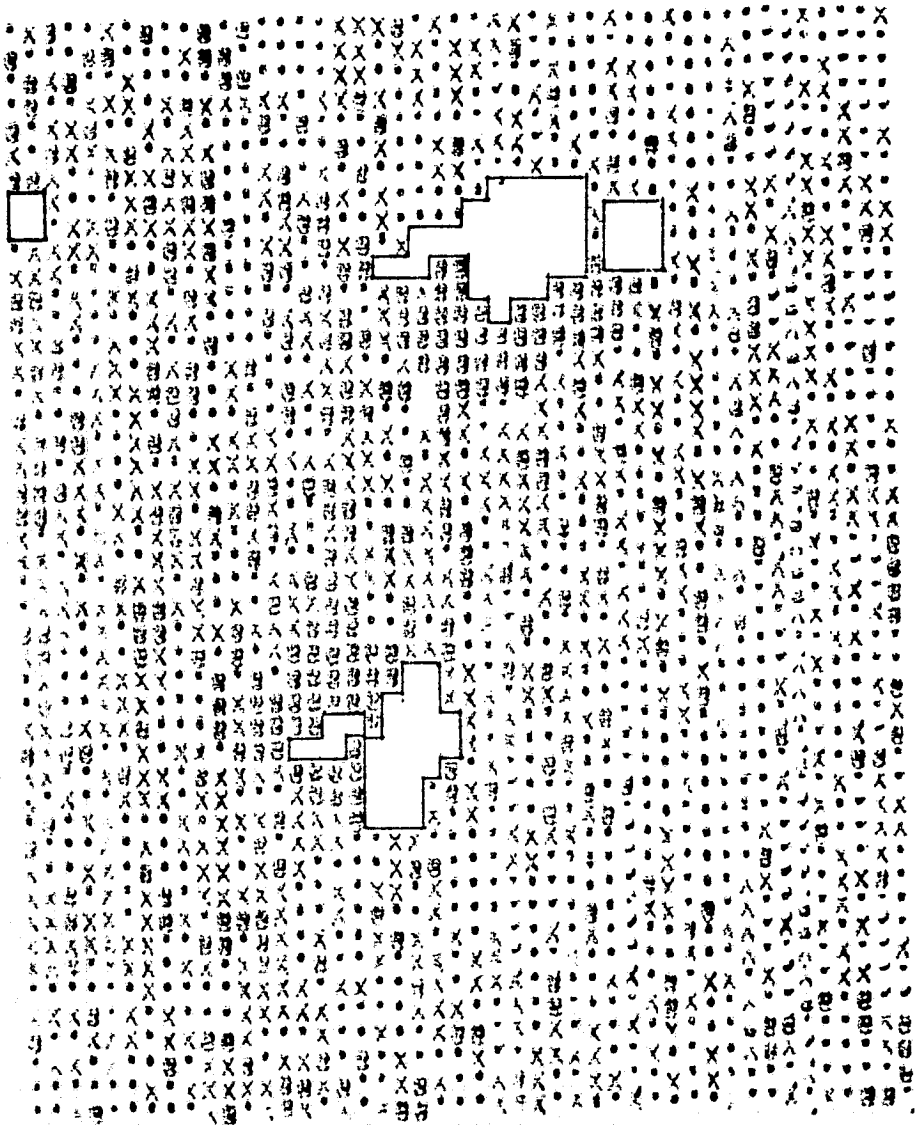

Figure 3.12 Portion of scene displayed as in Figure 3.10 for the night of 30 June 78.

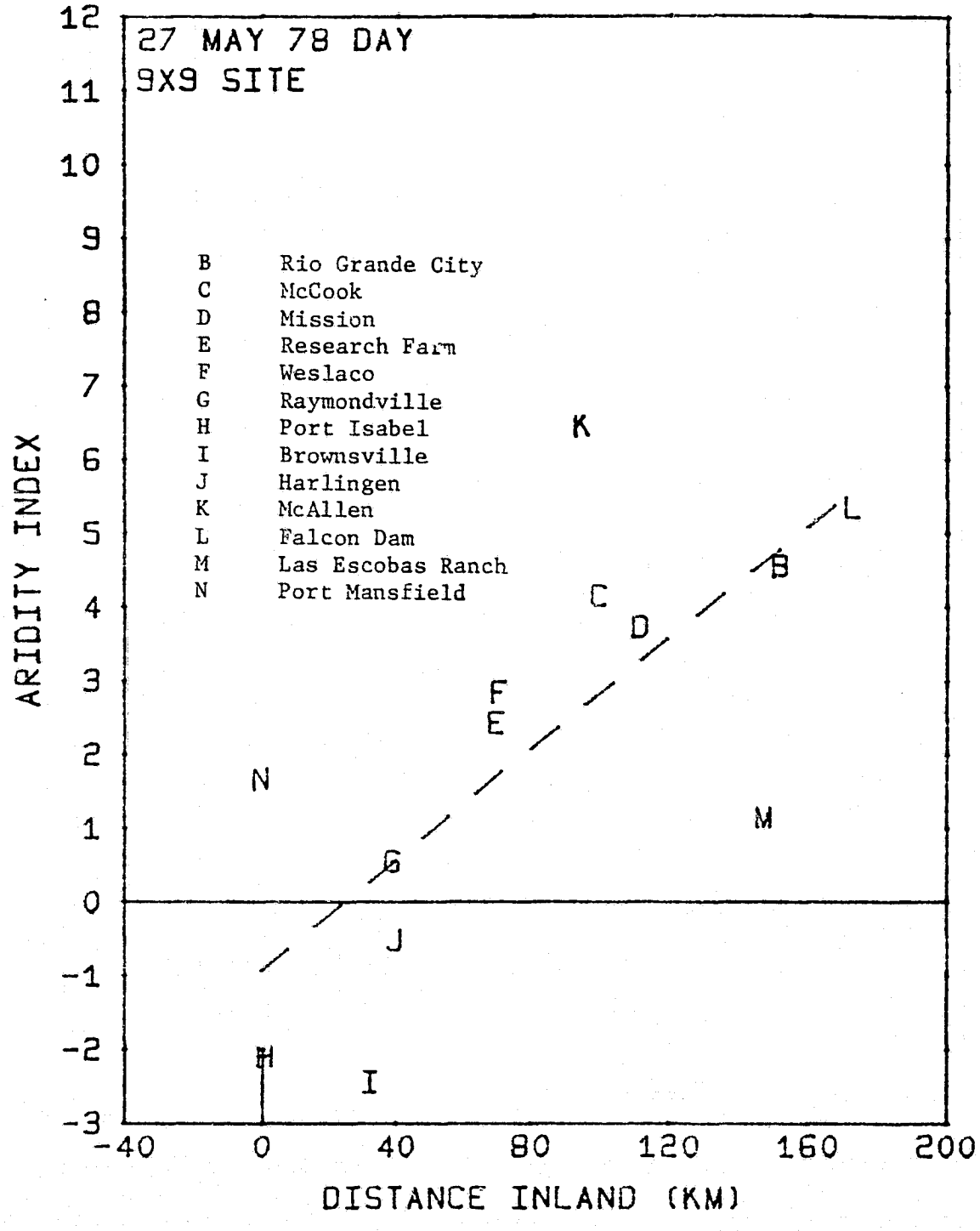

Figure 3.13 Aridity index (T_{HCMM}-T_{Max}) where T_{Max} is maximum air temperature for the day at weather stations and T_{HCMM} is the temperature mean of a 9x9 pixel sample surrounding the stations--the dashed line is the regression fit (see Table 3.8).

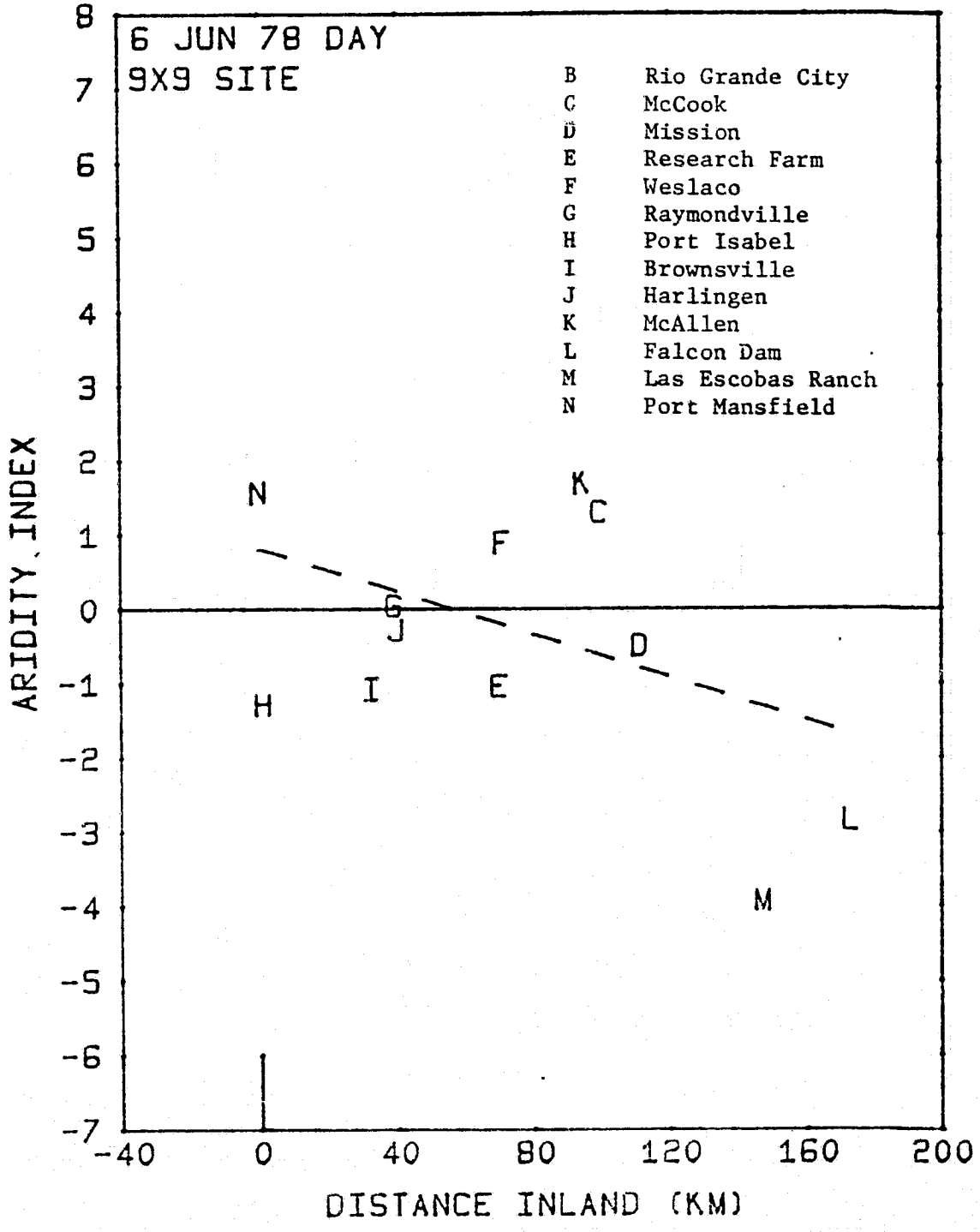

Figure 3.14 Aridity index as in Figure 3.13 for 06 June 78.

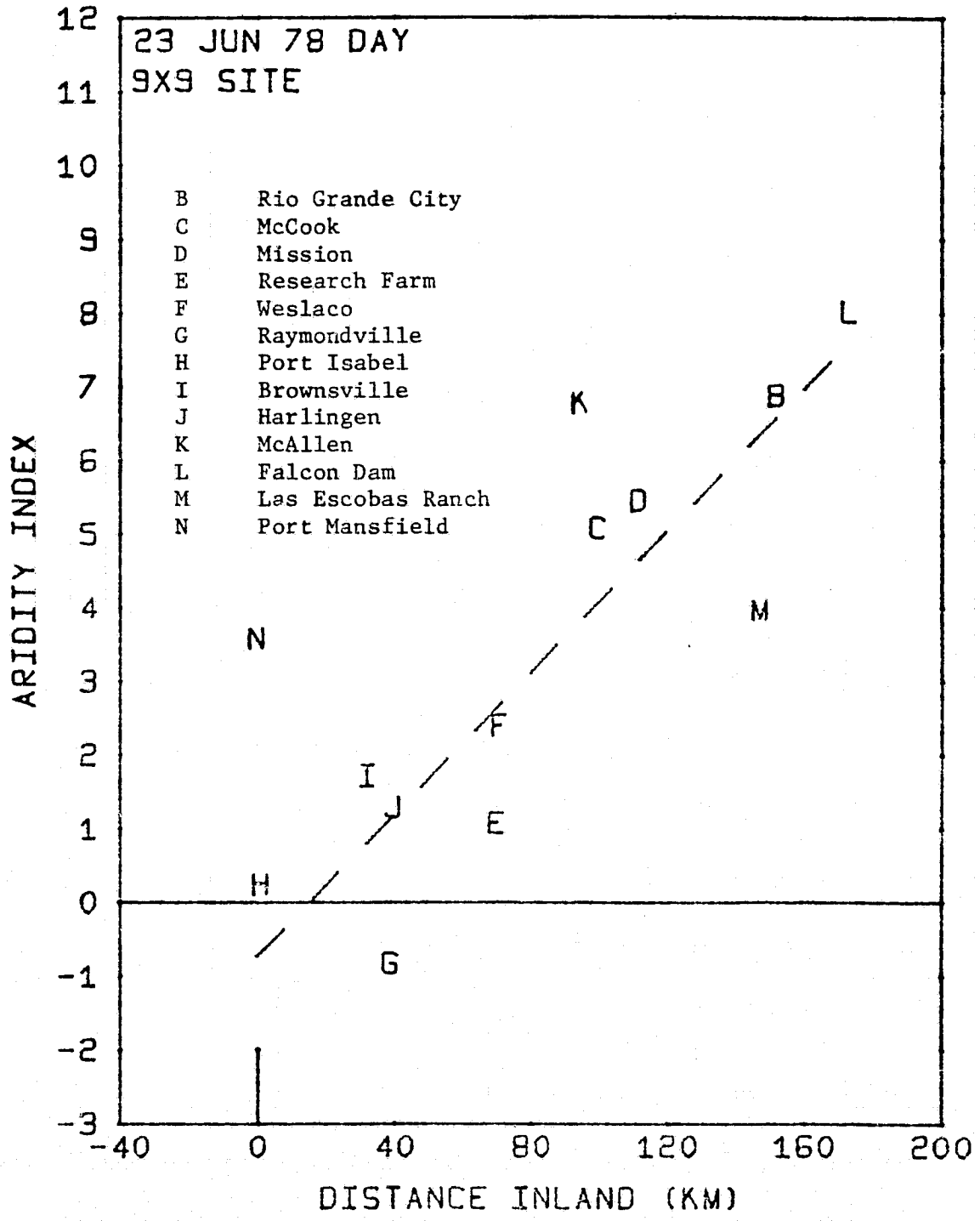

Figure 3.15 Aridity index as in Figure 3.13 for 23 June 78.

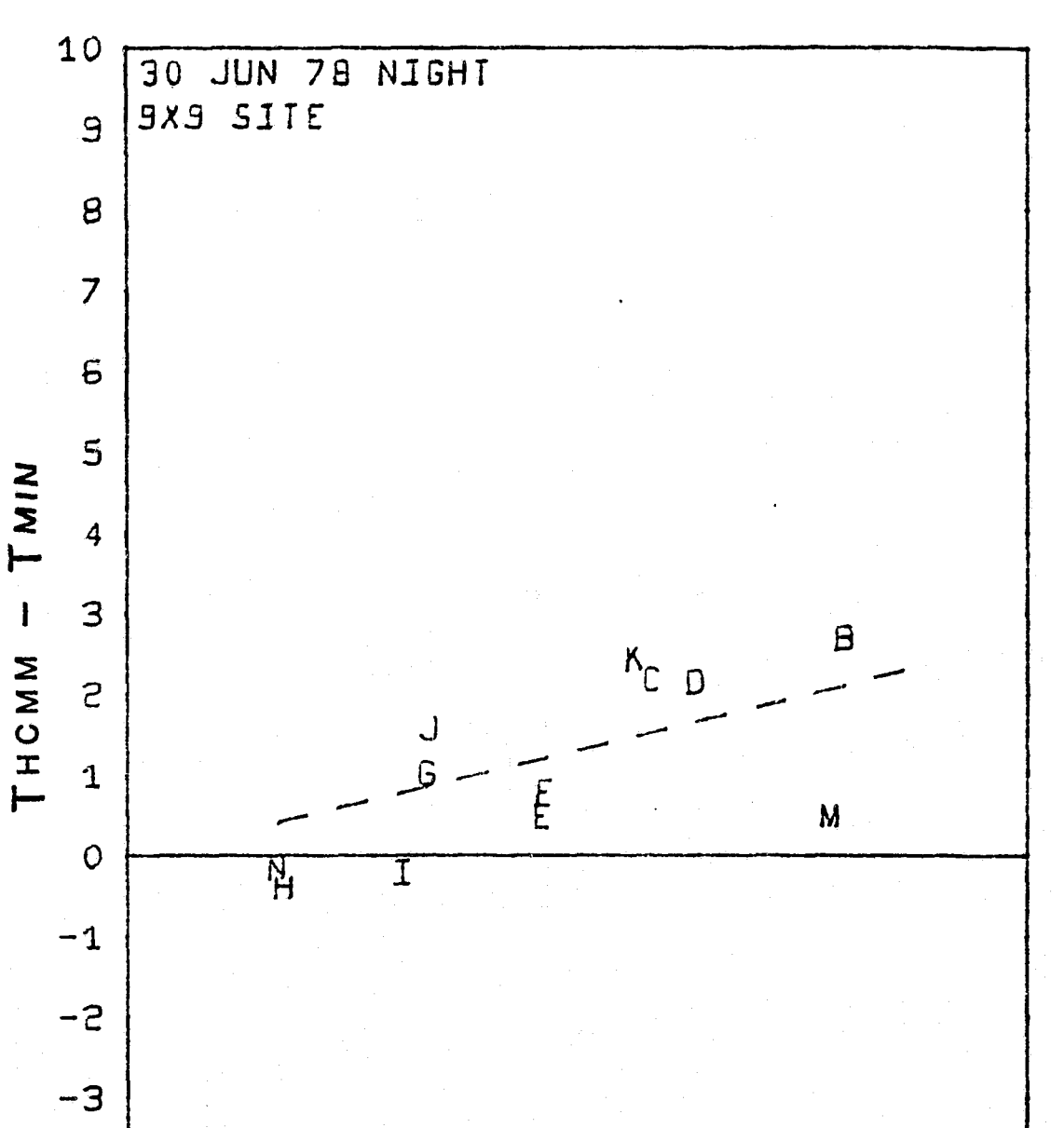

Figure 3.16 The difference between HCMM indicated nighttime surface temperature and daily minimum air temperature versus distance inland for the night of 30 June 78.

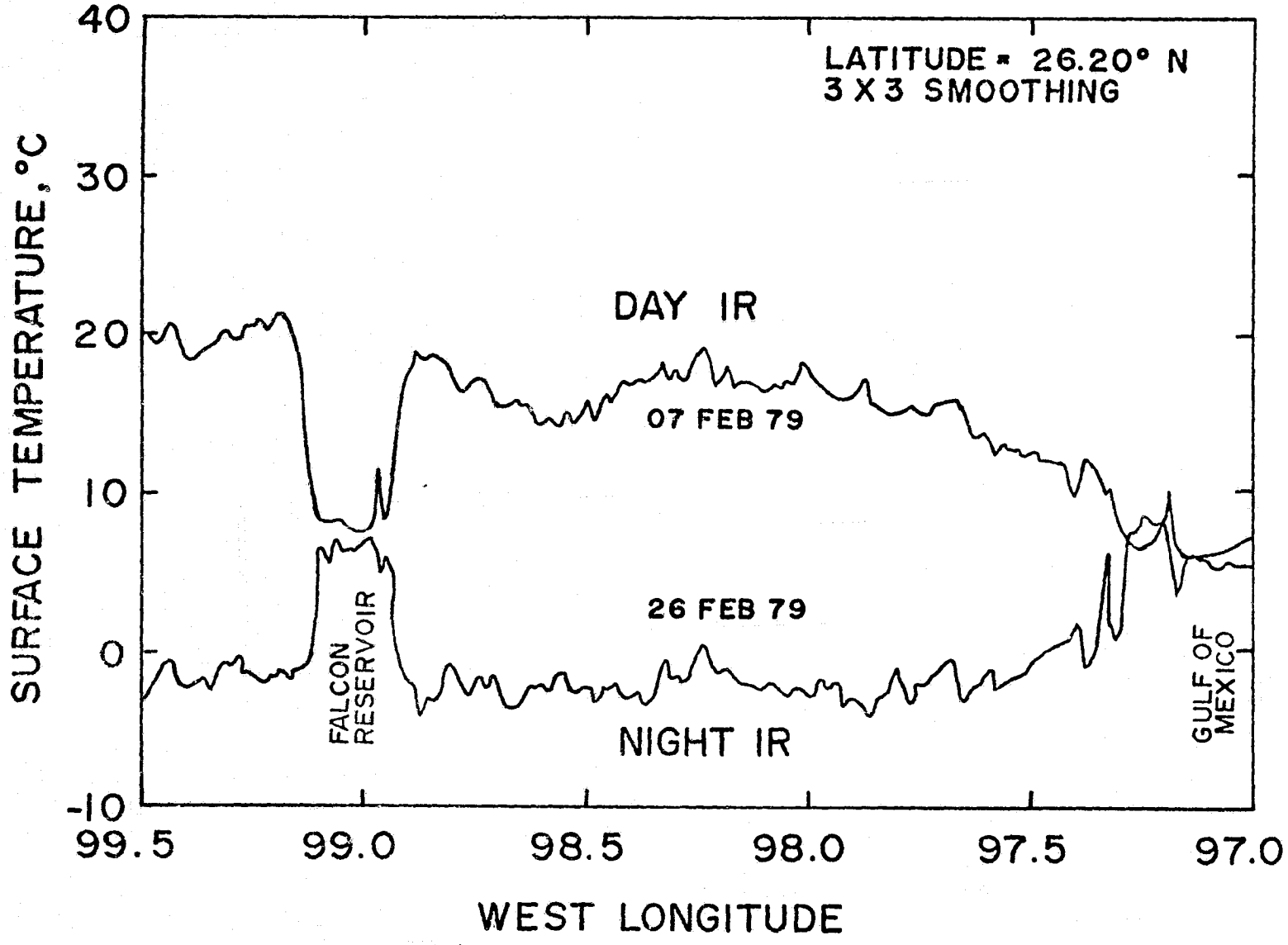

Figure 3.17 Daytime (07 Feb. 79) and nighttime (26 Feb. 79) Surface temperature profiles across the Lower Rio Grande Valley test sites on latitude 26.20° N.

Table 3.1 Summary of number of pixels, rank, percent of total, and number of acres represented (based on 600 x 600-m pixels) of each of the 36 soil associations in the Rio Grande Valley of Texas.

Soil Code No.	No. Pixels	Rank	% of Total	Acres	Soil Association
45	5483	1	15.351	487,775	McAllen-Brennan
54	2505	2	7.013	222,844	Nueces-Sarita
2	2139	3	5.989	190,284	water
81	1861	4	5.210	165,554	Sejita-Lomaita-Barrada
21	1827	5	5.115	162,529	Catalina-Copita
31	1648	6	4.614	146,605	Delmita-Randado
11	1518	7	4.250	135,041	Laredo-Olmito
25	1345	8	3.766	119,651	Raymondville
46	1340	9	3.752	119,206	McAllen-Zapata
13	1328	10	3.718	118,138	Rio Grande-Matamoros
48	1194	11	3.343	106,218	Willacy-Pharr-Hargill
92	1098	12	3.074	97,677	Willamar
29	1083	13	3.032	96,343	Willacy-Raymondville
61	984	14	2.755	87,536	Harlingen
43	952	15	2.665	84,690	Hidalgo-Pharr
42	884	16	2.475	78,640	Pharr-Brennan
23	847	17	2.371	75,348	Hidalgo
27	809	18	2.265	71,968	Raymondville-Lyford-Willamar
82	719	19	2.013	63,961	Mustang- coastal dunes
47	704	20	1.971	62,627	Willacy-Delfina-Hargill
62	645	21	1.806	57,378	Harlingen-Benito
28	626	22	1.753	55,688	Willacy-Racombes
55	594	23	1.663	52,842	Sarita-Falfurrias
24	565	24	1.582	50,262	Hidalgo-Raymondville
41	537	25	1.503	47,772	Copita
63	437	26	1.223	38,875	Mercedes
22	354	27	.991	31,492	Lyford-Raymondville-Lozano
71	340	28	.952	30,241	Jimenez-Quemado
12	306	29	.857	27,222	Reynosa-Runn
91	297	30	.832	26,421	Laredo saline-Lomalita
26	295	31	.832	26,243	Raymondville-Mercedes
52	231	32	.647	20,550	Comitas-Delmita
44	73	33	.204	6,494	McAllen
53	56	34	.157	4,982	dune land
1	47	35	.132	4,181	spoil banks
51	46	36	.129	4,092	Comitas
	35717			3,105,461	

Table 3.2 Number of cloud-free pixels (determined by the scatter diagram method) in each of the 36 soil associations on each of the 10 satellite passes.

		Dates of satellite pass									
	Soil	1979	1978								
No.	Code	2/07	5/27	6/06	6/12	6/17	6/23	7/03	7/08	8/15	11/08
1	1	47	47	34	36	44	38	33	47	47	44
2	2	2139	2139	1022	703	1808	1624	1738	2139	2139	1825
3	11	1518	1518	1076	1072	973	1345	1106	1518	1518	1491
4	12	306	306	303	302	56	305	302	306	306	305
5	13	1318	1328	1108	1208	911	1228	1176	1328	1328	1314
6	21	1827	1827	1785	1483	1289	1501	1720	1827	1827	1826
7	22	354	354	275	295	212	335	270	354	354	325
8	23	847	847	836	791	54	828	732	847	847	844
9	24	565	565	481	416	311	462	190	565	565	565
10	25	1345	1345	1191	1028	755	898	502	1345	1345	1338
11	26	295	295	281	234	295	251	103	295	295	292
12	27	809	809	625	778	515	753	620	809	809	795
13	28	626	626	504	382	200	370	2	626	626	614
14	29	1083	1083	856	928	613	741	423	1083	1083	1012
15	31	1648	1648	1207	1287	1257	992	1342	1648	1648	1635
16	41	537	537	517	483	443	431	515	537	537	536
17	42	884	884	861	859	218	849	822	884	884	854
18	43	952	952	875	847	505	874	641	952	952	952
19	44	73	73	73	71	53	70	73	73	73	63
20	45	5483	5483	4945	4790	4007	4300	4343	5483	5483	5025
21	46	1340	1340	1072	1134	952	866	1034	1340	1340	1317
22	47	704	704	571	535	625	502	245	704	704	696
23	48	1194	1194	1048	1018	627	957	175	1194	1194	1174
24	51	46	46	35	32	31	23	30	46	46	46
25	52	231	231	191	210	193	171	153	231	231	228
26	53	56	56	55	56	54	56	56	56	56	55
27	54	2505	2505	1636	1821	1890	1682	1907	2502	2502	2501
28	55	594	594	327	317	458	520	477	594	594	586
29	61	984	984	810	735	277	842	845	984	984	981
30	62	645	645	487	449	296	583	417	645	645	638
31	63	437	437	340	275	143	312	24	437	437	427
32	71	340	340	339	316	251	286	311	340	340	335
33	81	1861	1861	1511	1294	1761	1527	1497	1861	1861	1751
34	82	719	719	402	248	656	630	501	719	719	545
35	91	297	297	223	150	270	202	230	297	297	285
36	92	1098	1098	865	1066	945	947	981	1098	1098	1085
Total		35707	35717	28767	27649	23948	28301	25536	35717	35717	34505

Table 3.3 Soil association median temperatures obtained by the histogram peak method by using only pixels without clouds (WOC) compared with using all pixels including those with cloud contamination (WC) from each soil association for three cloudy satellite passes. The number of pixels at the peak in each comparison is also included; no data are presented for a soil or date when there was no temperature difference.

		Date: 12 Jun 78					17 Jun 78					3 Jul 78				
		Temperature			No. pixels		Temperature			No. pixels		Temperature			No. pixels	
		WOC[a]	WC[b]	Diff.	WOC	WC	WOC	WC	Diff.	WOC	WC	WOC	WC	Diff.	WOC	WC
		°C					°C					°C				
	Code															
1	1											23	15	8	5	9
2	2															
3	11															
4	12															
5	13															
6	21	27	26	1	287	329						30	31	1	385	605
7	22															
8	23						17	12	5	22	24					
9	24	19	18	1	70	85										
10	25															
11	26											13	11	2	22	26
12	27											24	23	1	119	124
13	28											21	-1	22	1	8
14	29															
15	31															
16	41															
17	42															
18	43															
19	44															
20	45															
21	46															
22	47											19	3	16	24	43
23	48											16	-2	14	17	34
24	51															
25	52															
26	53															
27	54															
28	55	25	21	4	31	42										
29	61															
30	62															
31	63	19	18	1	56	71										
32	71															
33	81															
34	82											14	25	11	178	183
35	91															
36	92															

a/ WOC = pixels without clouds.

b/ WC= all pixels including those with cloud contamination.

Table 3.4 Median temperatures of 36 soil associations in the Rio Grande Valley of Texas determined by the histogram peak method for the ten daytime satellite passes (Atmospheric corrections of Table 1.3 not applied).

		1979	1978								
No.	Code	2/07	5/27	6/06	6/12	6/17	6/23	7/03	7/08	8/15	11/08
		°C									
1	1	7	14	20	20	21	19	23	15	22	14
2	2	3	15	15	16	15	15	16	12	15	9
3	11	10	22	20	19	20	20	22	20	24	17
4	12	13	24	20	25	24	24	24	28	27	17
5	13	14	24	20	24	24	24	28	28	24	17
6	21	14	26	28	27	24	28	30	30	32	17
7	22	9	23	21	21	21	18	24	22	23	20
8	23	14	24	21	21	13	24	24	24	28	19
9	24	12	23	21	19	16	19	20	24	27	16
10	25	13	22	19	20	17	19	24	18	27	19
11	26	12	24	20	20	17	19	13	12	28	17
12	27	10	22	21	20	19	16	24	21	24	19
13	28	12	22	19	18	16	16	21	21	26	19
14	29	11	22	20	20	17	17	24	22	24	19
15	31	14	27	26	24	24	24	26	29	30	17
16	41	14	26	30	28	28	29	31	31	33	17
17	42	14	24	20	24	13	24	24	26	28	18
18	43	14	24	21	24	17	24	24	27	27	18
19	44	14	25	20	26	24	24	25	28	28	19
20	45	14	25	28	24	24	24	24	28	29	17
21	46	14	24	29	24	24	24	18	28	31	15
22	47	14	24	20	20	17	20	19	24	28	15
23	48	14	24	20	22	16	21	16	26	28	19
24	51	15	24	21	22	26	22	27	19	28	19
25	52	14	24	21	23	22	24	27	28	31	18
26	53	10	28	19	21	18	19	22	18	21	13
27	54	15	22	24	24	24	22	28	29	31	17
28	55	15	28	24	25	21	20	28	28	28	17
29	61	13	28	20	20	19	24	22	22	26	17
30	62	10	24	22	19	19	20	24	22	22	17
31	63	10	22	19	19	15	17	24	19	24	17
32	71	14	22	28	27	27	28	28	28	29	17
33	81	9	26	20	20	21	20	23	22	21	12
34	82	8	22	11	15	24	21	14	22	22	12
35	91	8	24	20	19	21	20	23	16	19	12
36	92	9	22	20	20	22	16	23	21	23	13

Table 3.5 Nighttime mean surface temperatures and standard deviations, °C, of south Texas soil association areas indicated by HCMM during 1978 and 1979.

Symbol	Distance Inland, km	Soil Associations	Mean Temperature & Standard Deviation, °C									
			30 Jun		23 Aug		10 Oct		21 Oct		26 Feb	
			Mean	S.D.	Mean	S.D.	Mean	S.D.	Mean	S.D.	Mean	S.D.
		(1) Shrink-Swell Clays										
Q	67	Harlingen	19.7	.9	20.1	.7	17.8	.6	14.8	.9	2.3	1.2
R	40	Harlingen-Benito	19.6	.9	20.1	.7	18.1	.6	15.4	1.0	3.4	1.0
S	34	Mercedes	19.7	.9	20.1	.6	17.7	.5	15.5	.6	3.6	1.0
		(2) Loams and clays										
1	34	Laredo-Olmito	19.6	.9	20.1	.7	18.1	.6	15.6	.9	3.9	1.3
2	104	Reynosa-Runn	19.8	.9	19.9	.7	17.7	.6	14.1	.9	2.8	1.1
3	100	Rio Grande-Matamoros	–	–	19.9	1.7	17.3	1.4	14.7	1.3	3.6	1.4
4	154	Catarina-Copita	–	–	20.3	.5	17.0	1.0	13.7	.9	3.3	1.2
5	20	Lyford-Raymondville	19.5	.7	19.9	.5	17.9	.5	15.5	.6	4.1	1.0
6	86	Hidalgo	20.2	.9	20.1	.6	17.5	.5	14.7	.7	3.1	.9
7	58	Hidalgo-Raymondville	19.7	.9	20.0	.5	17.9	.6	15.2	.7	2.8	1.0
8	50	Raymondville	19.6	.8	19.8	.5	17.6	.6	14.6	.8	2.6	.8
9	53	Raymondville-Mercedes	19.6	.8	19.9	.5	17.8	.6	15.1	.7	2.4	1.0
0	23	Raymondville-Lyford	19.3	.8	19.9	.5	17.6	.6	14.8	.8	3.1	1.1
A	43	Willacy-Recombes	19.5	.8	19.5	.5	17.8	.5	15.1	.7	3.0	.7
B	31	Willacy-Raymondville	19.4	.8	19.6	.5	17.6	.5	14.7	.7	3.0	.8
		(3) Loamy Upland										
C	92	Delmita-Randado	20.8	.8	20.6	.5	17.3	.5	14.2	.9	2.3	1.0
D	162	Copita	–	–	20.3	.5	16.4	1.2	14.0	.8	3.7	1.2
E	96	Pharr-Brennan	19.9	.8	19.9	.5	17.2	.5	13.2	2.1	3.3	.9
F	82	Hidalgo-Pharr	20.1	.9	20.1	.5	17.6	.6	14.0	16.1	3.1	1.0
G	115	McAllen	20.1	.7	20.4	.5	17.6	.5	14.3	.6	3.7	.7
H	115	McAllen-Brennan	20.5	4.6	20.0	.6	17.8	.6	13.9	1.0	2.8	1.3
I	134	McAllen-Zapata	20.2	.8	20.3	.6	17.2	.6	14.6	1.0	3.7	1.5
J	54	Willacy-Delfina-Hargill	20.1	.9	20.0	.6	17.7	.8	14.6	1.0	3.1	2.0
K	64	Willacy-Pharr-Hargill	19.9	.8	20.1	.6	17.7	.6	14.5	.8	2.9	1.2
		(4) Sandy Upland										
L	78	Comitas	20.1	.9	20.5	.7	17.4	.6	13.8	.7	1.9	.7
M	78	Comitas-Delmita	20.1	.8	20.0	.5	17.4	.5	14.4	.7	2.7	.8
O	5	Neuces-Sarita	19.5	.8	20.0	.6	17.2	.6	13.7	.8	1.3	1.0
P	68	Sarita-Falfurrias	19.5	.8	19.9	.6	17.4	.7	13.9	.7	1.3	1.0

Table 3.5, Continued

Symbol	Distance Inland, km	Soil Associations	Mean Temperature ± standard Deviation, °C									
			— 30 Jun		23 Aug		10 Oct		21 Oct		26 Feb	
			Mean	S.D.	Mean	S.D.	Mean	S.D.	Mean	S.D.	Mean	S.D.
		(5) Saline Clays and Loams										
U	88	Sejita-Lomalta-Barrada	20.3	1.0	20.7	1.0	19.2	.9	17.2	1.4	6.9	1.9
Y	5	Laredo saline-Lomalta	20.3	1.0	20.6	.8	18.7	.9	16/9	1.3	5.5	2.4
X	11	Willamar	19.6	.8	19.9	.6	18.1	.9	15.6	1.1	4.8	1.5
		(6) Sand and Dunes										
N	5	Duneland	19.6	.9	19.6	.4	17.8	.5	15.0	.7	5.4	1.0
V	14	Mustang-Coastal Dunes	19.7	2.1	22.6	.7	19.9	1.0	18.7	1.2	7.4	1.4

Table 3.6 Equations expressing dependence of daytime temperature (T9) observed by HCMM on distance inland from the coast, mean temperatures and distances, and standard deviations for eight dates in 1978.

Date	Equation	No. of Observ.	r^2
27 May	T(9)=31.87 + 0.010 (DIST)	18	0.075
06 June	T(9)=26.97 + 0.010 (DIST)	24	0.022
12 June	T(9)=26.22 + 0.061 (DIST)	17	0.491*
17 June	T(9)=22.68 + 0.054 (DIST)	20	0.220
23 June	T(9)=25.29 + 0.067 (DIST)	10	0.910**
03 July	T(9)=23.45 + 0.090 (DIST)	15	0.832**
08 July	T(9)=28.88 + 0.060 (DIST)	38	0.604**
15 Aug.	T(9)=32.06 + 0.052 (DIST)	26	0.633**

	Temperature, C		Distance, km	
	Mean	S. D.	Mean	S. D.
27 May	32.9	1.09	104.3	29.3
06 June	27.9	1.72	90.8	26.1
12 June	32.3	1.98	100.4	32.5
17 June	25.8	1.23	56.8	10.6
23 June	32.2	1.67	102.8	23.7
03 July	34.8	2.91	126.2	29.6
08 July	35.4	2.55	109.0	33.3
15 Aug.	38.3	1.93	119.0	29.4

Table 3.7 Weather station identification, description of surroundings, and deviation of daytime Aridity Indexes from the trend with distance inland.

Graph Symbol	Map Ident.	Station name & description	27 May	06 Jun	12 Jun	17 Jun	23 Jun	03 Jul	08 Jul	15 Aug	08 Nov	07 Feb	Sign recurrences minus/plus
A	1	Zapata (rangeland, lake)	-	-	-2.0	-	-	-7.1	-6.6	-5.2	-	-7.8	5/0
B	2	Rio Grande City (rangeland; irrigated agric.)	-2.0	-	-4.0	-1.0	0.3	0.8	-3.1	-7.2	1.4	-0.3	6/3
C	3	McCook (dryland grain sorghum)	1.3	1.9	4.7	3.9	1.0	0.1	2.1	3.3	4.2	2.7	0/10
D	5	Mission (irrigated field crops & citrus)	0.5	0.3	2.4	0.0	0.8	-0.1	1.1	0.6	0.5	0.3	1/8
E	9	Research Farm (irrigated agric.)	0.7	-0.8	1.4	1.2	-1.6	-3.1	-2.1	-0.9	-1.0	-0.2	6/4
F	10	Weslaco (irrigated agric. & urban)	1.1	1.1	0.0	0.6	-0.3	1.4	3.5	0.8	-0.9	-0.8	3/7
G	11	Raymondville (irrigated agric., urban)	0.0	-0.2	-1.0	-0.6	-2.0	-2.0	0.7	-3.0	2.0	-0.1	7/2
H	16	Port Isabel (water, urban, grassland)	-1.2	-2.1	0.5	2.2	0.9	2.6	0.6	0.0	-7.5	-10.5	4/5
I	17	Brownsville (irrigated agric., airport, urban)	-2.7	-1.4	0.5	2.8	0.9	1.9	-1.8	-1.2	-5.1	-1.8	6/4
J	20	Harlingen (irrigated agric., airport, urban)	-1.0	-0.5	-3.2	-5.4	0.1	-	-4.3	-0.6	2.1	0.5	6/3
K	21	McAllen (irrigated agric., airport, urban)	3.8	2.3	3.7	-	2.9	2.9	5.9	3.4	1.2	2.1	0/9
L	23	Falcon Dam (rangeland, lake)	-0.2	-1.2	-0.6	-2.0	0.4	-0.8	-3.9	0.7	3.6	-1.7	7/3
M	25	Las Escobas Ranch (rangeland)	-3.5	-2.6	5.3	-1.6	-2.3	-1.6	-2.3	2.9	-4.5	-2.2	8/2
N	26	Port Mansfield (salt grass, water)	2.6	0.7	1.9	4.0	4.3	5.2	2.8	-0.2	-5.4	-5.9	3/7

Table 3.8 Linear best fit of Aridity Indexes (daytime 9x9 pixel HCMM minus maximum air temperature, °C) with respect to distance inland (X, km), and atmospheric temperature correction used each date.

Date	Atmospheric Correction, C	Equation	Standard Deviation °C
27 May 78	6.43	-0.93 + 0.0377·X	2.65
06 Jun 78	6.83	0.80 - 0.0144·X	1.67
12 Jun 78	7.21	-1.00 + 0.0267·X	3.25
17 Jun 78	8.66	-1.58 + 0.0346·X	3.15
23 Jun 78	9.77	-0.73 + 0.0482·X	2.63
03 Jul 78	5.85	-5.36 + 0.0548·X	3.05
08 Jul 78	8.90*	-2.68 + 0.0755·X	4.58
15 Aug 78	7.73	2.02 + 0.0276·X	3.48
08 Nov 78	0.68	8.36 - 0.0173·X	3.04
07 Feb 79	0.92	4.73 + 0.0014·X	1.53

* Estimated value, radiosonde data missing for this date. Resulting intercept of the equation is consequently an estimate also.

Table 3.9 Mean daily maximum and minimum summertime and wintertime air temperatures (C), by months, for the period 1931 - 1962 (from Orton et al. 1967) for a coastal, an intermediate, and an interior location.

Month	Brownsville Station 17	Weslaco Station 10	Rio Grande City Station 2
May	30.3/21.7	32.2/21.1	34.4/20.4
Jun	32.2/23.9	33.8/22.9	36.6/22.8
Jul	33.4/24.5	34.9/23.4	37.6/23.5
Aug	33.6/24.4	35.1/23.2	37.9/23.2
Sep	31.9/22.9	33.1/21.8	34.7/21.4
Dec	21.9/12.1	22.8/11.2	22.4/8.7
Jan	20.7/11.2	22.0/10.4	21.7/7.9
Feb	22.7/12.8	24.4/12.2	24.4/9.8

4.0 FREEZE HAZARD

4.1 Abstract

Areas of least freeze hazard in our south Texas test area were identified by computer processing of HCMM data from two cold nights, 21 Oct 78 and 26 Feb 79. First, a temperature frequency distribution for individual pixels that comprised our test area identified all pixel locations where temperature was in the top third (Had usable data been available from other cold nights they would have been processed to determine the locations of warmest pixels on those nights also.). Then the locations of warm pixels from both dates were superimposed to form a map showing the areas that had least freeze hazard. A bold symbol was used to identify locations that were warm on both dates. This approach offers promise as a useful method of classifying land areas according to freeze safety. Because of variations in temperature patterns from date to date, information from several freeze or near freeze events should be used in determining the safest areas to grow temperature sensitive crops.

HCMM nighttime data from the serious freeze of 03 Jan 79 could not be validly analyzed for landscape temperatures because an absorbing-emitting atmospheric layer, probably subvisible cirrus (SCi), obscured surface emissions from view of the satellite. The SCi layer, which was not apparent to ground observers, retarded the loss of nocturnal terrestrial radiation to space and slowed the cooling of the landscape and air that night. This ability of satellites to detect an atmospheric layer that blocks the loss of terrestrial radiation should have important application in real-time freeze forecasting. Knowledge of the presence of such a blocking layer is justification for revising upward the minimum temperatures forecast for a cold night. This information could save growers from undertaking expensive freeze protection measures unnecessarily.

On the coldest SCi-free night for which we have HCMM data (26 Feb 79) the HCMM indicated surface temperature surrounding weather stations approximated the minimum air temperatures observed at the stations. In other words, presuming all calibrations were correct, the differences between air temperature and surface temperature at the 0209 CST HCMM overpass were approximately equal to the air temperature declines that occurred between overpass time and the minimums (usually at dawn). The cold-night temperatures of HCMM footprints surrounding the weather stations adjacent to water bodies did not closely match minimum air temperatures because of the mixed scene comprising warm water and cold land.

Cold nighttime temperatures in valleys and depressions were visible in the HCMM thermal image. In two cold air drainage situations investigated, the minimum air temperatures at dawn were lower than the satellite indicated surface temperatures surrounding the stations at overpass time.

The nighttime standard deviation from mean of pixels comprising footprints surrounding weather stations were typically 0.5 C to 0.8 C for cropland and rangeland locations, compared with 0.2 C to 0.4 C for offshore (Gulf of Mexico) water.

4.2 Introduction and objectives

Cold damage to crops usually occurs on clear, calm nights when radiational energy loss from the landscape results in critical vegetation temperatures. The low atmospheric moisture and lack of clouds usually associated with freeze events are ideal for observations by satellites. The HCMM overpass time is late enough to well establish nighttime surface temperature patterns.

Protection of vegetable and fruit crops against winter and spring freeze damage is becoming more difficult and expensive because of higher cost heating fuel. This makes it important to avoid planting temperature-sensitive annual and perennial crops in the coldest portions of local areas.

The objective was to test the suitability of HCMM data for identifying areas of least freeze hazard in south Texas. "Safe" warm areas and hazardous cold spots were to be examined for recurrence by comparing satellite data from all cold nights. Techniques developed in this study should be applicable to other areas where subtropical crops are grown (California, Arizona, Florida). The method may also be useful in selecting sites for deciduous fruits (prevention of bloom damage) and other temperature-sensitive crops.

A further objective was to determine the relationship between minimum air temperature and the surface temperature surrounding weather stations at the HCMM nighttime overpass.

4.3 Methods

The HCMM data were processed according to steps a through u (excluding f, g, h, o, p and q) outlined in section 2.1.1. The surface temperatures used in this chapter were corrected by a radiative transfer model (J. C. Price, personal communication) using 0600 CST radiosonde data from Brownsville, Texas applied to the entire test area.

4.4 Results

4.4.1 Identifying areas of least freeze hazard

Figure 3.11 shows the portions of the four southmost Texas counties that were warmest on two cold nights (21 Oct 78 and 26 Feb 79). Temperature patterns of additional cold nights would have been incorporated into the figure had more HCMM data been available. The freeze night of 03 Jan 79 for which HCMM data are on hand could not be used because the surface temperatures were obscured by an absorbing-emitting atmospheric layer believed to be subvisible cirrus (see section 4.4.2).

In preparation of Figure 3.11 a map-grid pixel was considered to be warm if its temperatures fell in the top third of all test area pixels. The darkest symbol used in the figure represents locations that were warmest on both dates; the lighter symbol indicates warmest on only one date. Blank areas were never in the top third of temperature, except that water bodies which were the warmest feature of the landscape have been left blank to facilitate identifying their location on the map.

The figure shows an extensive warm area in the immediate vicinity of the coastline (right side of figure). Apparent in these nighttime data are heat islands adjacent to inland water bodies (outlined). Other heat islands surround dots that locate the centers of cities and towns. The map shows warm areas in unexpected locations such as portions of Starr County (left side).

Such analysis based on several freeze nights could guide in selecting areas to plant temperature-sensitive crops. This is provided other factors such as availability of irrigation water and/or freedom from soil salinity are also favorable. The final site based on radiometric temperature surveys should consider the effects that vegetation density (amount of exposed bare soil) and emissivity may have had on a classification at a particular site.

4.4.2 HCMM-detected protective absorbing-emitting atmospheric layer during freeze night

A radiation absorbing-emitting layer prevented accurate assessment of surface temperatures on the only freeze night for which HCMM data are available for our test area, 03 Jan 79. The atmospheric layer is believed to have been subvisible cirrus (SCi). This was unexpected to ground observers because the sky was visibly clear, as it usually is on radiational cooling nights when energy loss from the landscape causes critical vegetation temperatures. The hourly weather records from the FAA McAllen, near station 21 (see Figure 1.3), also indicated the sky was clear. We had not observed absorbing-emitting layers in any of the five NOAA-2 through NOAA-5 cold night scenes of the test area that we had examined over a five year period.

The ability of the emissive (IR) channel of HCMM to detect essentially invisible absorbing-emitting atmospheric layers is discussed in section 2.2.2 of this report. The HCMM overpass on the freeze night occurred at 0205 CST on 03 Jan 79. The portions of the scene covered by the absorbing-emitting layer had an indicated temperature everywhere the same, or essentially so; much more uniform than landscape features outside the influence of the blocking layer.

Figure 4.1 infers that much of the test area was hidden from satellite view by a SCi layer during the HCMM nighttime overpass on 03 Jan 79. In the figure, temperatures at representative sites (means of 3x3 pixel footprints) are plotted against temperatures of the same sites in the NOAA-2 data of the historic 21 Dec 73 freeze (Nixon, Phinney and Arp, 1974; Nixon, Phinney and Gautreaux, 1978).

The figure shows that the representative sites (from which cities and sites adjacent to water bodies were excluded) had a narrow temperature range (-1.5 C to -2.4 C) on 03 Jan 79. These data were apparently dominated by the effect of the SCi layer. In contrast the satellite indicated temperatures for the same sites ranged from +2.0 C to -5.3 C during the 21 Dec 73 event, giving no suggestion of the presence of a SCi layer on that night.

A comparison of atmospheric-corrected surface temperatures (means of 3x3 pixel footprints) experienced at the same representative sites on cold, clear, SCi-free nights is made in Figure 4.2. In this case, 26 Feb 79 is compared with 21 Dec 73. Both dates have considerable temperature ranges. Even though several years elapsed between events the land use patterns have changed little in the interim.

A consistent temporal temperature relationship among sites would have resulted in a well defined linear grouping of points that plot diagonally across the figure from cold to warm. This was not the case, although there was a weak trend in this direction.

A further consideration entering into a comparison of the cold nights is that the NOAA-2 overpass was at 2107 CST December 73 in contrast to the HCMM overpass at 0209 CST on the later date. Thus the observations by satellite were made at different stages of nighttime landscape temperature development and this might have influenced the relationships among the stations.

However, practical conclusions related to freeze protection cannot be drawn from the figure because 26 Feb 79 was not a serious freeze event and because the overpasses were not at the same time of night. In any case, verification by study of additional freeze events would be prudent. The tentative conclusion to be drawn from Figure 4.2 is that comparative freeze damage from site to site varies from one event to another, as indicated by the wide scatter of points.

Meteorological data obtained on the night of 02-03 Jan 79 illustrate the effectiveness of an absorbing-emitting atmospheric layer in halting noctural temperature decline. Typically on clear, calm nights characteristic of radiational freezes, the air temperature continues to decline until a minimum is reached at dawn. In contrast, thermograph data (Figure 4.3) shows what happened during the night under discussion. This example is from station 9 (Figure 1.3) where there was a customary decline from the afternoon high to 2320. This drop of temperature from 4.4 C to -4.5 C in less than 9 hours forbode disaster to the subtropical crops and vegetation of the Lower Rio Grande Valley during the remainder of the night. The presence of clouds or a high dew point reading would have given hope of averting a continuing temperature decline. But visible clouds were not present and the dewpoint of -12.7 C was far below the prevailing temperature.

If the air temperature trend established before 2320 had continued throughout the night (dashed line of Figure 4.3), a minimum temperature of about -8.0 C would have been reached at dawn (Nixon 1974). However, the development of the atmospheric blocking phenomenon, invisible to the human eye but detectable in the HCMM emissive scene, caused a reduction of the net terrestrial radiation during the remainder of the night and a consequent air temperature increase. The surface air drift during this time was insufficient in itself to account for the marked change in temperature trend. Apparently the reduction of net-radiative energy loss from the surface resulted in a reapportionment of the soil heat flux to heating the air.

It appears that the absorbing-emitting atmospheric layer started to affect air temperatures at some locations between 2200 and midnight on the cold night of 02-03 Jan 79. Table 4.1 shows that nighttime temperature trends were moderated or reversed at or before midnight at stations 3, 4, 9, 13, 17 and 25 (Figure 1.3). These stations have a west-northwest east-southeast alignment across the test area. The moderation was short lived at western stations 3, 4, and 25 as the downward decline resumed at these sites. Haddock and Connolly (1979) have reported the thermograph of station 4 for this night. At stations 5, 11 and 21 on either side of the main alignment, the effects of radiation blockage were delayed until 0200 or later. The Rio Grande City area (station 2) benefited little, if any, from the atmospheric layer. At the time of HCMM overpass, the Vaso Marte Gomez, a reservoir in Mexico opposite Rio Grande City, was outside the influence of the atmospheric layer and showed clearly in the emissive scene. Delta Lake and La Sal Vieja in the vicinity of station 11 (Figure 1.3) could also be clearly seen on the emissive band imagery.

Falcon Reservoir was obscured in the HCMM emissive scene. Minimum air temperatures near the reservoir were -3.3 C at station 1 and -5.6 C at station 23. At station 1 the minimum was 0.6 C warmer than it had been the night before. These relatively warm air temperatures for locations so far inland can be partly attributed to their proximity to Falcon Reservoir, but they were mainly due to the absorbing-emitting atmospheric layer. These stations reached minimums of -6.7 C and -7.2 C, respectively, in the December 1973 freeze which was said to have been generally less severe than the January 1979 freeze.

The cold night of 02-03 Jan 79 caused serious freeze damage to citrus, sugarcane, vegetable and ornamental plants, but the damage was not nearly as disasterous as it would have been had the radiation absorbing-emitting atmospheric layer not been present. It can be seen from Figure 4.3 that the number of degree-hours of air temperature below some critical value would have been greater in the case of uninhibited temperature decline (dashed curve). The respective areas under the -3 C line suggest the relative extent of damage that would have been sustained by crops with that critical temperature.

Sugarcane freeze damage studies

It was hoped that the HCMM coverage on the freeze night of 02-03 Jan 79 would provide opportunity to verify the applicability of thermal satellite data to estimating relative amounts of freeze damage sustained by crops. The presence of the absorbing-emitting atmospheric layer prevented the test for which preparations were complete. The Rio Grande Valley Sugar Growers Association participated in the preparation by providing the coordinates of field loading sites so that the HCMM indicated surface temperatures of areas surrounding these sites could be correlated with sugarcane yields and mill processing records for these sites.

Surface temperatures observed with the NOAA-2 satellite on the occasion of the 20-21 Dec 73 freeze had correlated well with sugar contents of the crop harvested following that cold night (Nixon, Phinney and Gautreaux 1978). These comparisons between freeze-night satellite indicated temperatures at field locations and subsequent sugar contents of mill processed sugarcane showed that the freeze damage was least where the satellite-indicated surface temperatures were warmest.

According to t-tests made on data from individual field locations the correlations between freeze-night temperatures and percent commercially recoverable sugar was significant at $p = 0.10$. Since the sugar content of freeze-damaged sugarcane declines as it stands unharvested in the field following the freeze, the F-ratio was also calculated to take into account the multiple correlation of harvest dates and satellite sensed temperatures with recoverable sugar. The F-ratio for these test conditions was significant at $p = 0.05$. When satellite temperatures were adjusted for the additional temperature decline between overpass and the minimums at dawn the data were significant at $p = 0.01$.

Importance of absorbing-emitting atmospheric layer

The ability of satellites to detect the presence of an atmospheric layer that blocks the loss of terrestrial radiation to outer space should have important application in real-time freeze forcasting because as soon as the nocturnal radiation loss from the landscape is blocked, the rate of air temperature decline lessens. Consequently, the presence of a blocking layer justifies revising upward the minimum temperature forecast for the cold night. In borderline temperature conditions a more accurate low temperature forecast could save growers from undertaking expensive freeze protection measures unnecessarily.

Currently, polar orbiting weather satellites with a thermal band pass over the U.S. nightly. Since the thermal band responds to atmospheric layers such as developed on the night of 03 Jan 79, the potentital value of real-time processing of their data in conjunction with freeze warnings and advisories for growers is apparent. The development and operational testing of such procedures might be carried out under the multiagency AgRISTARS program. Under this program episodic events such as freezes are of high interest as an early warning of crop losses. The data would also be useful to the sugarcane, citrus and other fresh commodity industries

who need to react quickly to freezes. As mentioned above, the sugar content of the sugarcane stalks decreases fastest in the fields most seriously damaged so that such data would be a valuable tool in re-prioritizing harvest schedules following freezes to minimize sugar yield losses.

If multiple uses--such as real-time advisories to growers during the freeze, estimates of crop losses as they affect the market, and commodity industry quick reaction decisions--are all made from essentially the same data, then there is little doubt the effort can be cost effective. For the Lower Rio Grande Valley of Texas, there would only be three to five nights of interest in a normal winter. However, all parts of the data acquisition, transfer, interpretation and rapid dissemination system would need to be ready to function on about one day's notice. The data would not have sufficient resolution to make decisions about individual fields, but the gradient of temperature from the coast, relative temperature differences of production areas several kilometers apart and presence of any protective cloud or atmospheric vapor layer over any portion of the production area would be apparent.

4.4.3 Comparison of Tmin at weather stations and THCMM for weather station sites on cold nights

On clear, radiational freeze nights it is the temperature of vegetation that determines how much crop damage is sustained. Customarily the likelihood and extent of crop damage is estimated from air temperatures.

Table 4.2 compares the minimum air temperatures (Tmin) measured at weather stations with atmospherically corrected HCMM temperatures (THCMM) indicated for the footprints surrounding the stations. The station numbering in the table corresponds to locations in Figure 1.3. The size of the footprint varies from one pixel (20-seconds longitude by 20-seconds latitude) to 9x9 pixels (3-minutes longitude by 3-minutes latitude).

A study of this table for 26 Feb 79 shows that the minimum air temperatures which occurred several hours after overpass were roughly estimated by the HCMM indicated surface temperatures. In other words, presuming all calibrations were correct, the difference between air temperatures and surface temperatures at HCMM overpass at 0209 CST were approximately equal to the air temperature declines that occurred between overpass time and the minimums (generally at dawn).

While "on the average" the above statement is valid, the table shows that the relationship varied from site to site. Especially notable is Port Mansfield (26) where the surface temperature exceeded air temperature by 4.5 C for the single pixel to 2.4 C for the 9x9 footprints. The close vicinity of water at this station caused the discrepancy of temperatures. As the footprints increased in size there was a continuing improvement due to the influence of increased land area (land was colder than water).

An opposite effect occurred at Las Escobas Ranch (25) where increasing the footprint size increased the average surface temperature. Cold air drainage caused this rangeland site to have the lowest minimum air temperature of any station. Examination of the USGS Las Escobas Ranch 7.5-minute topographic quadrangle sheet shows the site to be on a flat area near the confluence of two ephemeral streams. The drainage ways apparently facilitated cold air drainage. As the footprints size was increased it included more sloping land, most of it higher in elevation and outside the cold pocket, thus resulting in a higher average temperature.

Apparently, cold air drainage was also the cause of the low minimum air temperature at the Rio Grande City (2) station. The location of this station, 5 km west of the city, is on the Rio Grande River flood plain near the toe of land that slopes from the upland. Table 4.2 shows the minimum air temperature at this site to be about 3 C lower than the satellite indicated temperatures at its overpass.

Several examples of the effects of cold air drainage are visible in the HCMM photographic image of 26 Feb 79 night for western Starr County (left portion of Figure 1.3 and Figure 3.11). This area has much more topographic relief than the remainder of the test area.

The degree of nighttime thermal homogeneity of the landscape is indicated by the standard deviations (second data line of each site) and standard errors (third data line). The marked differences of temperature between water and land are reflected in the large standard deviations (>1.5 C) of footprints that included both water and land: Zapata (1), Port Isabel (16), Port Mansfield (26) and the largest footprints at Falcon Dam (23). Several sites were thermally homogeneous, such as McCook (3), and had standard deviations less than 0.3 C.

4.5 Literature cited

Haddock, Don and Chan Connolly. 1979. Major freeze--Lower Rio Grande Valley of Texas. NOAA-USDA Weekly Weather and Crop Bulletin 66(3):10-13.

Nixon, P. R. 1974. Unit thermogram for minimum temperature prediction. Agricultural Research Service, Weslaco, Texas. Unpublished report. 3 pp.

Nixon, P. R., D. E. Phinney, and G. K. Arp. 1974. Mapping cold-night surface temperatures of the Lower Rio Grande Valley. Journal of the Rio Grande Valley Horticultural Society. 28:85-90.

Nixon, P. R., D. E. Phinney, and A. R. Gautreaux. 1973. Estimating sugarcane damage from regional freeze night temperature measurements. International Sugar Journal. 80:232-237.

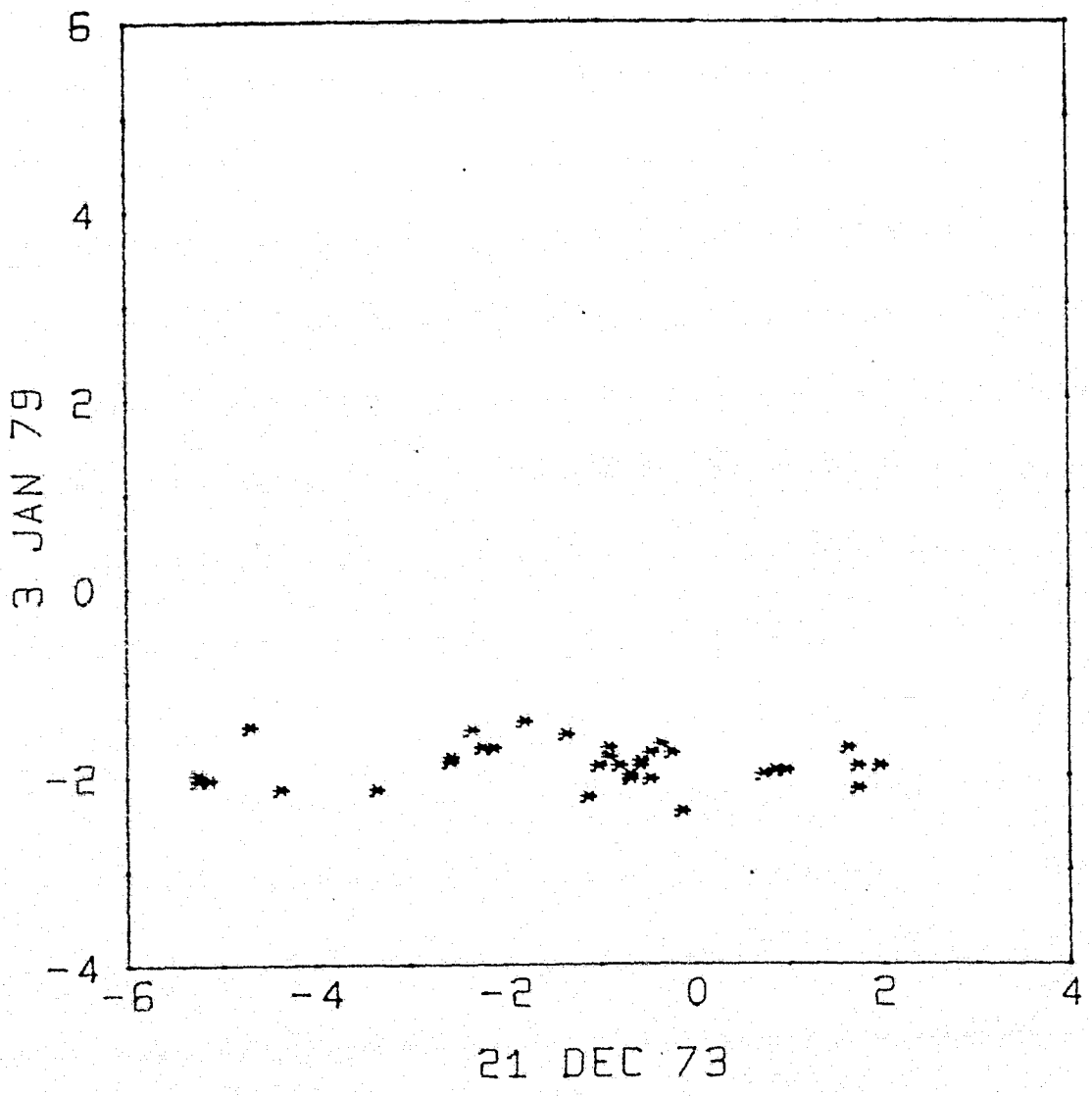

Figure 4.1 Temperature of 3x3 pixel samples (T3, C) of representative sites, excluding cities and water bodies, for two cold nights (03 Jan. 79 and 21 Dec. 73).

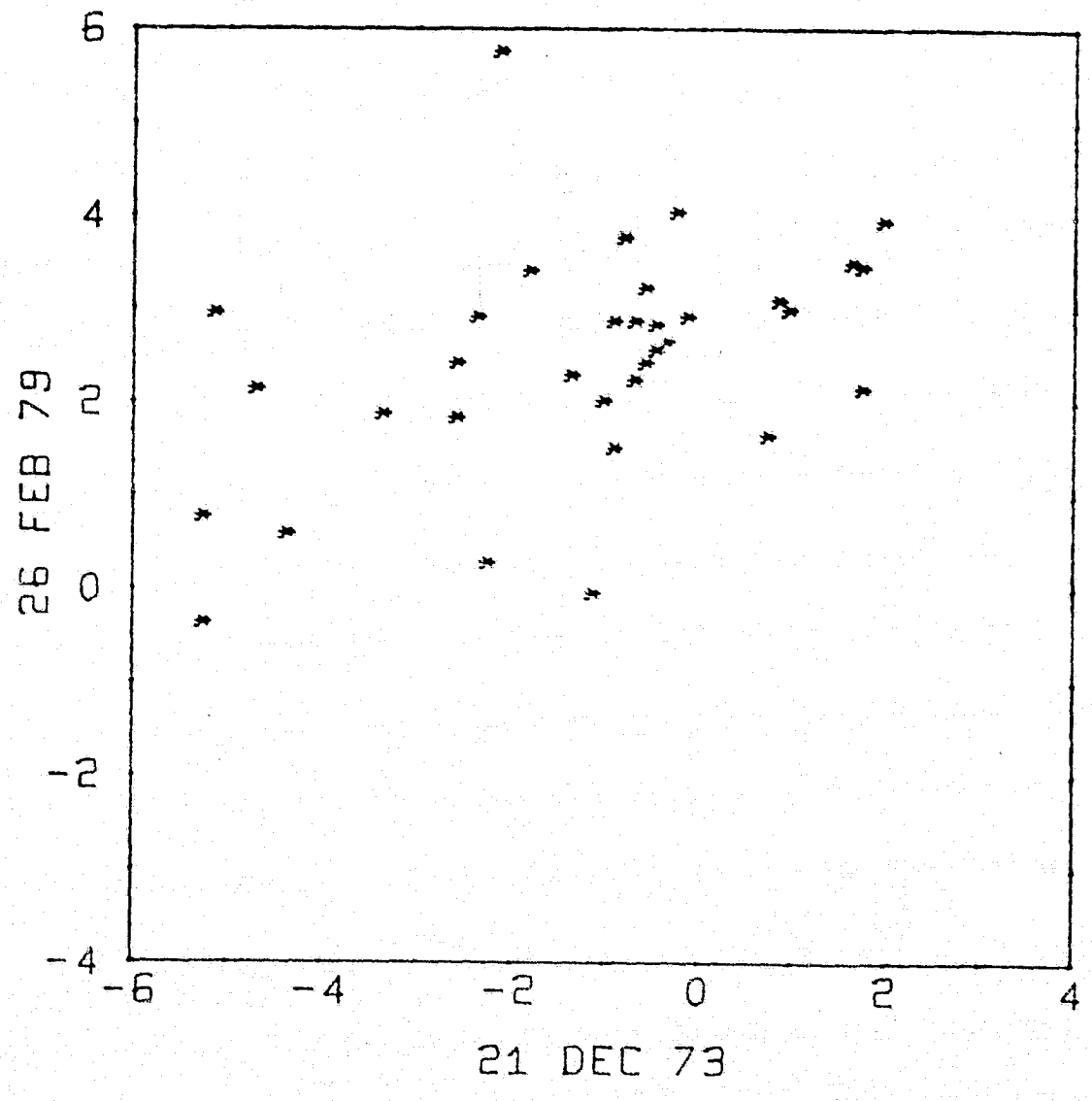

Figure 4.2 Temperature of 3x3 pixel samples (T3, C) of representative sites, excluding cities and water bodies, for two cold nights (26 Feb. 79 and 21 Dec. 73).

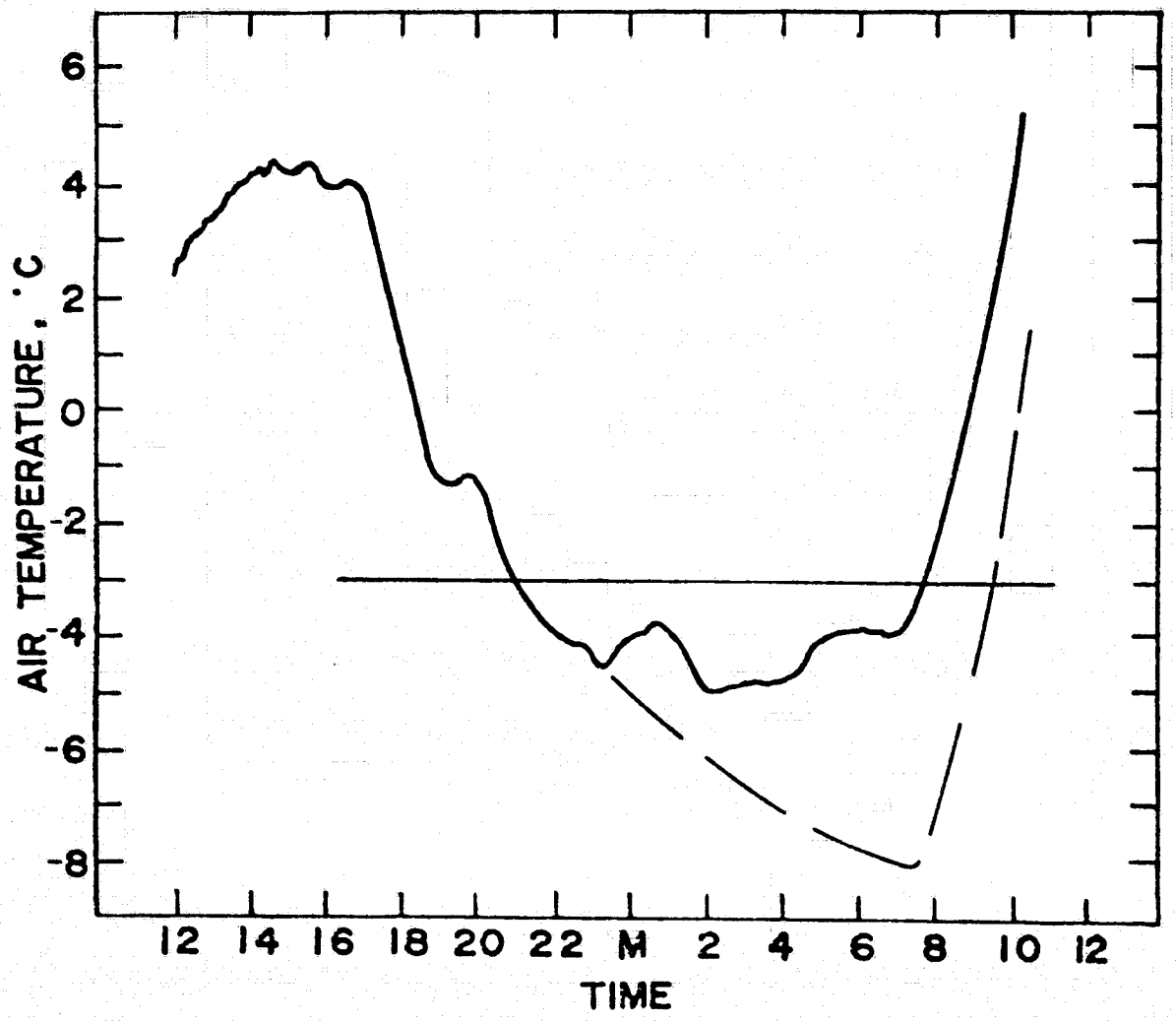

Figure 4.3 Thermograph trace from the Weslaco Environmental Station (station 9) spanning the 02 - 03 Jan. 79 freeze.

Table 4.1 Air temperatures at weather stations in the Lower Rio Grande Valley test area during the freeze of 02 - 03 January 1979.

Station		Time												
Name	No.	1900	2000	2100	2200	2300	0000	0100	0200	0300	0400	0500	0600	0700
Rio Grande City	2	-0.6	-1.1	-1.1	-2.2	-2.8	-3.3	-3.9	-3.9	-5.0	-6.1	-6.7	-7.2	-7.2
McCook	3	-0.6	-1.7	-1.7	-2.8	-3.9	-3.9	-3.9	-4.4	-4.4	-5.0	-5.6	-5.6	-6.1
Texan Gardens	4	-1.1	-1.7	-3.3	-3.9	-3.3	-3.3	-3.3	-3.9	-4.4	-5.0	-5.6	-6.1	-5.0
Mission, Bates Power	5	-0.6	-1.1	-1.7	-2.8	-2.8	-3.3	-3.3	-4.4	-5.0	-6.1	-6.7	-6.7	-5.0
Weslaco Environ. Sta.	9	-1.2	-1.2	-3.0	-3.8	-4.2	-3.9	-3.8	-4.9	-4.8	-4.7	-4.0	-3.9	-3.8
Raymondville	11	-1.1	-2.2	-1.1	-2.2	-3.9	-5.0	-5.0	-5.6	-5.6	-5.6	-5.6		-5.6
Adams Gardens	13	-2.2	-2.8	-3.9	-4.4	-4.4	-5.0	-4.4	-4.4	-3.9			-3.9	-3.9
Brownsville	17	-0.6	-1.1	-1.7	-2.8	-2.8	-2.8	-3.3	-2.8	-3.3	-2.2	-2.8	-3.3	-2.8
McAllen	21	1.7	1.1		-0.6	-1.1	-1.7	-2.2	-3.9	-3.3	-4.4	-3.3	-3.9	-3.9
Las Escobas Ranch	25	-0.8	-1.8	-2.6	-3.3	-4.8	-4.4	-2.6	-3.3	-3.3	-4.6	-4.7	-5.6	-6.1

Data for all stations except 9 and 25 are from Texas Citrus Mutual Freeze Report No. 1, dated 05 Jan. 79. Data were reported to the nearest degree F.

Table 4.2 Minimum air temperatures(T_{Min}) and nighttime HCMM radiometric surface temperatures(first lines) at weather station locations on 26 Feb. 79, standard deviations(second lines) and standard errors(third lines) of multipixel footprints.

Sta. No.	Sta. Name	T_{Min} (°C)	HCMM Radiometric Surface Temperature, C 1x1	3x3	5x5	7x7	9x9
1	Zapata	6.67	7.95	8.93	9.30	9.27	8.95
				1.75	2.40	2.63	2.85
				.58	.48	.38	.32
2	Rio Grande City	0.00	2.83	3.37	3.54	3.64	3.61
				.40	.61	.77	.80
				.13	.12	.11	.09
3	McCook	2.78	1.20	2.15	2.23	2.29	2.10
				.50	.63	.54	.61
				.17	.13	.08	.07
5	Mission	1.67	2.42	2.74	2.86	2.65	2.68
				.63	.74	.75	.75
				.21	.15	.11	.08
9	Research Farm	2.22	3.23	2.60	2.39	2.41	2.38
				.90	.73	.69	.70
				.30	.15	.10	.08
10	Weslaco	3.33	3.23	3.28	2.94	2.63	2.72
				.58	.75	.77	.76
				.20	.15	.11	.08
11	Raymondville	1.67	4.04	3.65	3.36	3.07	2.78
				.98	.96	.90	.85
				.33	.19	.13	.10
16	Port Isabel	11.11	9.49	10.86	11.17	11.22	11.19
				1.51	1.60	1.86	2.07
				.50	.32	.27	.23
17	Brownsville	3.89	3.23	3.10	3.23	3.53	3.74
				.60	.76	.85	.80
				.20	.15	.12	.09
20	Harlingen	3.33	4.44	3.63	3.55	3.28	3.33
				.85	.94	1.10	1.17
				.28	.19	.16	.13
21	McAllen	4.44	3.23	4.04	3.80	3.75	3.74
				.49	.57	.62	.76
				.16	.12	.09	.08
23	Falcon Dam	4.44	3.64	3.50	3.63	3.93	4.21
				.28	.78	1.04	1.55
				.09	.15	.15	.17
25	Las Escobas Ranch	-0.67	1.61	2.42	2.74	3.09	3.25
				.70	1.05	1.20	1.22
				.23	.21	.17	.14
26	Port Mansfield	8.33	12.85	11.77	11.20	10.95	10.77
				1.75	2.07	2.31	2.55
				.58	.42	.33	.28

5.0 PLANTING DATE ADVISORY

5.1 Abstract

HCMM radiometric temperatures on a clear night early in the 1979 planting season (26 February), when there was little atmospheric attenuation, were very close to minimum air temperature, 3.1 C. Minimum temperature at the 10-cm soil depth was about 10 C higher. The radiometric temperature of the sandy uplands (1.4 C) differed from that of the loams and clays (3.3 C). Three variables--average daily air temperature, insolation at ground level, and extraterrestrial radiation--accounted for from 89 to 93% of the variation in maximum daily (Tmax), minimum daily (Tmin), and average daily ($\overline{T5}$) temperature at the 5-cm soil depth in dry plots and for from 88 to 91% of the variation for wet plots. Standard errors of the estimate of Tmax, Tmin, and $\overline{T5}$ from the three environmental variables ranged from 1.5 to 1.9 C.

Estimation of planting depth soil temperatures from radiometric temperatures appears feasible, provided the relation between planting depth and surface temperature is understood. The estimates should be superior to estimates currently made from air temperature observations and can probably have coefficients to tailor them to major surface texture groupings (soil associations).

5.2 Introduction and objectives

The flow of heat in soils follows linear-flow laws, the same as for the flow of water and air in soils. The calories of heat Q transmitted per unit area per unit time through a soil in the x direction, where the temperature is T and the temperature gradient is dT/dx, is given by:

$$Q = -K \frac{dT}{dx}$$

where K is defined as the thermal conductivity. The negative sign is used because heat flows in the direction of decreasing temperature. In soils K can vary considerably with moisture content and soil type. It can be shown (Kirkhum, 1964) that vertical heat flow is expressed by

$$k \frac{\partial^2 T}{\partial x} = \frac{\partial T}{\partial t}$$

where the thermal diffusivity $k=k/\rho c$, and ρ is density and c is specific heat.

In this manner diurnal and annual soil surface temperature fluctuations are transmitted to the deeper soil layers. Practical implications (Chirkov, 1979) of the above equations are that: (1) At a given depth in the thermallly active soil zone the interval between minima and maxima is 24 hours and 12 months; (2) The amplitude of the temperature range decreases in geometric progression in relation to the arithmetic progression of depth; and (3) There is a lag in occurrences of minimum and maximum temperatures with depth. This time lag is directly proportional to depth.

Soil temperatures are critical for germination of crop seeds. For example, it is recommended that seed of corn, sorghum, and cotton not be planted in the spring until average soil temperature at the 2-inch (5-cm) depth reaches 55, 60, and 65 F (or 13, 15, and 18 C), respectively, and a warming trend is forecast for the subsequent five days. Coarse-textured soils (sands and sandy loams) are better drained, retain less water and warm up earlier in the spring than fine-textured soils (clays and clay loams). Thus synoptic soil radiant temperatures should relate generally to soil association patterns if antecedent precipitation was similar and the emissivities are the same for all soil types. Then, because of the correlation between surface temperature and temperatures at shallow soil depths, one would expect radiometric surface temperatures to give guidance on adequacy of soil temperature for planting.

In this task, we proposed to examine the nighttime soil temperature patterns in the HCMM data for one or more nights as spring planting time approached and compare them with the soil association patterns as mapped by the Soil Conservation Service. Also available were (a) daily maximum and minimum soil temperature at the 10-cm depth for four monitoring sites during the period 01 Jan through 31 Mar 79, which the NWS, NOAA, used for planting advisories, and (b) soil temperatures in wet and dry plots we maintained at the Research Farm, along with the environmental station, during the HCMM investigation period. The soil temperatures recorded by NWS observers could be compared with the HCMM temperatures, and the continuous wet and dry plot and environmental station data enabled an examination of the dependence of soil temperature at various depths on the ambient environmental variables.

Toy et al. (1978) produced and reported linear equations relating monthly, seasonal, and annual air temperature (F)--which is widely available in climatic summaries--and soil temperature (F) at the 10-cm depth for eight widely separated sites in the U.S.. Mean monthly soil temperatures, based on data from all stations combined, could be estimated to ±2.3 C from the air temperature data. Meikle and Treadway (1979) used fourth degree polynomials to estimate maximum and minimum temperature at the 10-cm depth from air temperature for 114 U.S. locations. For Weslaco, Texas (Willacy fine sandy loam soil) the standard error of the estimate of soil temperature was 2.4 C for the maximum and 2.0 C for the minimum. Bonn (1977) found that the coefficients relating radiometric temperature (equivalent blackbody temperature observed with a Barnes PRT) and thermistor probe temperatures are close to unity for bare soil but vary with the seasons for vegetated surfaces. The closest correlations between remotely sensed temperature was with surface soil temperature for bare ground and with air temperature at the half canopy height over vegetated areas.

5.3 Methods

There were three sources of data for looking at soil temperature as it related to planting crops: (a) daily maximum and minimum soil temperature at the 10-cm depth for the period 01 Jan through 31 Mar 79 from four sites within the test area as made by volunteer observers for the NOAA NWS office at Brownsville, (b) HCMM radiometric temperatures for the night of 26 February 1979, and (c) soil temperature for the first 90 days of 1979 (except for a few days when equipment was down) as measured with thermocouples in the small wet and dry plots maintained at the Research Farm. Of these data sources "a" and "c" are described somewhat more fully in section 1.2.8.

The data for the 10-cm soil depth at four sites and the maximum and minimum daily air temperature for these same sites were tabulated, keypunched, and graphed for each site to display the time trends and the relations between air and ground temperature.

The radiometric temperatures from HCMM were displayed in relation to soil associations by the same procedures as for other dates under Synoptic Analyses (see section 3.4.2).

For the thermocouple data of the wet and dry plots, the methods of acquisition and reduction were as follows:

The center areas (about 1.5 m dia.) of each of two soil plots 6.1 m square and 6.1 m apart were instrumented with type T thermocouples at the following depths: 0.5, 5, 10, 20, and 100 cm. In order to reduce "stem conduction error" at the thermocouple junctions special wire configurations were incorporated which placed the first several centimeters of wire from the junctions in the junction isotherm. Each junction buried 5-cm and deeper was located in a spiral of 20-gage lead wire totaling about 50 cm in length (Figure 5.1A). Because the thermal conductivity of copper is about 10 times that of the mating copper-nickel alloy about 45 cm of the wire in the spiral was copper and the remainder was the mating alloy wire.

Because the vertical temperature gradient in the vicinity of the 0.5-cm depth thermocouples was so steep even more precautions were taken to minimize stem conduction and to preserve the integrity of the thin layer of soil above the thermocouple junctions. For these thermocouples the junction was part of a grid consisting of 0.13-mm dia. wire wound on a rectangular frame made of vinyl-insulated, 20-gage copper wire as shown in Figure 5.1B. The 20-gage lead wire was joined to the grid wire outside the frame. An electrical insulating spray material was applied to all uninsulated wire surfaces in both junction designs.

Each plot had 3 independent thermocouples at the 0.5-cm depth and 3 thermocouples connected in parallel at the 5-cm depth. One thermocouple was located at each of the remaining depths. In addition, two shielded, air-temperature sensing thermocouples were mounted on a nearby tower at .5 m and 1.5 m heights. All of these instruments terminated at a Brown, 20-point, strip-chart recorder located in an instrument shelter.

The Brown recorder was timed to scan the thermocouples once every hour. The "wet" plot was watered weekly if rainfall did not exceed 0.7 of the amount of weekly pan evaporation less the sum of the antecedent rainfall as described by Linsley, et al. (1958) using a factor of 0.9. The "dry" plot received only rainfall. Data were transcribed from the strip charts to IBM cards preparatory to computer processing.

5.4. Results

5.4.1 Soil association and NWS observer temperatures

Figure 5.2 summarizes the mean temperature, of all HCMM pixels representative of each soil association, and the standard deviation for each soil association in the HCMM data for 26 February 1979. The symbols used are decoded in Table 3.5. It is evident that the scatter of temperatures versus distance (km) inland of soil association centroids has a "V" pattern. Sand dunes (V symbol) on Padre Island and saline coastal clays have temperatures of about 7 C. At the bottom of the "V" pattern at about 60 km inland, the "P" and "O" represent the sandy upland soil associations, Sarita-Falfurrias and Nueces-Sarita which had radiometric temperatures of about 1 C. T, I, and D at the upper right arm of the "V" with radiometric temperatures of about 4 C identify the loamy upland inland soil associations Jimenez-Quemado, McAllen-Zapata, and Copita, respectively. When the soil associations were grouped by soil surface texture into six categories and displayed as in Figure 5.3, it was obvious that the mean temperature (1.4 C) of the sandy uplands (category 4) differed from that of the loams and clays (category 2) which had a mean temperature of 3.3 C. The two categories are equidistant from the coast and the standard deviations do not overlap. The shrink-swell clays (category 1) are a fraction of a degree cooler than the loams and clays (category 2) even though the shrink-swell clays are closer to the coast.

By comparison, the trend line in soil temperatures at the 10-cm depth, as measured by NWS observers with indicating maximum and minimum thermometers was a minimum on 09 Feb at all four sites; Adams Gardens (12.5 C), Mercedes (13.9 C), Weslaco (13.3 C), and McCook (12.5 C). Thereafter the temperature increased an average of 0.21 C per day through the end of March. On 26 Feb, the mean daily 10-cm soil depth temperature estimated from the trend line was 16.6, 16.2, 17.3, and 16.4 C at Adams Gardens, McCook, Mercedes, and Weslaco, respectively and the minimum averaged 12.7 C. Thus the soil was warm enough to plant corn and sorghum, but it was still about a week too early to plant cotton.

The average minimum air temperature at these four sites on 26 Feb was 3.1 which is very close to the mean radiometric temperature of Figure 5.2.

In summary, although there are many sources of variation in the data (differing vegetative cover conditions, mixture of irrigated and nonirrigated sites) the data show that radiometric temperature of the sandy uplands (1.4 C) differed from the temperature of the loams and clays (3.3 C) on a night of strong radiational cooling and that the radiometric temperatures were close to the minimum air temperatures that night.

5.4.2 Wet and dry plot temperatures

Although soil temperature data was recorded hourly at 5 levels, in each plot from late in 1978 until the middle of 1980, only the complete data for the three days around the HCMM overpass date of 26 Feb 79 was reduced and evaluated in detail together with selected daily data points during the period from 01 Jan through 31 Mar 79.

The 26 Feb, 3-day period data provides an example of how wet and dry soil temperatures varied as functions of depth and time, as shown in Figure 5.4 and 5.5. At the 100-cm depth the diurnal variation disappeared from the temperature traces leaving an almost constant average daily temperature increase of 0.1 C for the wet plot and 0.23 C for the dry plot for this 3-day period. The 20-cm traces exhibit time lags ranging from three to eight hours from the 0.5-cm temperature traces. Air temperature (shown in Figure 5.6) exhibits a more consistent lag of 1.5 to 2.6 hours from the 0.5-cm temperature traces. The variation in surface temperature changes seems to be the chief cause of the wide variation in the lag times of the 20-cm deep soil temperatures.

Figures 5.6 and 5.7 illustrate how the wet and dry plot soil temperatures compared with each other at depths of 0.5, 5, 20, and 100-cm. The average difference between the wet and dry soil temperatures for this period is 3.7 C at 0.5-cm deep, 3.3 C at 5-cm, 3.3 C at 10-cm (not shown), 2.9 C at 20-cm and 0.9 at 100-cm.

The low air temperature of 26 February, lower than any wet and dry plot soil temperature (Figure 5.6), may be lower than we would expect if it were measured over a large area of uniformly bare, hard-packed soil. Hard-packed, bare soils cool less radiatively than the loose-packed and vegetative-covered soils that surround our test area. The temperature of the air that we recorded was affected far more by the general character of the surrounding, up-wind terrain than it was by our small test plot area.

5.4.3 Prediction of wet and dry plot 5-cm soil temperatures from meteorological variables

Daily maximum (Tmax), daily minimum (Tmin), average daily temperature ($\overline{T5}$) and daily maximum minus minimum temperature (M-M) at the 5-cm depth in each of the wet and dry plots, as measured by thermocouples, were regressed on the following ten environmental variables:

Ta - average daily air temperature, C

ICDPD - average of current day and previous day's insolation, Ly day^{-1}

TW - air temperature times wind movement, °C km day^{-1}

INSOL - insolation, Ly day^{-1} (same as current day insolation in ICDPD)

I/W - ratio of insolation for current and previous day to wind movement current and previous day, Ly day^{-1}/km day^{-1}

IOA - insolation outside the atmosphere incident on a surface of unit area parallel to the earth's surface--extraterrestrial radiation--, Ly day^{-1}

BP - barometric pressure, inches Hg

MDP - mean dew point, °C

SDEF - saturation deficit of the air, inches Hg

SDW - saturation deficit times wind movement, inches Hg km day^{-1}

These eight analyses as well as an additional one, the average daily temperature difference between the wet and dry plots, are summarized in Table 5.1. From the simple correlation coefficients, r, in the upper part of Table 5.1, it is evident that:

(1) The 10 "independent" variables are all significantly correlated with maximum daily temperature (Tmax) and mean daily soil temperature at the 5-cm depth ($\overline{T5}$) (Any $r \geq 0.217$ is significant at p=.05). Seven of the 10 independent variables are significantly correlated with Tmin and 6 are correlated with maximum minus minimum (M-M) temperature in both wet and dry plots.

(2) Mean daily air temperature is the most influential environmental variable affecting Tmax, Tmin, and $\overline{T5}$ for both wet and dry plots (The simple correlations range from 0.847 to 0.945). Variables containing air temperature, such as air temperature times wind (TW), also yield highly significant correlations.

(3) Variables containing insolation are more highly correlated with Tmax of the soil and (M-M) than with either Tmin or $\overline{T5}$.

(4) For a given variable pair, the correlations are about the same for both wet and dry plots.

The means summarized at the bottom of the simple correlations table show that maximum and minimum daily temperatures in the dry plots were both warmer than in the wet plots and that the average daily temperature difference was 1.8 C. The daily excursion in temperature (M-M) was greater in the dry plots by 2.1 C.

At the bottom of Table 5.1 information is presented on the order in which the independent variables were added in the step-wise multiple regressions, on the proportion of the sum of squares (R^2) accounted for at each step where the new variable added had a regression coefficient that significantly deviated from zero (t-test) and on the standard error of estimate for each dependent temperature variable in this particular data set.

For estimating Tmax, Tmin, and $\overline{T5}$, average daily air temperature was always the first variable chosen. The second or third variable chosen was always either I/W (ratio of insolation for the current and previous day to wind run the current and previous day) or IOA (insolation outside the atmosphere or extraterrestrial radiation). The current day's insolation (INSOL) was the 2nd, 3rd, or 4th variable chosen in 5 out of the 6 analyses. The first three variables accounted for from 89 to 93% of the variation in Tmax, Tmin, and $\overline{T5}$ for the dry plots and for from 88 to 91% for the wet plots.

For estimating the max-min temperature at the 5-cm depth, INSOL was the first variable chosen, average of current and previous day's insolation (ICDPD) was the second variable chosen, and TW was the third variable chosen. These three variables could account for 78% of the variation for the dry plots but for only 65% for the wet plot. Had we had a soil water content measurement daily it undoubtedly would have been included and would have probably been more important for the wet than for the dry soil plot.

Still a different set of independent variables accounted best for the average daily soil temperature difference between the wet and dry plots ($\overline{T}$wet-$\overline{T}$dry). The first variable chosen was I/W, the second was IOA, and the third was saturation deficit of the air times daily wind run, SDW. They accounted for 66% of the variation in ($\overline{T}$wet-$\overline{T}$dry). It is noteworthy that two of these involve windspeed.

The standard errors of estimate of Tmax, Tmin, and $\overline{T5}$ were all similar and ranged from 1.5 to 1.9 C. From air temperature alone (data not presented) Tmax, Tmin, and $\overline{T5}$ could be estimated with standard errors 2.6, 2.0, and 1.6 C for the wet plots and 3.6, 2.1, and 2.1 C for the dry plots, respectively.

In general these findings indicate that Tmax, Tmin, and $\overline{T}$ for shallow soil temperatures correlate well with average daily temperature, as in the literature cited. The variables ICDPD, INSOL, I/W, and IOA are all insolation measurements and they were always the 2nd, 3rd, and 4th variables chosen to estimate soil temperature. Consequently, soil temperature estimates would be improved if ground level daily insolation data were routinely available from some source. Extraterrestrial radiation, IOA, is evidently a surrogate for daylength or season in the relations.

The simple correlations between the independent variables used in the multiple regression analyses are summarized in Table 5.2. The insolation variables derived from ground level measurements ICDPD, INSOL, and I/W are closely correlated and hence any one would suffice. Likewise $\bar{T}a$ and TW are highly correlated (r=0.832) so that TW is dominated by the information it contains about temperature, not wind. IOA correlates highest with $\bar{T}a$ (0.618) and mean dewpoint temperature, MDP (0.545), but contains significant additional seasonal or daylength information. Barometric pressure, BP, is negatively correlated with every other variable. It and SDEF were not included in any of the multiple regression equations. Saturation deficit times wind (SDW) which correlates most highly with variables containing ground level insolation and air temperature variables but contains some other information was the third variable chosen in estimating the wet minus dry soil temperature difference, $\bar{T}wet-\bar{T}dry$.

In summary, of 10 variables we used, air temperature, ground level insolation, and extraterrestrial radiation could be used to estimate the 5-cm soil temperature parameters daily maximum (Tmax), daily minimum (Tmin), and average daily temperature (T5) with average standard errors of 1.87, 1.77 and 1.53, respectively. Multiple regression equations containing these variables accounted for 88 to 93% of the variation in the 5-cm soil depth temperature measured with thermocouples for the period (preplant and planting) 01 Jan to 31 Mar 79.

5.5 Literature cited

Bonn, F. J. 1977. Ground truth measurements for thermal infrared remote sensing. Photog. Engin. and Remote Sensing. 43:1001-1007.

Chirkov, Y. I. 1979. Soil Climate. IN Seemann, J., Y. I. Chirkov, J. Lomas, and B. Primault. Agrometeorology. Sringer-Verlag, N.Y. 324 p.

Kirkham, D. 1964. Soil Physics. IN Chow, V. T. (ed.). Handbook of applied hydrology. McGraw-Hill Book Co., Inc. N.Y.

Linsley, R. K., Jr., M. A. Kohler, and J. L. H. Paulhus. 1958. Hydrology for Engineers. McGraw Hill Book Co., Inc., N.Y. 340 p.

Meikle, R. W. and T. R. Treadway. 1979. A mathematical method for estimating soil temperatures. Soil Science. 128:226-242.

Toy, T. J., A. J. Kuhaida, Jr., and B. E. Manson. 1978. The prediction of mean monthly soil temperature from mean monthly air temperature. Soil Science. 126:181-189.

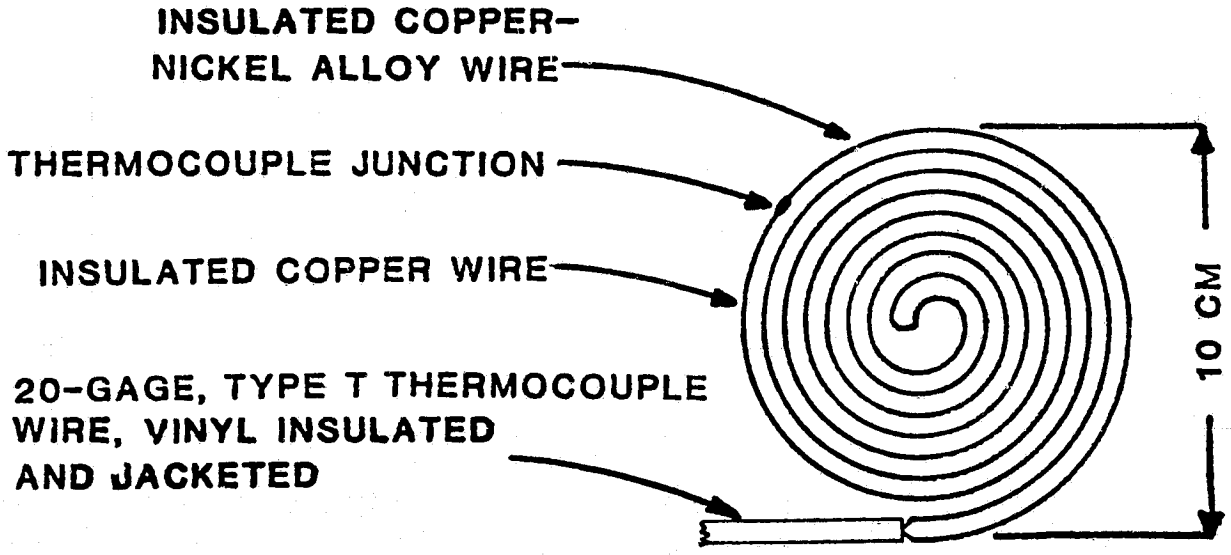

(A)

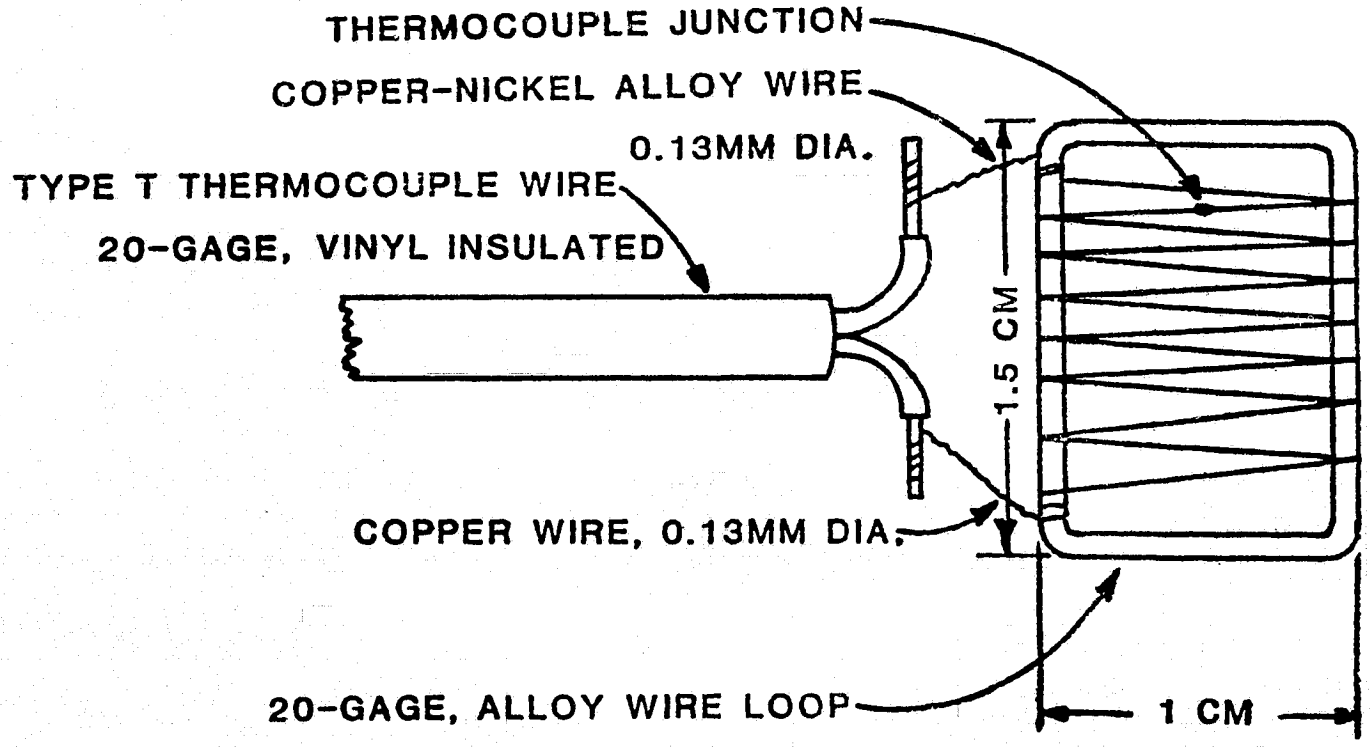

(B)

Figure 5.1 Thermocouple configurations for 5-cm and deeper depths (A) and 0.5-cm depth (B).

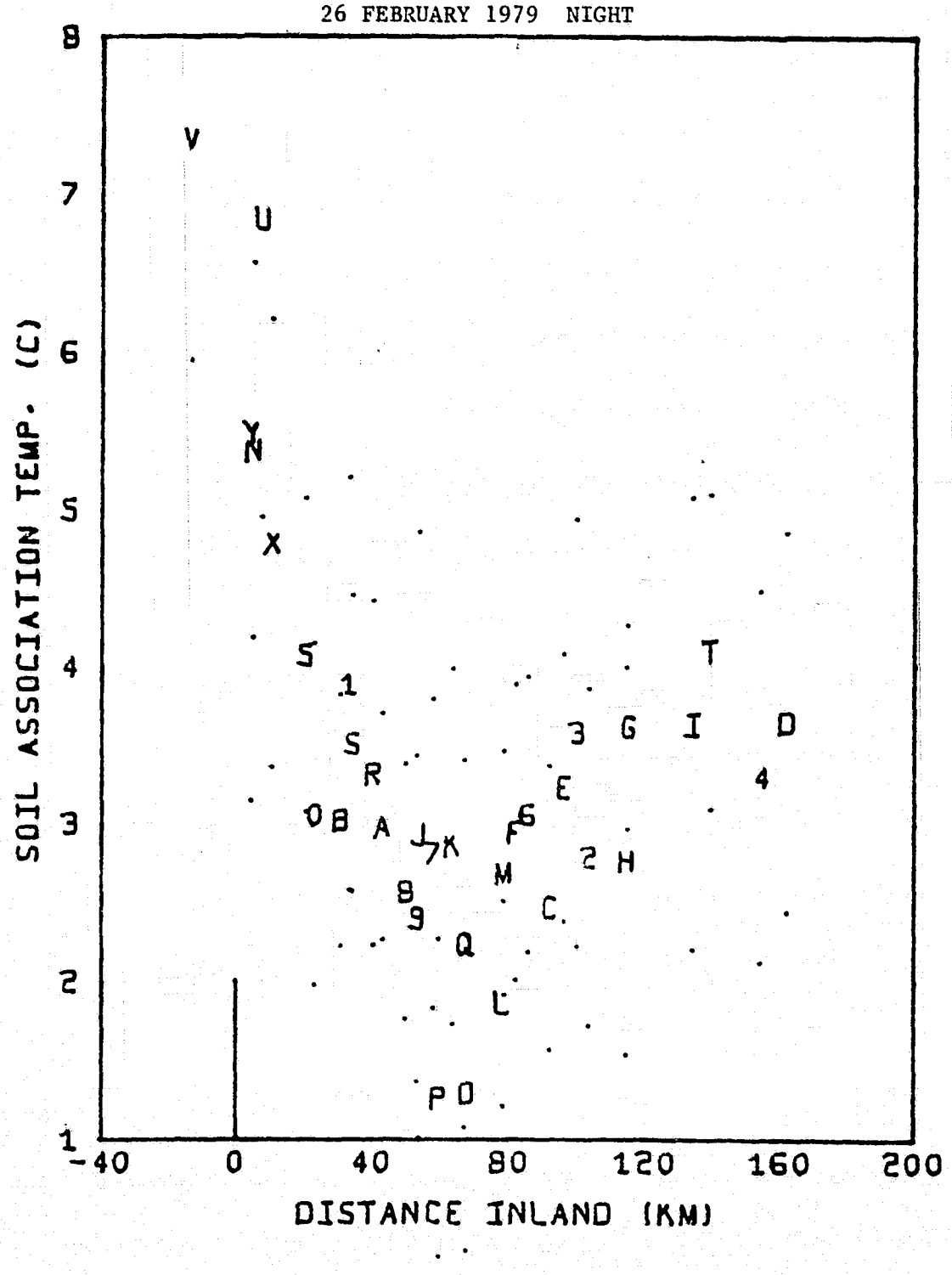

Figure 5.2 Nighttime HCMM radiometric temperatures and standard deviations (dots equidistant above and below identifying symbols) by soil associations versus mean distance of the association from the coastline (Table 3.5 defines the soil association symbols.).

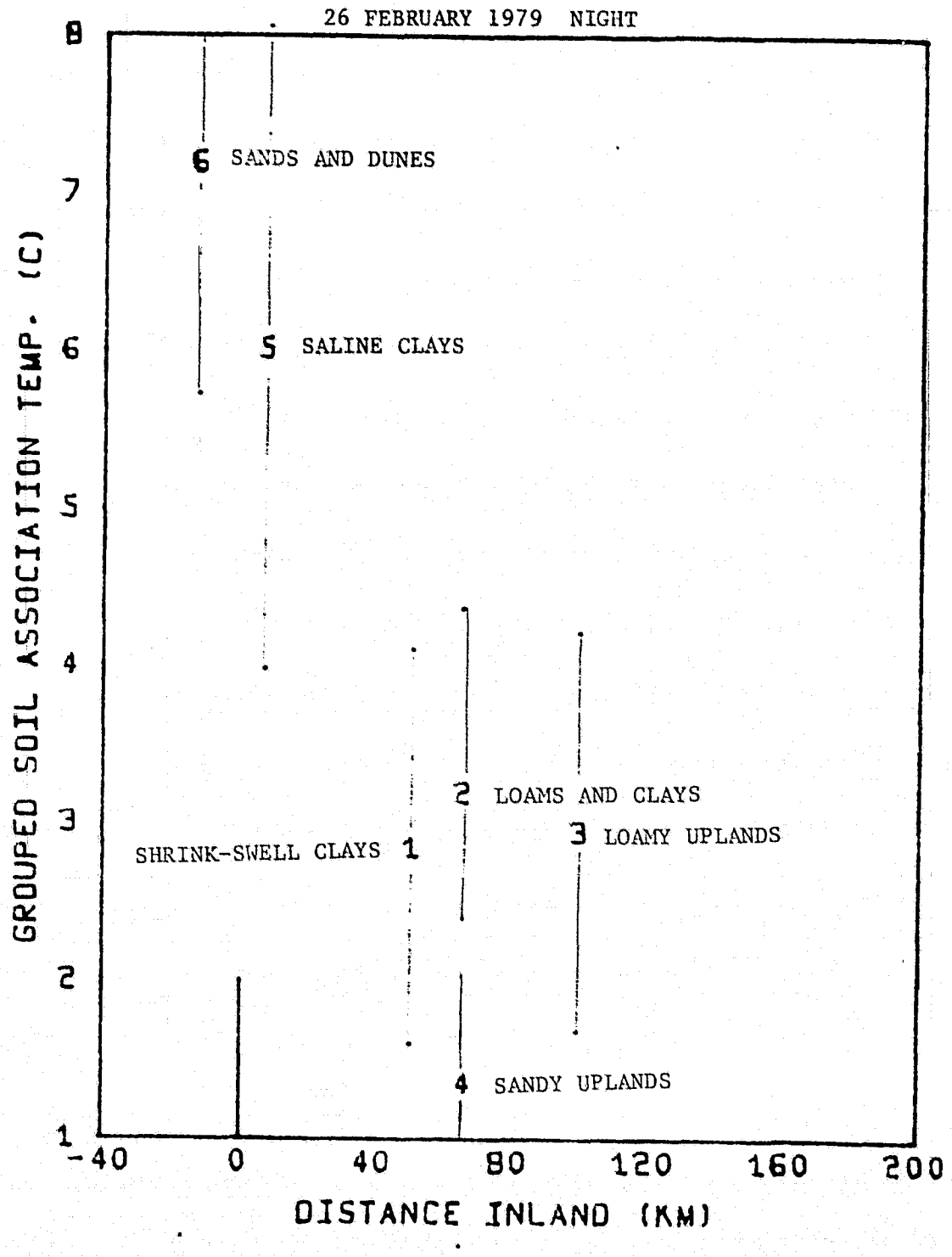

Figure 5.3 Radiometric temperature for soil association categories grouped by texture.

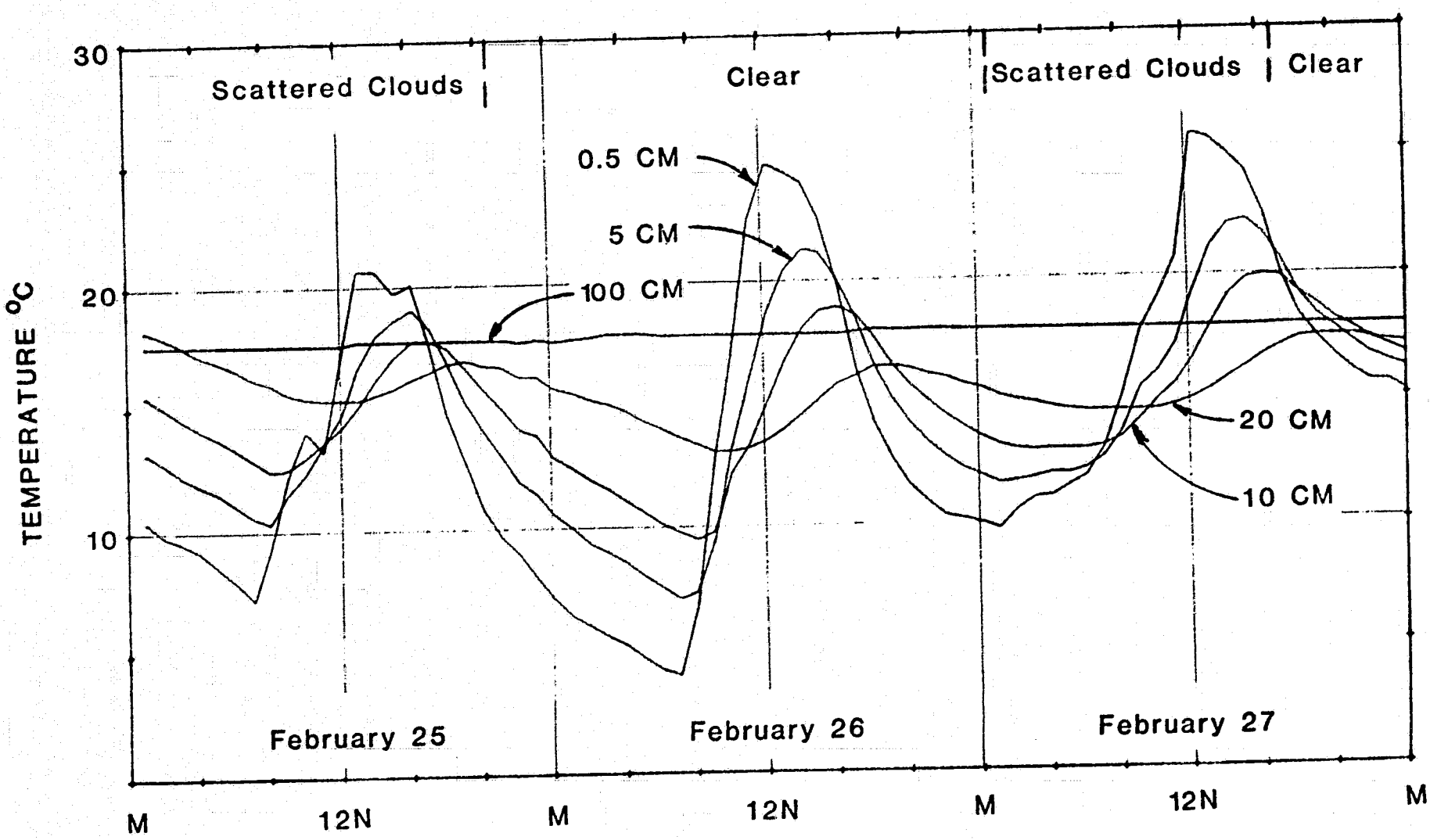

Figure 5.4 Soil temperatures, wet plot, 25 through 27 Feb. 79.

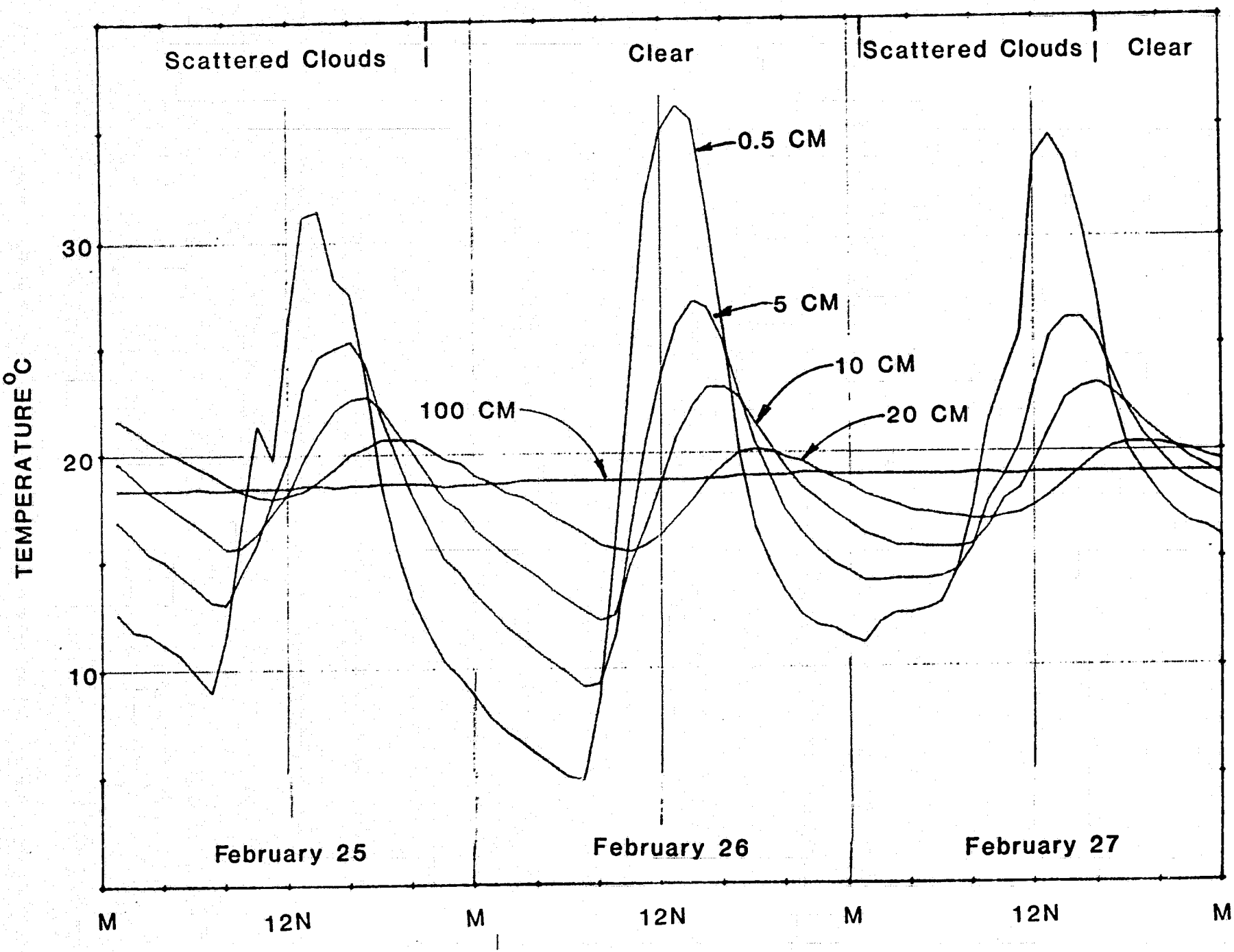

Figure 5.5 Soil temperature, dry plot, 25 through 27 February, 1979

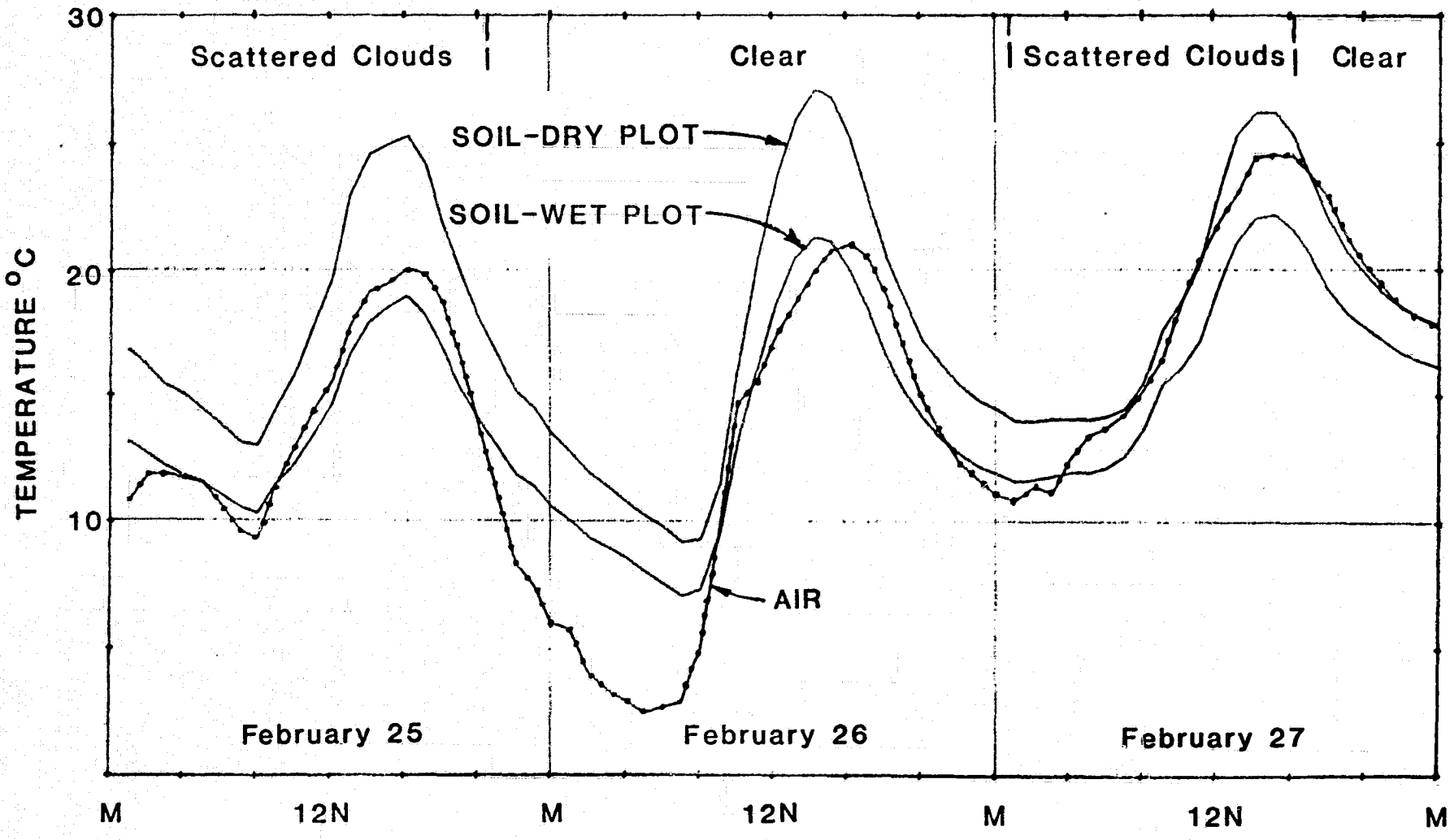

Figure 5.6 Air and 5-cm soil temperatures, 25 through 27 Feb. 79.

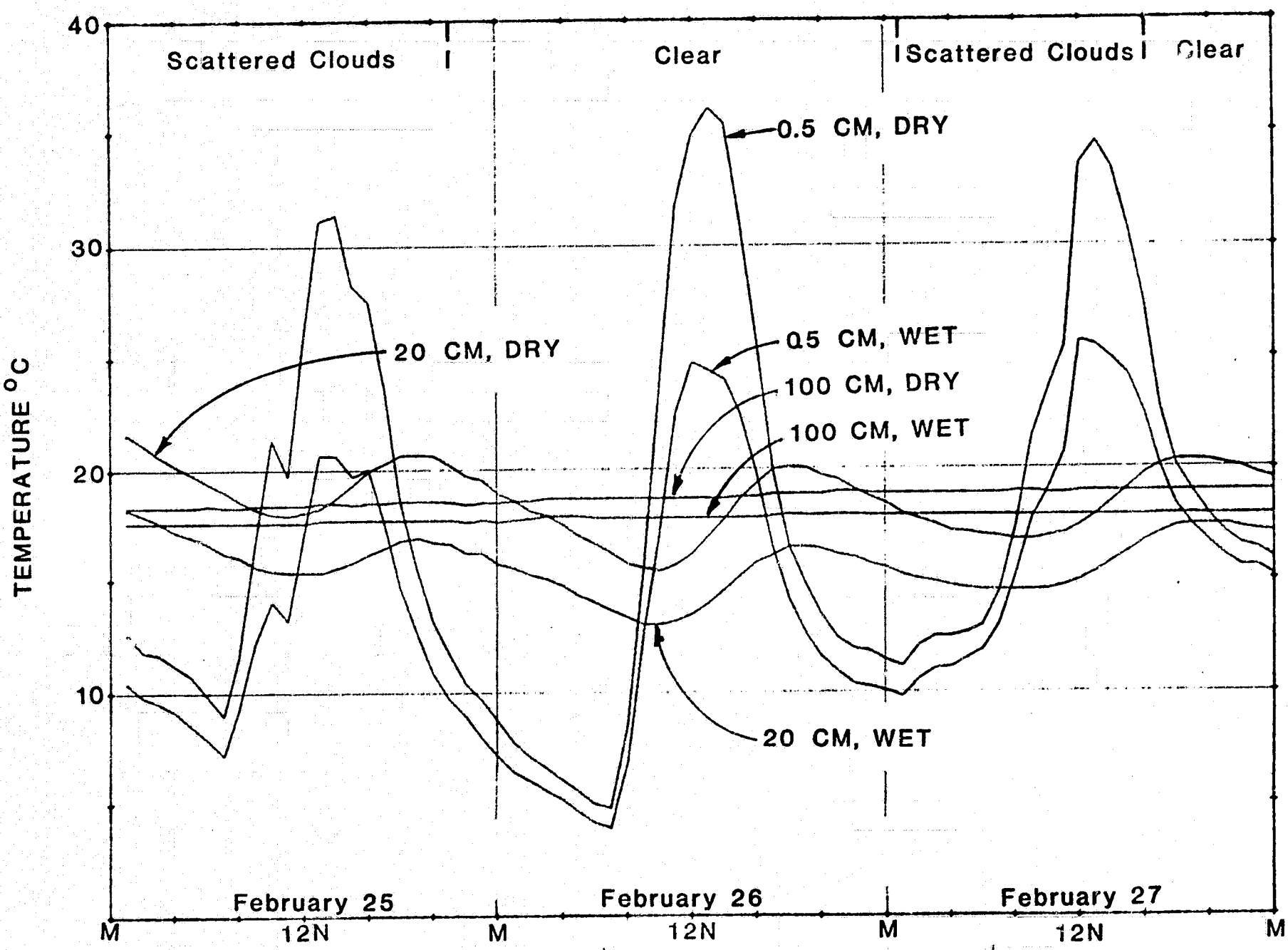

Figure 5.7 Soil temperature, 25 through 27 February, 1979

Table 5.1 Correlation coefficients between nine dependent soil temperature variables and ten environmental variables (upper part); and summary of multiple regression variables chosen, R^2, and standard errors of estimate of nine soil temperature variables (lower part).

Independent variable	Dependent Variable: Wet Plots T_{max}	Wet Plots T_{min}	Wet Plots $\bar{T}5$	Wet Plots (M-M)	Dry Plots T_{max}	Dry Plots T_{min}	Dry Plots $\bar{T}5$	Dry Plots (M-M)	$(T_{wet}-T_{dry})$
	r								
(1) $\bar{T}_a$	.875	.920	.945	.017	.847	.923	.934	.136	-.553
(2) ICDPD	.588	.186	.414	.672	.670	.240	.505	.749	-.653
(3) TW	.676	.819	.786	-.152	.641	.805	.758	-.035	-.379
(4) INSOL	.574	.138	.382	.724	.675	.168	.473	.850	-.631
(5) I/W	.536	.104	.344	.713	.627	.171	.448	.770	-.663
(6) IOA	.628	.624	.659	.067	.653	.684	.707	.142	-.625
(7) BP	-.631	-.642	-.671	-.045	-.607	-.654	-.667	-.106	-.408
(8) MDP	.547	.800	.705	-.333	.474	.782	.649	-.270	-.209
(9) SDEF	.668	.420	.577	.447	.727	.438	.633	.581	-.605
(10) SDW	.608	.476	.573	.262	.648	.480	.607	.402	-.507
Mean:	20.00	13.13	16.54	6.84	22.93	13.96	18.42	8.95	-1.83
S.D.:	5.32	5.00	4.90	3.27	6.67	5.49	5.73	4.21	1.31
	n=80 r(.05)=0.217 ; r(.01)=0.283								
Significant variables in the order added in step-wise multiple regression:									
	1	1	1	4	1	1	1	4	5
	4	5	2	3	4	6	2	3	6
	5	6	6	5	5	4	6	5	10
	-	4	-	-	6	-	-	-	-
Coefficients of determination, R^2, for one, two, three,... variables with t-value significant at the 0.05 level.									
	.766	.846	.893	.524	.717	.852	.872	.722	.440
	.867	.872	.902	.613	.904	.872	.912	.765	.615
	.876	.884	.908	.648	.920	.893	.927	.785	.659
	-	.885	-	-	.927	-	-	-	-
Standard error of the estimate, C(for maximum no. of terms in regression):									
	1.90	1.72	1.50	1.98	1.84	1.81	1.56	1.99	.78

Table 5.2 Simple correlation matrix among input environmental variables for estimating 5-cm soil temperature in wet and dry plots.

	$\bar{T}_a$	ICDPD	TW	INSOL	I/W	IOA	BP	MDP	SDEF	SDW
						r				
(1) $\bar{T}_a$	-	.339	.832	.310	.278	.618	-.730	.780	.569	.582
(2) ICDPD		-	.234	.827	.905	.360	-.242	-.125	.697	.606
(3) TW			-	.195	.023	.506	-.622	.725	.417	.664
(4) INSOL				-	.772	.295	-.203	-.156	.717	.617
(5) I/W					-	.354	-.174	-.175	.670	.431
(6) IOA						-	-.373	.545	.250	.217
(7) BP							-	-.571	-.401	-.453
(8) MDP								-	-.019	.087
(9) SDEF									-	.882
(10) SDW										-
Mean	16.2	69.7	5693.	270.4	.78	667.1	29.9	9.68	0.19	67.1
S.D.	6.4	124.3	3045.	149.9	.45	97.2	.22	7.62	.12	44.7

n=80 r(.05)=0.217 ; r(.01)=0.283

6.0 CROP WATER STRESS

6.1 Abstract

HCMM temperatures for sorghum, citrus, and sugarcane crop sites were related to soil water depletion (DEPL) since the last rain or irrigation calculated from the USDA-ARS Irrigation Scheduling Program (ISP), to days since irrigation or rainfall (DSR), and to the ratio of estimated actual to potential evapotranspiration (ET/ETp) the day of and the day prior to HCMM overpasses. For a combined crops data set involving three HCMM overpasses, temperatures observed by HCMM (means of 3 x 3 pixel arrays, T_3) were highly significantly correlated with ET/ETp (r=-.704**) and positively correlated with DSR (r=.484*). Temperatures were also highly significantly correlated with insolation on the day of the pass (IDOP) r=.812**, the vegetation greenness index (PVI6) calculated from Landsat for the corresponding dates (r=-.642**) and maximum air temperature (Tmax) the day of the HCMM pass. The simple correlation between HCMM-observed surface temperatures and variables important in evapotranspiration for seven dates (27 May through 08 Jul 78) consisting of 51 observations were: insolation the hour of the HCMM overpass (IHROP), r= .668**), IDOP, r=.660**, ET/ETp, r=-.581**; DSR, r=-.477**, Tmax, r=.378**; and, percent vegetation cover (PC), r=-.277**. For this data set, Tmax was highly significantly correlated with DSR, DEPL, and ET/ETp. The data demonstrate the strong correlation between variables related to evapotranspiration and HCMM surface temperatures, as well as the strong coupling of maximum daily air temperature to availability of water for evapotranspiration. In general, the findings indicate that surface temperatures observed by satellites, such as HCMM and the NOAA-6 to -9 series, are responding to shifts in the energy balance of the Earth's surface that are strongly affected by vegetative cover and availability of water for evapotranspiration. Operational applications of such interpretations may be forthcoming under AgRISTARS.

6.2 Introduction and objectives

The remote sensing of plant canopy temperatures appears feasible in studying a broad array of situations: assessing the need for irrigation, conversely, the extent and severity of drought; distribution of rainfall as revealed by vegetative thermal patterns; proximity of water tables to the soil surface; plant-temperature variation with distance from coastal or inland water bodies; ecological studies of plant communities; crop inventories related to gross thermal patterns; and, estimating evapotranspiration from farmland, forest, and rangeland (Myers, et al., 1970; Wiegand and Bartholic, 1970, and Wiegand, 1971).

Plant canopy temperature is a function of the energy balance that is dominated by incident radiation (Wiegand and Namken, 1966) and by availability of water at the leaves for transpiration (Ehlig and Gardner, 1963; Byrne, et al., 1979). When water supply to the leaves is restricted by root zone water depletion, soil salinity (Thomas and Wiegand, 1970), or restricted rooting, transpiration is reduced and the energy balance shifts to a higher temperature equilibrium consistent with increased sensible heat loss. The energy balance is also affected by advected

energy, water vapor pressure gradient between the crop and the air (atmospheric demand) (Jackson et al., 1981), by crop stomatal resistance (physiological), surface roughness (turbulent transfer), and albedo. Thus plant, soil, and ambient environmental variables all affect crop canopy temperatures.

Crop canopy temperature is normally very close to ambient air temperature, a degree or two below at low light intensities and relative humidities (Pallas and Harris, 1964) to a few degrees above under severe water stress. The magnitude of effects are illustrated by the following examples from the literature: Cotton leaf temperatures were 3.5 C higher for plants with a leaf relative turgidity* of 59% (severely wilted) than for plants with a relative turgidity of 83% (well watered) (Wiegand and Namken, 1966). Tanner (1963) reported a 0 to 3 C foliage temperature difference between irrigated and nonirrigated potatoes; he estimated that a 10% decrease in transpiration by a full cover of alfalfa evapotranspiring at 0.76 mm hr^{-1} would cause a temperature increase of approximately 1 C when the associated windspeed at the 1-m height was 3.1 m sec^{-1} and the net radiation was 0.95 ly min^{-1}. Gates (1964) calculated the energy balance for single leaves and concluded that for each 0.10 mm hr^{-1} of transpiration, the temperature of the transpiring leaf would be 5, 2.5, and 1 C cooler than a similarly exposed nontranspiring leaf at windspeeds of 1, 5, and 15 mph, respectively. Wiegand and Namken (1966) who measured cotton leaf temperatures under partly cloudy conditions in early afternoon in June found a linear increase in leaf temperature of 9 C when insolation ranged from 0.6 ly min^{-1} (cloud shadowed plants) to 1.6 ly min^{-1} (full sun).

In this task, we proposed to relate HCMM temperatures to soil water depletion and to days since irrigation or rainfall; and, to look at how canopy temperatures differed among the crops sorghum, citrus, and sugarcane.

6.3 Methods

A computerized irrigation scheduling program developed by Jensen, Wright, and Pratt (1971), commonly referred to as the USDA-ARS Irrigation Scheduling Program, (ISP) (Wright and Jensen, 1978), provides estimates of the timing and amount of irrigation water needed using weather data, crop coefficients, and soil data. The necessary crop coefficients for local use of the method have been developed for cotton, sugarcane, and citrus (Salinas and Namken, 1977). Coefficients for grain sorghum were developed in this study. Given the date of the last irrigation or rainfall, daily weather data, applicable crop coefficients, soil water holding characteristics, and rooting depth, the method calculates daily water depletion. At the time of the proposal submission, we were routinely scheduling the irrigations of about 150 fields and experimental plots

---

* Relative turgidity (RT) = 100 (FW-DW)/TW-DW), wherein FW is the fresh or field condition weight of leaf samples, TW is the turgid weight achieved by floating the leaf samples on distilled water overnight under illumination, and DW is the dry weight of the samples after drying at 60 C.

of sugarcane, citrus, and cotton for our own research and farmer-cooperators. The method is used to schedule irrigations for about 400,000 ha in the irrigated west (EPA, 1975). Thus we chose the cumulative water depletion and actual evapotranspiration estimate on the day of and the day prior to the HCMM overpass dates calculated by this procedure as the acceptable standard to relate the HCMM indicated crop canopy temperatures to.

Because of the nominal 40 ha instantaneous field of view of the HCMM data, we utilized various precautions in selecting fields for study. One precaution was to find fields surrounded by other fields of the same crop so that an ample area of crop, even if not all within the same field was obtained. Part of the cotton and sorghum fields were also chosen in nonirrigated areas where soil water conditions would be uniform among adjacent fields. These considerations as well as ground travel and manpower resulted in our selecting 22 fields that ranged from 18 to 1240 ha in size (only three <40 ha) that were devoted to sorghum, sugarcane, cotton, citrus, and improved pastures (grass). Ground truth acquired on weekly visits from 30 May to 13 Jul 78 included crop species, plant height (PH), percent crop cover (PC), percent weed cover, stage of maturity, and dates of irrigation (See section 1.2.2 for more detail).

Ideally, the crops should have attained about 70% ground cover at maximum canopy development to eliminate exposed sunlit soil effects on the canopy temperatures and evapotranspiration rates (Tanner and Jury, 1976). However, the crops did not all reach such ground covers, so we include percent cover (PC) and spectral vegetation indexes (Kauth and Thomas, 1976; Richardson and Wiegand, 1977) as variables in the analyses. The latter were available from two Landsat Satellite overpasses--for 15 Jun and 12 Jul 78--that could be paired with HCMM data for 12 and 17 Jun, and 8 Jul 78, respectively. (See section 1.2.4 for additional detail). Because ground cover ranged from 20 to >70%, we developed crop coefficient curves to cover the ranges, <40 PC, 40-60 PC, and >60 PC.

The equation ET = Kc ETp was used to estimate the soil water depletion where

ET = estimated evapotranspiration (cm/day) for a given crop

ETp = the evapotranspiration potential

= 0.0112 (Tm-20)Rs

Rs = incident solar radiation converted to equivalent depth of water evaporated (cm/day)

Tm = mean daily temperature (°F) as obtained from the closest weather station

Kc = Kco Ka + Ks

where Kco is the crop coefficient

Ka is a soil moisture availability factor

Ks is a factor that lets evaporation directly from the soil contribute to ET for a short time (3 days in summer) when the soil surface is wet from irrigation or rainfall. When Kco $\leq$.9, Ks does not apply.

The mean daily temperature from the weather station geographically closest to the chosen field was used to calculate ETp. Daily insolation as needed for Rs in the irrigation scheduling program (ISP) and hourly insolation for relating to the HCMM overpass temperatures were taken from the central weather station at Weslaco. (See section 1.2.5 for more details).

Rooting depth and plant available water in the root zone were estimated for each crop on each soil type as shown in Table 6.1. ET was calculated for the dates 21 May through 15 Jul 78 inclusive. The bookkeeping of soil water took rainfall, irrigations, and drainage in excess of field capacity into account.

We acquired digital magnetic tapes for the reflective (0.55 to 1.1 μm) and emissive (10.5 to 12.5 μm) bands of HCMM for afternoon overpasses on 27 May; 6, 12, 17 and 23 Jun; and 3 and 8 Jul 78. The overpass on 27 May was 1416 LST; the overpass time became slightly earlier on succeeding passes and was 1400 on 8 Jul. The scenes were subjected to a long series of processing steps including registration to the ground scene, assignment of latitude and longitude to each pixel, etc. (See report section 2.1.1 for more detail). From these procedures it was possible to extract the single pixel that centered on the individual site of interest or to use the mean of 3x3, 5x5, 7x7 or 9x9 arrays of pixels centered on the central pixel as representative of the site. For the analyses of this task, we used only the central pixel (1x1 matrix of pixels) and the mean of the 3x3 array of pixels for analysis. We used the "original" HCMM calibration to calculate the HCMM temperatures from the digital counts not the "recalibration" (Barnes and Price, 1980). The original calibration yields temperatures 5.5 C higher than the recalibration.

We merged the data from HCMM (albedo and surface temperatures for 1x1 (T_1, R_1) and 3x3 (T_3, R_3) pixel matrices) with ground truth (crop species; days since irrigation or rainfall (DSR); plant height (PH); percent cover (PC)), weather station (daily maximum (TMAX) and minimum temperatures (TMIN); rainfall), Landsat (vegetation indices KVI, BRT, PVI, PVI6), and central environmental station (insolation the day of the pass (IDOP) and insolation the hour of the pass (IHROP)) with outputs from the irrigation scheduling program (cumulative depletion (DEPL) since rainfall or irrigation), ratio of actual evapotranspiration to potential evapotranspiration for the day of and the day preceding the HCMM overpass (ET/ETp), and calculated site distance from the coast (DIST) into three data set combinations:

(1) HCMM data for 3 dates paired with Landsat data for 2 dates plus the ground truth, weather station, irrigation scheduling and central environmental station data for the appropriate dates. This set was available with cloud and water vapor contaminated pixels included and with the affected data deleted.

(2) HCMM data for 7 dates (27 May through 8 Jul) paired with ground truth, weather station, irrigation scheduling, and central weather station data for the same period (15 Aug 78 data (see Table 1.2) not included for lack of ground truth and irrigation scheduling data past 15 Jul).

(3) T_1, R_1, and T_3, R_3 segregated by the crops sugarcane, citrus, and sorghum for 7 dates. (Did not include cotton or grass because of insufficient number of observations).

The raw and derived data for the 22 intensive sites are summarized in Appendix A. The cloud and vapor contaminated data have been deleted. Our approach in analyzing the data was to use the most complete data set we could initially, then delete sources of variation such as cloud and vapor contaminated pixels and then highly correlated variables. We used a statistical program W1106 included by IBM with its basic statistical package for our IBM 1800 computer. This step-wise multiple regression program calculates the simple correlation among all the variables in the data set before performing a step-wise multiple regression analysis.

6.4 Results

We were extremely fortunate that 7 usable overpasses of HCMM occurred while we were ground truthing and obtaining the data for the irrigation scheduling computations, and that Landsat data were available for two dates to augment the ground truth taken.

Results from the various data sets may be summarized as follows:

6.4.1 Correlation of crop water stress parameters and vegetation indexes with HCMM temperatures and albedos

6.4.1.1 Before and after removal of atmospherically contaminated data

Data set 1 consisting of HCMM data for 3 dates paired with corresponding LANDSAT, ground truth, weather station, irrigation scheduling, and central weather station data were used for these analyses.

The simple correlation of the albedo (R) and surface temperature (T) and the other variables are summarized in Table 6.2. Results are presented for the central pixel for each site (field) and a 3x3 matrix of pixels centered on the central pixel. In the upper portion of Table 6.2 results are presented for the data that included cloud and vapor contaminated pixels (n = number of observations = 46) and in the lower part with the cloud contaminated pixels and some of the variables deleted (n=22).

Conclusions reached from considering the content of Table 6.2 are:

(a) The simple correlations among variables is higher for the sample of 9 pixels (R_3, T_3) than it is for the central pixel (R_1, T_1) in both the upper and lower parts of Table 6.2.

(b) The simple correlation of other variables with temperature are improved by deleting the cloud and vapor contaminated pixels, but the correlations of albedo are weakened. (This occurs for albedo even though the standard deviation about the mean is lessened whereas it remains about the same for temperature.)

(c) Albedo is significantly correlated with water depletion (DEPL) and insolation on the day of the pass (IDOP) before contaminated pixels are removed but only with IDOP after removal of contaminated data.

(d) Before deletion of contaminated data, T_1 and T_3 are most closely correlated with distance from the coast (DIST) but they are also significantly correlated with the ratio of actual to potential evapotranspiration the day of and the day prior to the pass (ET/ETp), maximum air temperature the day of the pass (Tmax) and the vegetation indices PVI, PVI6, and GVI. After deletion of the variable DIST (to be discussed under synoptic analyses), all but PVI6 of the vegetation indices (because they are highly intercorrelated and PVI is least affected by atmospheric conditions) and the contaminated data, HCMM temperatures are significantly correlated with days since rainfall (or irrigation) (DSR), ET/ETp, Tmax, IDOP, PVI6, and albedo.

The multiple regression analyses are useful for indicating the amount of variation explained by the environmental variables. Table 6.3 lists the variables in the order they were included in the stepwise regression, gives the multiple correlation coefficients, and provides the standard error of estimate of 3x3 pixel temperature (T_3) for the first eight variables included in the analyses for data set 1 before and after removing cloud contaminated pixels and DIST.

Table 6.3 shows that eight variables explained 66% of the variation in T_3 before removal of cloud and vapor contaminated pixels and 96% of the variation after their removal. These results point out the overwhelming variability imposed on the HCMM thermal data by atmospheric effects. The standard error of estimate of mean temperature, $S\bar{T}_3$, decreased as additional variables were added to the regression analysis. It was 1.1 C for the noncontaminated data and 2.8 C for the contaminated data when eight variables were included in the respective regression equations.

The corresponding R^2 and $S\bar{T}$ for the central pixel (data not presented) for eight variables in the analyses were .601 and 3.3 before contaminated data were deleted and .941 and 1.4 after they were deleted.

Generally these results show the strong effect of an unclean atmosphere on the observations, a strong correlation between variables related to evapotranspiration and temperatures observed by HCMM, and that well over 90% of the variation in observed temperature is explained by the variables included in the analyses when samples from cloud or vapor contaminated atmosphere are deleted.

6.4.1.2 Within the crops sugarcane, citrus, and sorghum

Data set 3 consisting of T_3 and R_3 data for 7 dates segregated by crops were used for this analysis.

Table 6.4, which summarizes the statistically significant simple correlation coefficients between each pair of variables by crops for 7 HCMM overpass dates, is an attempt to get a further feel for the variables that were consistently related. In interpreting the data, it is worthwhile to keep in mind that the sorghum fields were mainly from non-irrigated areas, the fields were large and most of the fields had been harvested by 08 Jul. The sugarcane fields were making rapid growth and both plant height and ground cover were increasing rapidly; to maintain the growth they had to be irrigated regularly after the rainfall in early June. The citrus orchards were the smallest sites used, the age and condition of groves within the test sites varied considerably, and citrus is moderately drought tolerant.

From Table 6.4 we see that T_3 for the sorghum sites is significantly correlated with 8 other variables (PC, DEPL, ET/ETp, IDOP, IHROP, DSR, Tmax, and PH) whereas it is significantly correlated with only two for sugarcane (IDOP, IHROP) and one for citrus (Tmax). Plant height (PH) is significantly correlated for all 3 crops with PC, DEPL, and Tmax.

Regarding variables that affect water use, we see that calculated depletion (DEPL) is significantly related to PC as in the real world; the two could be significantly related because the crop coefficients used to estimate evapotranpsiration are ground cover dependent. But crop coefficients used here were either taken from the literature or were derived from independent data. Days since rainfall or irrigation (DSR) and ET/ETp, two variables that are not methodologically dependent are very highly correlated for each of the crops (SC=-.945**, CT=-.778**, and SR=-.910**). Such findings support the validity of the evapotranspiration estimation procedures and their utility for irrigation scheduling.

Figure 6.1 presents the cumulative percent of the variation in T_1 and T_3 as variables were added to the multiple regression for 1x1 and 3x3 pixel samples representing sugarcane, citrus and sorghum fields. For every crop by the time 6 variables had been included in the regression equations for the 3x3 pixel sample, > 95% of the variation in T_3 was explained. For the 1x1 pixel sample, from 85% (sugarcane) to 92% (sorghum) of the variation was explained by 6 variables. For citrus and sorghum 3 variables explain over 80% of the variation in T_1 and T_3, but not for sugarcane.

From a look at Figure 6.1, it appears that 6 variables are desirable to describe the behavior of T_3. Numerical values of R^2 and $S\overline{T}_3$ for 3 and 6 variables, and the variables included were (where variables with significant regression coefficients are underscored):

6.4.2 Correlation of PC, DEPL, IDOP, IHROP, TMAX, ET/ETP, and PH with HCMM temperatures and albedos for seven observation dates

Data set 2 consisting of HCMM data for 7 dates (27 May through 8 Jul 78) during which ground truth and evapotranspiration calculations were being made were used for the analyses. The simple correlation coefficients for 8 variables with the central pixel albedo and temperature (R_1, T_1) and with the 3x3 pixel mean of albedo and temperature (R_3, T_3) for 7 HCMM overpass dates are summarized in Table 6.5. The same variables that correlated with R and T for the three dates of data (Table 6.2) again correlate. However, the simple correlation coefficients are larger; they are, therefore, significant at a higher probability level because the number of observations is greater. Also as in Table 6.2, the simple correlations are slightly higher for the 3x3 pixel mean data (R_3, T_3) than for the central pixel (R_1, T_1) data. The only exception is the correlation with percent vegetative cover (PC).

The simple correlation between albedo and temperature is highly significant, whereas it was not for the three dates of Table 6.2. This seems to be related to the facts that the additional dates in the data set were associated with a greater range in the variables such as insolation the day of (IDOP) and the hour of the HCMM pass (IHROP), and in other influencing variables such as percent vegetative cover (PC) and plant height (PH). IHROP was not significantly correlated with any other variable in the data set in Table 6.2 because those dates had quite similar insolation the hour of the HCMM overpass.

The finding that insolation (IDOP, IHROP) strongly affects surface temperature is as it should be because the sun's energy is the "driver" of the earth's energy balance. The highly significant negative correlation between the ratio of actual to potential evaporation (ET/ETp) for the day of and day prior to the pass indicates that as water becomes less available for transpiration, the canopy temperature increases. This finding, again, agrees with reality and the physical and physiological processes involved. The significant positive correlation between maximum air temperature (Tmax) the day of the HCMM overpass and the site surface temperature observed by HCMM is also in agreement with reality; that is, the two are coupled.

In the energy balance equation,

$$Rn = G + H + LE,$$

if incident solar radiation remains constant for a series of summer days and heat flux into the ground G is a small, essentially fixed proportion of net radiation Rn for daily periods, it is obvious that a decrease in water availability which reduces the latent heat of evapotranspiration LE has to be compensated for by an increase in sensible heat flux from the canopy to the air, H.

Jackson et al. (1981) and Monteith (1973) further show that H and LE, respectively, can be expressed by

$$H = \rho c_p (Tc-TA)/ra$$

$$\text{and } LE = \rho c_p (e^*_c - eA)/[\gamma(ra+rc)]$$

where ρ is the density of the air, c_p the heat capacity of air, Tc canopy temperature, TA air temperature, e^*_c the saturated vapor pressure at Tc, eA the vapor pressure of the air, γ the psychrometric constant, ra the aerodynamic resistance of air to vapor transport, and rc is the canopy resistance to water vapor transfer to the air.

In our studies ET = LE became smaller the longer it had been since rain had fallen or irrigation water had been applied. Consequently, (Tc-TA) which is directly proportional to H had to increase. If ground cover was essentially complete, THCMM was sensing Tc. From May through July when the data for these studies were being obtained, TA was also increasing seasonally.

Jackson et al. (1981) also defined a crop water stress index (CWSI) as CSWI = 1-ET/ETP. In Appendix Table A.2 we list ET/ETP for 7 sorghum, 6 sugarcane, 4 cotton, 3 citrus, and 2 grass fields for each of 3 dates. The very low ET/ETP for a number of the dryland sites on JD 189 means they were under severe stress.

Jackson et al. (1981) also document that there is a linear relation between Tc-TA and the vapor pressure deficit of the air, e^*_A-eA. When we performed the step-wise multiple regression analyses for several dates (see Figure 2.5) we found that the saturation deficit of the air (SDEF) was the first variable selected and that it alone explained over 50% of the variation in THCMM. Consequently, we believe interpretation of canopy or "Earth surface" temperatures between geographical locations that differ widely in water vapor pressure of the air will have to include the effect of differing saturation deficits of the air in interpreting Tc and Tc-TA observations.

In Table 6.6 the simple correlation matrix among the "independent" variables of Table 6.5 are presented. Tmax is highly significantly positively correlated with millimeters water depletion (DEPL) (.486**) and days since rainfall or irrigation (DSR) (.567**) and highly significantly negatively correlated with ET/ETp (-.474**). These correlations indicate clearly that availability of water for evapotranspiration is affecting partitioning in the energy balance. Consequently, a decrease in availability of water for evapotranspiration is associated with an increase in the daily maximum air temperature. The actual to potential evapotranspiration ratio (ET/ETp) is significantly correlated with vegetative cover (PC), and days since rainfall or irrigation (DSR) as well as Tmax. DSR and DEPL are calculated for the same time interval and are highly correlated. Plant height (PH) is weakly correlated with only one variable, PC. PH is not a sensitive variable when the crops are pooled because only cotton and sugarcane were changing in plant height; sorghum had headed by 27 May, citrus is a perennial whose height remained constant for the two month period, and grass height changed little during the observation period.

The multiple regression equations for estimating the 3x3 pixel HCMM temperatures (through the first 4 variables), and the R^2 and the standard error of the estimate, $S\bar{T}_3$ (through 5 variables) were:

	R^2	$S\bar{T}_3$ (°C)	No. of Variables
$T_3 = 24.67 + .090\ (IHROP)$	.446**	2.9	1
$= 29.61 + .079\ (IHROP) - 6.863\ (ET/ETp)$	.672**	2.3	2
$= 23.59 + .070\ (IHROP) - 6.830\ (ET/ETp) + .386\ (R_3)$	.701**	2.2	3
$= -26.93 - .162\ (IHROP) - 7.273\ (ET/ETp) + .989\ (R_3) - .162\ (IDOP)$	.781**	1.9	4
	.803**	1.8	5

A t-test of the regression coefficients was significant for each of the first five variables (R_3, ET/ETp, IDOP, IHROP, Tmax) included in the multiple regression equations; they accounted for 80% of the variation in T_3. The standard error of the estimated temperature decreases from 2.9 C for inclusion of the first variable to 1.9 C by the time the fourth variable is included. The corresponding multiple correlation and $S\bar{T}x$ for the central pixel data were: for 4 variables, $R^2 = .722$, $S\bar{T}_1 = 2.3$ C and for 8 variables $R^2 = .764$, and $S\bar{T}_1 = 2.2$ C.

6.5 Literature cited

Barnes, W. L. and J. C. Price. 1980. Calibration of a satellite infrared radiometer. J. Applied Optics. 19:2153-2161.

Byrne, G. F., J. E. Begg, P. M. Fleming, and F. X. Dunin. 1979. Remotely sensed land cover temperature and soil water status--A brief review. Remote Sensing of Environ. 8:291-305.

Ehlig, C. F. and W. R. Gardner. 1963. Relationship between transpiration and the internal water relations of plants. Agron. J. 56:127-130.

Environmental Protection Agency. 1975. Scientific irrigation scheduling for salinity control of irrigation return flows. EPA-600/2-75-064. U.S. Environmental Protection Agency. Ada, OK.

Gates, D. M. 1964. Leaf temperature and transpiration. Agron. J. 56:273-277.

Jackson, R. D., S. B. Idso, R. J. Reginato, and P. J. Pinter, Jr. 1981. A canopy temperature based crop water stress index. Water Resources Res. (In press).

Jensen, M. E., J. L. Wright, and B. J. Pratt. 1971. Estimating soil moisture depletion from climate, crop and soil data. Transactions ASAE. 14:954-959.

Kauth, R. J. and G. S. Thomas. 1976. The tasseled cap--A graphic description of the spectral-temporal development of agricultural crops as seen by LANDSAT. Proc. Sympos. Machine Proc. of Remote Sensing Data. (LARS, Purdue Univ.) IEEE Cat. No. 76, Ch. 1103-1 MPRSD.

Monteith, J. L. 1973. Principles of environmental physics. Edward Arnold, Ltd. London. 241 p.

Myers, V. I., M. D. Heilman, R. J. P. Lyon, L. N. Namken, D. S. Simonett, J. R. Thomas, C. L. Wiegand, and J. T. Woolley. 1970. Soil, water and plant relations. In Remote Sensing With Special Reference to Agriculture and Forestry, pp. 253-297. National Academy of Sciences, Washington, D.C.

Pallas, J. R., Jr. and D. G. Harris. 1964. Transpiration, stomatal activity and leaf temperatures of cotton plants as influenced by radiant energy, relative humidity, and soil moisture tension. Plant Physiol. 39:xliii (Abstr.)

Richardson, A. J. and C. L. Wiegand. 1977. Distinguishing vegetation from soil background information. Photogram. Engin. and Remote Sensing. 43:1541-1552.

Salinas, F. and L. N. Namken. 1977. Irrigation scheduling for sugarcane in the Lower Rio Grande Valley of Texas. Proc. Amer. Soc. Sugar Cane Tech. 6:186-190.

Tanner, C. B. 1963. Plant temperatures. Agron. J. 55:210-211.

Tanner, C. B. and W. A. Jury. 1976. Estimating evaporation and transpiration from a row crop during incomplete cover. Agron. J. 68:239-243.

Thomas, J. R. and C. L. Wiegand. 1970. Osmotic and matric suction effects on relative turgidity, temperature, and growth of cotton leaves. Soil Science. 109:85-92.

Wiegand, C. L. 1971. Agricultural applications and requirements for thermal infrared scanners. Proc. International Workshop on Earth Resources Survey Systems, Univ. of Michigan, Ann Arbor. Vol II, pp. 66-81. U.S. Govt. Printing Office, Washington, D.C.

Wiegand, C. L. and J. F. Bartholic. 1970. Remote sensing in evapotranspiration research on the Great Plains. Proc. Great Plains Agric. Council Evapotranspiration Seminar, Public. No. 50, pp. 137-180. Kansas State Experiment Station. Manhattan, KS.

Wiegand, C. L. and L. N. Namken. 1966. Influences of plant moisture stress, solar radiation, and air temperature on cotton leaf temperatures. Agron. J. 58:582-586.

Wright, J. L. and M. E. Jensen. 1978. Development and evaluation of evapotranspiration models for irrigation scheduling. Transactions ASAE. 21:88-91, 96.

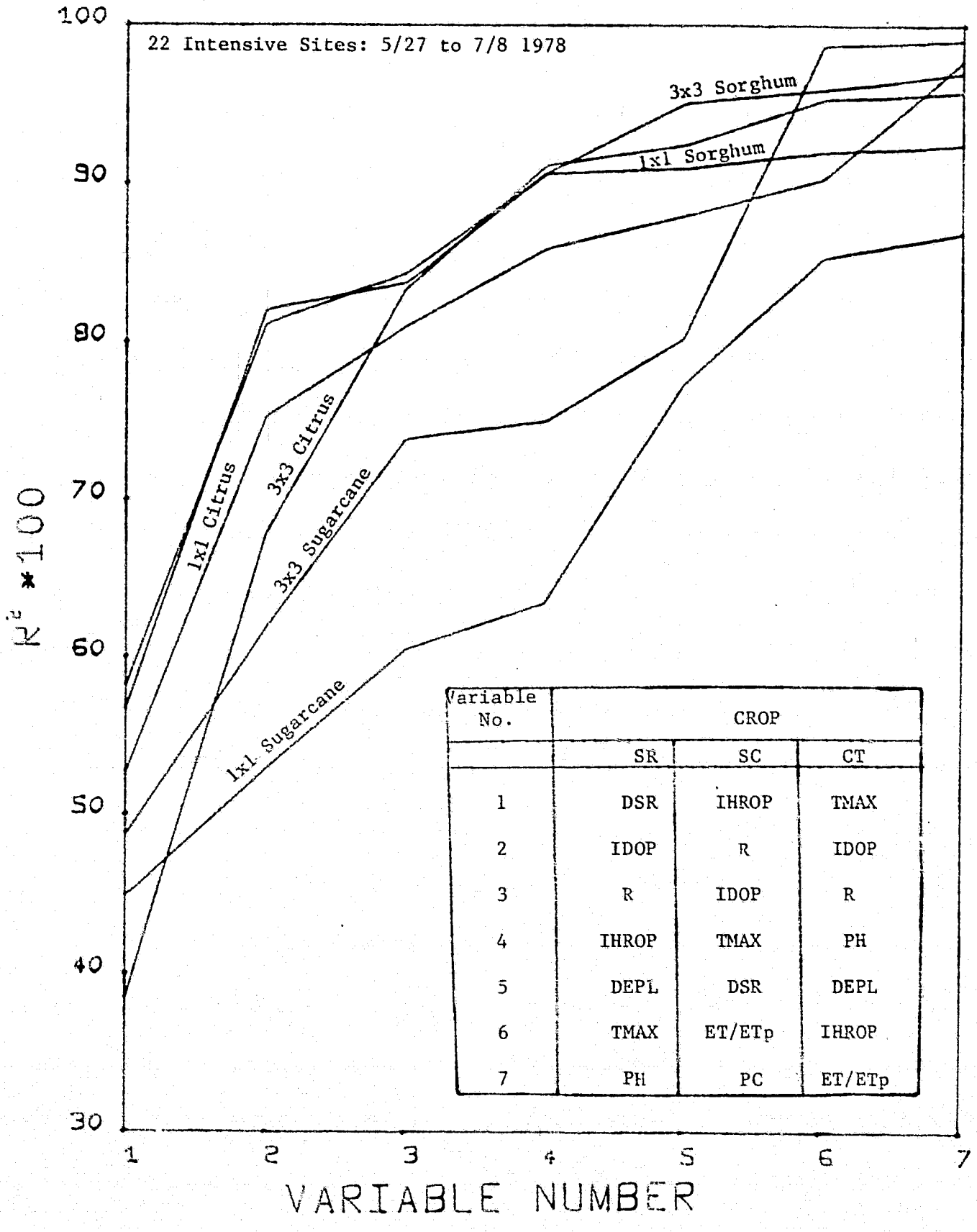

Variable No.	CROP		
	SR	SC	CT
1	DSR	IHROP	TMAX
2	IDOP	R	IDOP
3	R	IDOP	R
4	IHROP	TMAX	PH
5	DEPL	DSR	DEPL
6	TMAX	ET/ETp	IHROP
7	PH	PC	ET/ETp

Figure 6.1 Percent of variation explained as variables were added to the multiple regression for 1x1 and 3x3 pixel samples of sugarcane, citrus, and sorghum.

Table 6.1. Soil types, crops, rooting depth, and water characteristics of fields and sites for which evapotranspiration was determined.

Soil type	Crop[a/]		Rooting depth	Water holding capacity of soil		Plant available water	Allowable depletion	
			cm	in.H_2O/ ft.soil	cm.H_2O/ cm.soil	cm	%	cm
Swelling clay	Sorghum	✓	90	2.34	.195	17.8	50	8.9
	Sugarcane	✓	90	2.34	.195	17.8	50	8.9
	Cotton	✓	90	2.34	.195	17.8	50	8.9
	Citrus			(This soil type not suitable for citrus)				
Loamy & clayey (clay loam)	Sorghum	✓	120	2.1	.175	21.3	50	10.7
	Sugarcane	✓	120	2.1	.175	21.3	50	10.7
	Cotton	✓	120	2.1	.175	21.3	50	10.7
	Citrus		90					
	Grass		120					
Loamy upland (sandy clay loam)	Sorghum		120					
	Sugarcane	✓	120	1.86	.155	18.9	50	9.4
	Cotton		150					
	Citrus	✓	90	1.86	.155	14.2	60	8.5
	Grass	✓	120	1.86	.155	23.6	50	11.8
Fine sandy loam	Sorghum	✓	150	1.56	.130	19.8	60	11.9
	Sugarcane	✓	120	1.56	.130	15.8	60	9.5
	Cotton	✓	150	1.56	.130	19.8	60	11.9
	Citrus		120					
	Grass	✓	150	1.56	.130	19.8	60	11.9

[a/] Sample of fields included crops within soil types as indicated by a check mark, ✓

Table 6.2. Linear correlation coefficients for all variables with the central pixel albedo and temperature (R_1, T_1) and with the 3 x 3 pixel mean value of albedo and temperature (R_3, T_3) for 22 intensive sites. Top portion of table is for cloud and vapor contaminated pixels in the analysis, and the lower part is with them deleted.[a/]

Variable Acronym	Mean ± SD	R_1	T_1	R_3	T_3	Mean ± SD
		Correlation coeff., r				
PC(%)	50.0 ± 22.4	.095	-.156	.145	-.203	Same as for central pixel
PH(cm)	136. ± 116	-.015	.145	.068	.125	
DSR(days)	14.6 ± 10.6	-.276	.266	-.388**	.286	
DEPL.(mm)	59 ± 37.6	-.299*	-.116	-.359*	-.123	
ET/ETp	.56 ± .29	.102	-.441**	.275	-.505**	
Tmax(°C)	36.1 ± 1.5	-.151	.350*	-.258	.375**	
IDOP(Ly)	415. ± 50	.367*	.278	.454**	.317*	
DIST(Km)	79.4 ± 22.4	.221	.696**	.107	.761**	
PVI	14.2 ± 7.1	-.058	-.343*	.113	-.387**	
PVI6	19.8 ± 10.1	-.030	-.404**	.152	-.450**	
GVI	23.4 ± 11.3	-.039	-.374**	.139	-.419**	
BRT	76.3 ± 9.3	-.037	.217	-.086	-.221	
R(%)	17.6 ± 2.1	-	.080	-	-.017	17.6 ± 1.6
T(°C)	29.7 ± 4.8	.080	-	-.017	-	29.7 ± 4.4
PC	49.2 ± 23.2	.107	-.255	.270	-.269	Same as for central pixel
DSR	14.9 ± 9.9	-.030	.448**	-.173	.484*	
DEPL	55.7 ± 30.5	-.220	-.126	-.242	-.082	
ET/ETp	.51 ± .27	-.190	-.681**	-.069	-.704**	
Tmax	36.0 ± 1.6	.081	.583**	.043	.619**	
IDOP	408 ± 54.4	.614**	.773**	.679**	.812**	
PVI6	19.0 ± 9.9	-.206	-.635**	-.106	-.642**	
R	17.2 ± 1.6	-	.537*	-	.492*	17.2 ± 1.3
T	31.9 ± 4.7	.537*	-	.492*	-	31.9 ± 4.5

[a/] For upper portion of table, number of observations of each variable, n = 46 whereas in the lower part n = 22.

Table 6.3. Effect of cloud and vapor contamination on proportion of the sum of squares explained by regression (R^2) and the standard error of estimate ($S_{\bar{T}_3}$) of mean temperature (T_3).

Contaminated pixels included (n = 46)				Contaminated pixels deleted (n = 22)		
Variable No.	Acronym	R^2	$S_{\bar{T}_3}$ (^oC)	Acronym	R^2	$S_{\bar{T}_3}$ ^oC
1	ET/ETp	.255	3.9	IDOP	.659	2.7
2	DEPL	.332	3.7	PVI6	.824	2.0
3	Tmax	.457	3.4	ET/ETp	.884	1.6
4	DSR	.496	3.3	R_3	.887	1.7
5	BRT	.587	3.2	Tmax	.895	1.7
6	PH	.587	3.1	DEPL	.923	1.5
7	PVI6	.635	2.9	DSR	.944	1.3
8	GVI	.661	2.8	PC	.960	1.1
	t-test of regression coefficients significant for each of first 3 variables and for DEPL, PH, and BRT among 8 terms.			t-test of regression coefficients significant for each of first 3 variables and for Tmax, DEPL, DSR, R_3, ET/ETp and PC for 8 terms.		

Table 6.4 Summary of statistically significant linear correlation coefficients between each variable measured for sugarcane (SC, n=12), citrus (CT, n=11), and sorghum (SR, n=18) for seven overpass dates from 27 May to 08 July, 1978.

Crop	Variable	DEPL	ET/ETp	IHROP	DSR	TMAX	PH	T3
SC CT SR	R3			.661*				.581*
SC CT SR	PC	-.633* -.646** -.624**	.810**		.623* -.703**	.593* .681** -.618**	.568* .999** .727**	-.600**
SC CT SR	DEPL		-.939** -.856**		.998** .920**	.553* .880**	.796** .646* -.563*	.555*
SC CT SR	ET/ETp				-.945** -.778** -.910**	-.853**	-.763** .644**	-.690**
SC CT SR	IDOP			.975** .975** .975**				.676** .571*
SC CT SR	IHROP							.698** .574*
SC CT SR	DSR					.938**	.778** -.640**	.763**
SC CT SR	TMAX						-.748** -.683* -.581**	.620* .741**
SC CT SR	PH							-.538*

* designates statistical significance at the 0.05 level
** designates statistical significance at the 0.01 level

Table 6.5 Linear correlation coefficients for 8 variables with the central pixel albedo and temperature (R_1, T_1) and with the 3 x 3 pixel mean value of albedo and temperature (R_3, T_3) for 7 dates (27 May through 8 July, 1978) during which ground truth observations and evapotranspiration calculations were being made (n = 51).

Variable Acronym	Mean ± SD	R_1	T_1	R_3	T_3	Mean ± SD
		r				
PC (%)	49.7±19.4	.028	-.282*	.067	-.277**	Same
DEPL (mm)	41.6±29.4	.108	.018	.086	.074	as
ET/ETp	.61±.27	-.098	-.553**	-.072	-.581**	for
IDOP (Ly)	414±47	.174	.650**	.211	.660**	central
IHROP (Ly)	68±29	.329*	.647**	.371**	.668**	pixel
DSR	10.4±9.4	.157	.429**	.124	.477**	↓
Tmax (°C)	35.4±2.1	.173	.357*	.137	.378**	
PH (cm)	147±112	.097	.021	.113	.053	
R (°)	17.3±2.2	-	.360**	-	.412**	17.2±1.8
T	30.8±4.1	.360**	-	.412**	-	30.8±3.9

Table 6.6 Linear correlation coefficient matrix among the independent variables of Table 6.5.

	PC	DEPL	ET/ETp	IDOP	IHROP	DSR	Tmax	PH
PC	-	.112	.450**	-.170	-.167	-.246	.022	.310*
DEPL		-	-.230	-.236	-.205	.730**	.486**	.035
ET/ETp			-	-.143	-.168	-.734**	-.474**	.164
IDOP				-	.971**	.021	.092	.196
IHROP					-	.065	.165	.241
DSR						-	.567**	-.117
Tmax							-	.174
PH								-

7.0 PLANT COVER

7.1 Abstract

HCMM temperatures[a] for five crops (sorghum, citrus, sugarcane, cotton and grass pastures) as one data set were significantly linearly correlated with the vegetation indexes GVI, PVI, and PVI6 but not with percent cover (PC) or plant height (PH). For sorghum, PC (as well as the vegetation indexes) was significantly correlated with HCMM temperatures. Weather (insolation, saturation deficit of the air, and maximum daily air temperature on HCMM overpass dates), geographic (distance of sample sites from the coast) and time (days since irrigation or rainfall) variables influenced HCMM temperatures as much as or more than vegetative conditions when crops that differed in stage of maturity, planting configuration, and PC vs PH relation were combined in one data set. For cotton and sugarcane which were increasing in ground cover during the observation period (27 May to 15 Aug 78), the cooling effect of increasing ground cover was about equally offset by the seasonal increase in ambient air and agricultural landscape temperature. In general, the spread in HCMM temperatures among crops was narrow and the temperatures were below ground-observed air temperatures at the time of the HCMM data acquisitions, 1400 to 1416 hours LST.

From these studies we anticipate that surface temperatures observed by the polar orbiting operational meteorological satellites (NOAA-6 to -9 series) will correlate with vegetation indexes calculated from their visible and near-infrared bands and be interpretable in the AgRISTARS program for synoptic seasonal crop development and drought occurrence applicatons.

7.2 Introduction and objectives

We anticipated that the surface temperature of bare fields would be approximately 20 C higher than those with a dense crop canopy (Wiegand, et al. 1968) and that there would be an approximately linear relation between plant cover, LAI or spectral vegetation indexes (Kauth and Thomas 1976; Richardson and Wiegand 1977) and temperature.

Success in identifying fields that differ in amount of ground cover by living or dead vegetation would have many applications in protecting the soil against water and wind erosion.

Also, the thermal data could be used for the synoptic monitoring of drought. For this application, the more severe the drought the higher the observed surface temperatures should be; that is, the energy balance (Byrne et al. 1979; Soer 1980) would shift to more of the energy going into sensible heat associated with increased soil heating and relatively less into the latent heat flux associated with evapotranspiration. Drought would also limit plant growth, hence ground cover, leaf area indexes, or crop canopy greenness. Although we could not anticipate a drought, we selected fields in both irrigated and dryland farming areas.

---

[a] The HCMM temperatures reported were not adjusted for atmospheric attenuation.

This comparison simulated a drought vs nondrought situation in that the annual free water evaporation is approximately 180-cm for the study area compared with the normal 60-cm of rainfall, so that dry cropland and rangeland sites experience plant growth limiting water deficits periodically throughout the year.

In this study we wanted to document the effect of crop cover on HCMM surface temperature. The extent to which this objective could be met using HCMM data depended upon selection of adequately sized homogenous areas, degree of atmospheric attenuation of emitted energy, registration of HCMM data to the ground scene and other considerations that impacted the quality of data available and on the ability to implement the analysis, and not on the technical soundness of the objectives per se in ground level or low altitude aircraft investigations.

For bare soil, Idso et al. (1975) have shown that the difference between daytime maximum and nightime minimum surface temperature (ΔTs) was inversely related to soil water content in the surface 2 to 4-cm of soil. Cihlar et al. (1979) expressed water content of fallow fields as percent of field capacity (PFC) and confirmed the inverse linear Ts versus PFC for the 0 to 2- and 0 to 4-cm depths.

The relationships are more complicated when plant canopies and crop residues partially cover the ground, but shallow soil moisture apparently continues to dominate. For example, Cihlar et al. (1979) who measured percent bare ground, plant height, percent plant cover, and percent straw cover in cropped and post harvest barley fields were able to explain from 5 to 15% more of the variation in ΔTs by including percent straw cover and percent bare ground in the regression analyses. Wiegand et al. (1968) found that the equivalent blackbody temperature from aircraft scanner data of grain sorghum in small thinned plots at 1400 hours LST was a linear inverse function of leaf area index (LAI); the temperature difference between LAI's of 0.8 and 4.2 was 17 C. Heilman and Moore (1980) found that 1330 hour soil temperature, beneath a barley canopy that changed from 30 to 90% ground cover (PC) over the 45 day study period, as measured by thermocouples 1-mm below the soil surface could be predicted (r^2=.86, S.D.=2.6 C) from canopy temperature measured by a Barnes infrared thermometer and an exponential function of PC. There was no improvement in estimating soil temperature by including LAI, insolation, or maximum daily air temperature. Cihlar (1980) studied the day minus night temperature difference, ΔTs, as a function of plant available water in the 0 to 2 and the 0 to 20-cm surface soil layer for barley canopies that ranged from 60 to 98% ground cover. The correlation between the two decreased as plant cover decreased, and he concluded that plant water stress would be accurately indicated by infrared thermometry only for sufficiently dense canopies. Sutherland and Bartholic (1977) considered the emissivity appropriate for correcting aircraft scanner apparent temperatures to true temperatures and concluded that if the crop height-to-spacing ratio is greater than 1, the composite emissivity of agricultural areas is between 0.98 and 1.00 and temperature errors

are <2 C. Byrne et al. (1979) urged that canopy temperature data be supplemented by data from other sources that document atmospheric demand, root density, and plant and soil characteristics since leaf water status--hence canopy temperature--is affected by these as well as mean moisture content in the root zone.

7.3 Methods

The data for this task are described in report sections 1.2.2 through 1.2.4, and they were processed as described in report sections 2.1.2, 2.1.3, and 2.1.5. Other information on methods used that are necessary for understanding the data and how they were used are given in the particular results section where it applies. The variables used are of general information to all results subsections, however, and are defined as follows:

R3 - average albedo relative to the solar constant at the top of the atmosphere from HCMM reflective band (0.55 to 1.1 μm) for 3x3 arrays of ground site pixels (%). The digital counts given in the HCMM data were ratioed to 255, the digital count for a perfect reflector normal to the sun's rays, and multiplied by 100 to convert to percentage.

T3 - average temperature from HCMM thermal band (10.5 to 12.5 μm) for 3x3 arrays of ground site pixels (°C). The equation used that applies to the temperature range 260 K (0 digital counts, DC) to 340 K (255 digital counts) was

$$T3 = \frac{1251.6}{\ln\left(\frac{14421.6}{DC + 118.21} + 1.0\right)}$$

PC - plant cover estimated visually from a nadir view as fraction of ground area obscured by crop plants and weeds (%). It is an integrated value for the field that incorporates skips in rows into the estimate.

PH - plant height as measured from the soil surface to the uppermost plant part as determined by sighting across the tops of plants (cm).

PVI - perpendicular vegetation index calculated from Landsat bands 5 (0.6 to 0.7 um) and 7 (0.8 to 1.1 μm) digital counts (unitless).

specifically,

$$PVI = \left((Rgg^5 - Rp5)^2 + (Rgg7 - Rp7)^2 \right)^{1/2}$$

where Rp5 and Rp7 are the digital counts for the candidate pixels in Landsat data and Rgg5 = 0.851 Rp5 + 0.355 Rp7 and Rgg7 = 0.355 Rp5 + 0.148 Rp7 are the points of intersection on the soil background line of perpendiculars from Rp5 and Rp7

PVI6 - perpendicular vegetation index calculated from digital counts of Landsat bands 5 and 6 (0.7 to 0.8 μm) (unitless).

GVI - Kauth's green vegetation index = -0.290 (4) - 0.562 (5) + 0.600 (6) + 0.491 (7) where 4, 5, 6, and 7 denote digital counts of Landsat multispectral scanner (MSS) bands 4, 5, 6, and 7, respectively (unitless).

BRT - Kauth's brightness index = 0.433 (4) + 0.632 (5) + 0.586 (6) + 0.264 (7) wherein 4, 5, 6, and 7 denote the digital count of Landsat MSS bands 4, 5, 6, and 7, respectively (unitless).

IDOP - insolation on the day of the pass up to the hour of the overpass (langleys = cal cm^{-2}).

IHROP - insolation the hour of the overpass, measured from 1300 to 1400 hour (langleys).

SDEF - saturation deficit of the air for the hour of the overpass (mb)

Note: IDOP, IHROP and SDEF were measured at one site, the central weather station at Weslaco, TX.

Tmax - air temperature maximum the day of the pass from the observation station, of 22 in the study area, nearest the ground site of interest (°C).

DSR - days since rainfall (or irrigation) from rainfall reporting station nearest the ground site of interest and ground observations of irrigations in process (days).

For readers who may not be familiar with the vegetation indexes, experience indicate that PVI, PVI6, and GVI are most responsive to the amount of living (green) vegetation present whereas BRT responds to the amount of exposed soil in the sensor field of view. As mentioned in Chapter 5, percent cover (PC) may be living or nonliving vegetation (plant residue or senescent plant parts). When the vegetation present is healthy and green, PC and the greenness indicating vegetation indexes are correlated; however, if the vegetation present is a mixture of living and nonliving plant parts, PC may not be correlated with the vegetation indexes or BRT.

The albedo (or reflectance) from the 0.55 to 1.1 um band of HCMM straddles the visible wavelengths from 0.55 to 0.70 um wherein soils are more reflective then plants and the 0.70 to 1.05 um range where plants are more reflective than soil. Consequently, albedos over this wavelength interval are nondescript and may not relate to any of the vegetation indicators.

7.4 Results

7.4.1 Vegetation indexes, percent cover (PC) and plant height (PH) in relation to HCMM temperatures and albedos

We used the data for the 22 intensive sites where PC and PH had been measured weekly from 30 May to 13 Jul. These data were supplemented with Landsat data for two dates (15 Jun and 12 Jul 78) that could be paired with HCMM albedo and temperature data for three dates (12 and 17 Jun and 08 Jul 78). Because clouds obscured some of the fields on Landsat overpass dates and some of the HCMM data were deleted due to cloud and vapor contamination, we were left with 32 data points from the three dates for the intensive sites. There were 30 Landsat vegetation index data points from the representative and weather station sites, but ground observations of PC and PH were not taken. These data sets were analyzed separately and then were combined into one set. The linear correlation coefficient matrices for the HCMM albedo (R3) and temperature (T3) with the vegetation data are presented in Table 7.1.

The linear correlation coefficient matrices of Table 7.1 show that HCMM-observed temperatures correlated significantly and positively with albedo and highly significantly and negatively with PVI, PVI6 and GVI (part C of Table 7.1) the same as for the intensive sites only (part A of Table 7.1). Thus, temperature decreased as amount of green vegetation increased. The positive linear correlation between R3 and T3 indicated that exposed soil dominated the albedo, probably because the sun's energy is concentrated in the visible wavelengths where soil is more reflective than vegetation.

The data for the intensive sites where PC and PH were observed (part A of Table 7.1) indicated that percent cover and plant height were linearly correlated (r=0.422*). However, the correlation was weak due to the variety of crops and planting configurations involved. As shown at the bottom of Part A, the 22 observations were composed of 9 sorghum, 5 sugarcane, 4 citrus, 1 cotton, and 3 grass pasture sites. The noncorrelation between PH and T3 is probably due to the same reasons. For example, the citrus averaged 370 cm in height as opposed to Bermudagrass sod that was only 10 cm tall. The citrus trees are typically planted on 6 or 7 m spacing, and in spite of their height, they averaged only 53% ground cover. The row spacing of sugarcane is typically 1.5 m compared with 90-cm for sorghum and cotton. Sugarcane was growing rapidly during the experimental period; it averaged 146 cm in height on 27 May and 201 cm in height on 08 Jul. Sorghum was at the grain filling stage by the time the measurements were begun so its maximum height and greenness had already occurred; it was, in fact, senescing (lower leaves drying up) during the observations period and two fields had been harvested by 08 Jul. There was little rainfall during the growing season except the first week in June; consequently, dryland cotton and sorghum were water stressed on 27 May and after mid-June.

The vegetation index GVI is very highly correlated (r=0.97** to 0.99**) with the vegetation indexes PVI and PVI6. Whereas GVI is derived by rotation and translation of the coordinate axes in Landsat data space so that one of the axes contains the maximum amount of information about green or living vegetation, PVI and PVI6 are based on the perpendicular distance from the soil background line in Landsat data for pixels containing vegetation. For PVI and PVI6 the greater the displacement from the soil background line (PVI and PVI6=0 for the soil background line) the greater the vegetation density or green leaf area index (LAI) (Wiegand et al. 1979). The high interrelation among these independently derived vegetation indexes adds confidence that they describe vegetation conditions. The PVI6 is less affected by atmospheric conditions than PVI; consequently it gives higher linear correlation coefficients with R3 and T3 than does PVI.

The Kauth brightness (BRT) is negatively correlated with the green vegetation indexes and with PC and PH. This is evidence that BRT is dominated by the exposed soil sensed by Landsat. In fact, BRT is commonly called the soil brightness index. The linear correlation (r= -0.739**) between PH and BRT in Table 7.1, part A, was the highest correlation coefficient observed in the data set, excluding the greenness vegetation index intercorrelations.

In summary, the various analyses presented show that temperature as observed by HCMM is negatively correlated with the greenness vegetation indexes. Consequently, as the amount of living vegetation increased surface temperature decreased. On the other hand, the Kauth brightness (BRT) was negatively linearly correlated with the ground estimates of PC (r=-0.501*) and PH (r=-0.739**), but BRT was not significantly correlated with HCMM measured temperature nor with the greenness vegetation indexes. Therefore, the amount of green vegetation apparently had a stronger effect on surface temperature than did the amount of exposed (bare) soil. Perhaps this is so because vegetation actively affects several aspects of the energy balance--aerodynamic roughness, light energy partitioning per se, and transpiration, a dominant process among the energy dissipation mechanisms.

The linear correlation coefficient matrix is given in Table 7.2 for the 9 sorghum data points from the pooled crops data set of Table 7.1. Percent cover was significantly negatively correlated (r=-0.682**) with HCMM temperature and both PC and PH were significantly positively correlated with each of the vegetation indexes and significantly negatively correlated with BRT. The greenness vegetation indexes were negatively correlated (r=-0.706* to -0.719*) with HCMM temperatures, and brightness was positively correlated (r=0.835**) with HCMM temperature.

The relation between PC and the vegetation indexes PVI and GVI is displayed in the upper part of Figure 7.1, and the relation between the vegetation indexes and HCMM indicated temperatures is shown in the lower part of the figure. The data were pooled for three dates and it is evident that the 08 Jul ground covers are low (due to harvest of the fields) and the temperatures are high.

7.4.2 Influence of other variables relative to that of vegetation on HCMM temperatures and albedos

The data set of part C, Table 7.1, was segregated into irrigated and dryland test sites for the analyses of this section. The objective was to look at variables other than vegetation that affected temperature and albedo.

The results are summarized in Table 7.3 where the analysis of the irrigated sites in Part A of the table and the nonirrigated sites are Part B. For the irrigated sites, seven variables were highly significantly correlated with HCMM temperature for a 3x3 matrix of pixels; the variables, in order of decreasing correlation coefficients, were: insolation on the day of the pass (IDOP), maximum air temperature (Tmax), distance from the coast (DIST), saturation deficit of the air (SDEF), perpendicular vegetation index from Landsat bands 5 and 6 (PVI6), Kauth greenness (GVI) and days since rainfall or irrigation (DSR). For the dryland sites, five variables were highly significantly correlated with the HCMM temperature. They were, in order of decreasing magnitude of the correlation coefficients, SDEF, Tmax, DIST, IDOP, and DSR.

The step-wise multiple regression equations that included six variables are given at the bottom of each part of Table 7.3. For both the irrigated and dryland sites, six variables explain 90% of the variation in the HCMM observed temperatures. The standard error of the estimate of temperature is 1.4 C for the irrigated sites and 1.5 C for the dryland sites. The variables included in the regression analyses are predominantly weather related (insolation, saturation deficit of the air, and maximum daily air temperature), geographic (distance from the coast) and related to evapotranspiration (days since rainfall or irrigation). For the mixture of crops and planting configurations represented in the data set, the spectral vegetation index, PVI6, was the third variable chosen in the regression equation for the dryland sites but no vegetation index was among the first 6 variables chosen for the irrigated sites, although PVI and GVI were the 7th and 8th variables chosen.

From these analyses we conclude that when several crops are pooled, variables such as insolation which relates directly to energy available, air temperature which responds to the sensible heat component, saturation deficit of the air which is a measure of the capacity of air to take on moisture, and days since irrigation or rainfall which is indicating availability of water for evapotranspiration relate more directly to the HCMM temperatures than do indicators of vegetation greenness. When crops are pooled that differ in stage of maturity (or senescence), planting configurations, and that vary crop to crop in relation between height and percent ground cover (or its inverse, exposed soil) then the vegetation indexes are not as closely correlated with observed HCMM temperatures as are the weather variables. These observations are borne out for the nine sorghum fields of Table 7.2 The multiple regression equation for

estimating T3 using 5 variables was T3=-6.70 - 1.075(SDEF) - 2.107 (PVI) + 1.990(PVI6) + 0.030(PC) - 0.005(PH) for which R^2=0.998 and the standard error of the estimate of T_3 was 0.13 C. Within this single crop, 4 of the 5 variables included were vegetation parameters and only one was weather related. The SDEF alone explained 76% of the variation in surface temperature of the grain sorghum fields, SDEF + PVI6 explained 91%, and SDEF + PVI6 + PVI explained 99.2% of the variation. These findings suggest the desirability of looking at relationships within crops. We attempt that in the following sections.

7.4.3 Percent cover versus plant height within crops

The data for the analyses are the ground truth for the intensive sites corresponding to the eight HCMM overpass dates (27 May; 06, 12, 17 and 23 Jun; 03 and 08 Jul; and 15 Aug 78). Table 7.4 describes the data in terms of number of observations per crop, summarizes the means and standard deviations in both PC and PH, and presents the equations that relate PC to PH. The intercept values differed considerably among crops and so did the coefficients for the PH term. The growing season was well along before plant measurements were begun in this study so that an intercept value greatly different from zero (the predicted PC at zero PH) is not alarming. The quadratic equation for sorghum resulted from head extension above the leaf canopy and the fact that some plant heights following combining and even tillage are included in the data set (Consequently, there are observations at low PC and PH.). Within row crops, plant population (plants per unit area) was variable; this introduced variability in PC without affecting PH. In plotting the data by soil type for cotton and sugarcane for the water use studies (Chapter 6.0), it was evident that on clay soils the PC was greater for a given plant height than for the nonclay soil types. The slopes were the same, but the intercepts differed. Thus soil type caused some of the variability in the relation between PC and PH.

In summary, there was a highly significant relation between PH and PC for sorghum, sugarcane, cotton, and citrus. However, no two crops gave similar percent cover prediction equations due to differing slopes and intercepts.

7.4.4 Temperature versus percent cover within crops

The data for this analysis are the ground truth for the intensive sites corresponding to the eight HCMM overpass dates from 27 May to 15 Aug 78. Table 7.5 describes the data in terms of number of observations per crop, summarizes the means and standard deviations in both PC and T3, and presents the equations that relate PC to T3.

Grain sorghum was the only crop for which the relationship was significant (r^2=0.522**). The regression equation predicted a surface temperature of 36.5 C for 0% ground cover and a decrease in temperature of 1.3 C for each 10% increase in ground cover. This result appears physically meaningful until one considers that sorghum was senescing during the period Jun to Aug so that the ground cover was decreasing at the same time air temperature was increasing. Sugarcane increased

in ground cover during the 27 May to 15 Aug time period, and it had no correlation between ground cover and crop canopy temperature. Thus we believe that for sugarcane the cooling effect of an increase in ground cover was offset by the seasonal increase in ambient air and agricultural landscape temperature during the observation period. The citrus sites all had 54 ±2% ground cover so that changes in their temperature were a function of time and other variables besides ground cover. There were only 8 observations for cotton and they seemed to behave like sugarcane. Cotton had a lower temperature than the other crops because the temperature observations were limited to the first three dates 27 May, 06 Jun and 12 Jun 78.

Within the range of ground covers of the four crops studied, ground cover was not very strongly related to observed surface temperature. For the crops that were increasing in ground cover during the observation period (sugarcane, cotton), the cooling effect of increasing ground cover was about equally offset by the seasonal increase in ambient air and agricultural landscape temperature during the observation period.

7.4.5 Temperature comparison among crops

One of the objectives of this study was to determine whether surface or canopy temperature differed among crops, HCMM resolution permitting. Although we had eight HCMM overpasses in a 2½ month period from the end of May to mid-August, we deleted approximately one-third of the temperature observations due to cloud or vapor contamination. Therefore, no ground site was consistently represented in the data. In addition, one date (17 Jun 78) yielded low temperatures - probably due to high cirrus cloud contamination - and was eliminated completely. However, by scanning the summaries of the temperature data by individual ground site, we found three sorghum sites, two sugarcane sites and two citrus sites were represented on five of the eight dates.

The comparison of temperature among crop surfaces as well as relative to that of a deep water body and maximum air temperature at the central weather station are presented in Figure 7.2. The data show the average temperature for the vegetated sites is 4.4 C lower on 06 Jun than on 27 May. These observations were made preceding and just after heavy rains on 04 to 06 Jun, respectively. It was essentially rainless again for the remainder of the study period.

The sorghum grain was maturing in June, the crop was harvested by mid-July, and the land was fallow by 15 Aug. By contrast, sugarcane (an irrigated crop) was growing rapidly from June to August. The perennial citrus trees, also irrigated, were essentially invariant in ground cover during this fraction of a growing season.

The temperature of all the crops increased after the 06 Jun observation date. The temperature of sugarcane and citrus tends to be similar and both are cooler than the grain sorghum fields. On 15 Aug the citrus was about 3 C cooler than the fallow sorghum, and the Lake water is about 10 C cooler than the cropped sites. For these uncorrected temperature data, maximum daily air temperature was above crop surface temperature, except on 15 Aug 78 when the fallow sorghum was above air temperature.

Generally, the data show that the temperature spread among crops is narrow and that the uncorrected crop surface temperature was below daily maximum air temperature when the sites were vegetated.

7.5 Literature cited

Byrne, G. F., J. E. Begg, P. M. Fleming, and F. X. Dunin. 1979. Remotely sensed land cover temperature and soil water status--a brief review. Remote Sensing of Environment. 8:291-305.

Cihlar, J., T. Sommerfeldt, and B. Peterson. 1979. Soil water content estimation in fallow fields from airborne thermal scanner measurements. Canadian J. Remote Sensing. 5:18-32.

Cihlar, J. 1980. Soil water and plant canopy effects on remotely measured surface temperatures. Int'l. J. Remote Sensing. 1:167-173.

Heilman, J. L. and D. G. Moore. 1980. Thermography for estimating near-surface soil moisture under developing crop canopies. J. Applied Meteorol. 19:324-328.

Idso, S. B., T. L. Schmugge, R. D. Jackson, and R. J. Reginato. 1975. The utility of surface temperature measurements for the remote sensing of soil water status. J. Geophys. Res. 80:3044-3049.

Kauth, R. J. and G. S. Thomas. 1976. The tasseled cap--A graphic description of the spectral-temporal development of agricultural crops as seen by LANDSAT. Proc. Sympos. Machine Proc. of Remote Sensing Data. (LARS, Purdue Univ.) IEEE Cat. No. 76, Ch. 1103-1 MPRSD.

Richardson, A. J. and C. L. Wiegand. 1977. Distinguishing vegetation from soil background information. Photogram. Engin. and Remote Sensing. 43:1541-1552.

Soer, G. J. R. 1980. Estimation of regional evapotranspiration and soil moisture conditions using remotely sensed crop surface temperatures. Remote Sensing of Environment. 9:27-45.

Sutherland, R. A. and J. F. Bartholic. 1977. Significance of vegetation in interpreting thermal radiation from a terrestrial surface. J. Applied Meteorol. 16:759-763.

Wiegand, C. L., M. D. Heilman, and A. H. Gerbermann. 1968. Detailed plant and soil thermal regime in agronomy. Proc. 5th Sympos. Remote Sensing of Environment. pp. 325-342. Univ. Michigan, Ann Arbor.

Wiegand, C. L., A. J. Richardson, and E. T. Kanemasu. 1979. Leaf area index estimates for wheat from LANDSAT and their implications for evapotranspiration and crop modeling. Agron. J. 71:336-342.

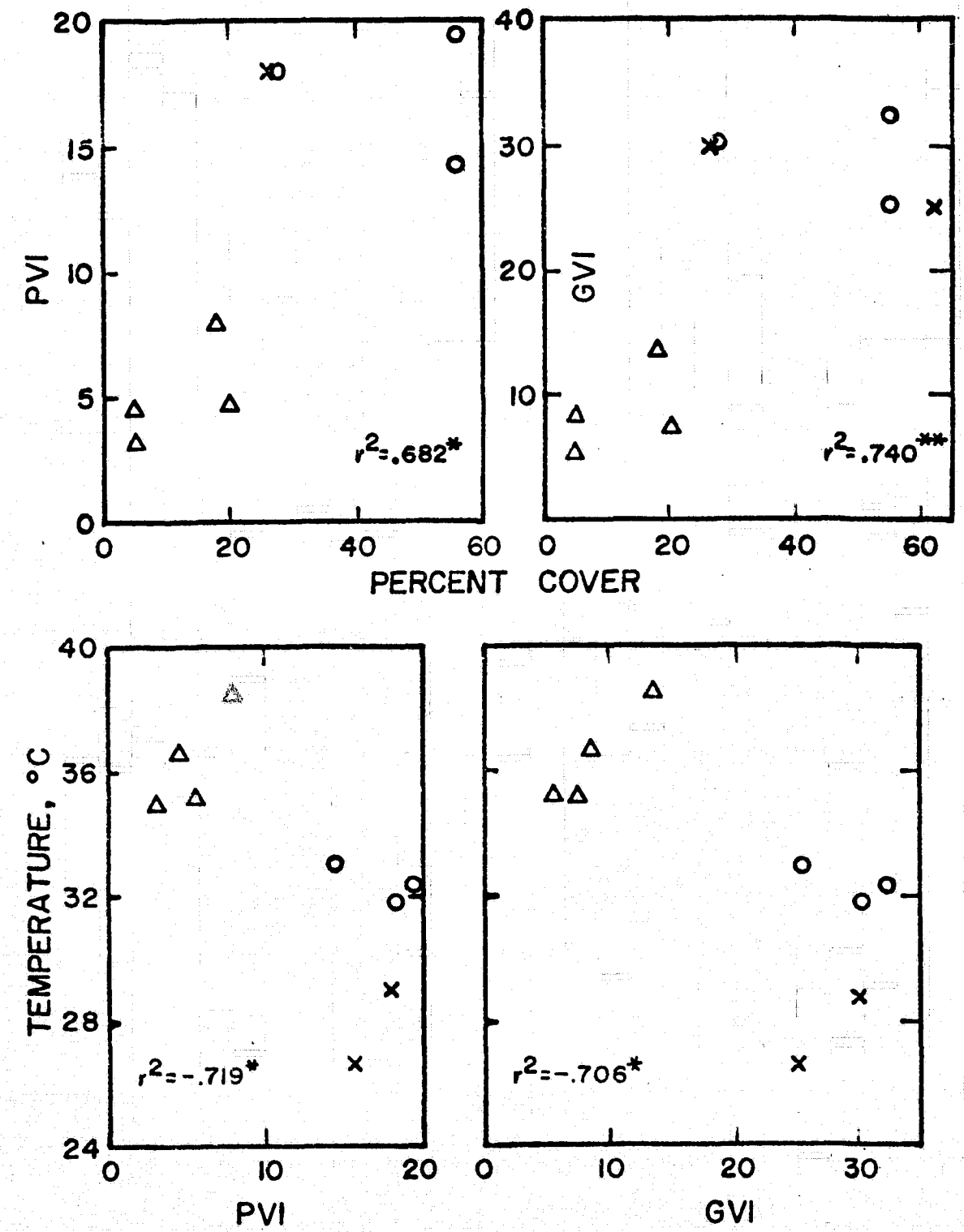

Figure 7.1 Relation between PC and vegetation indexes PVI and GVI (upper figures) and between vegetation indexes and HCMM indicated temperature (lower figures). Data are from sorghum fields for three dates: 12 Jun. 78, o ; 17 Jun. 78, x; and 08 Jul. 78, Δ.

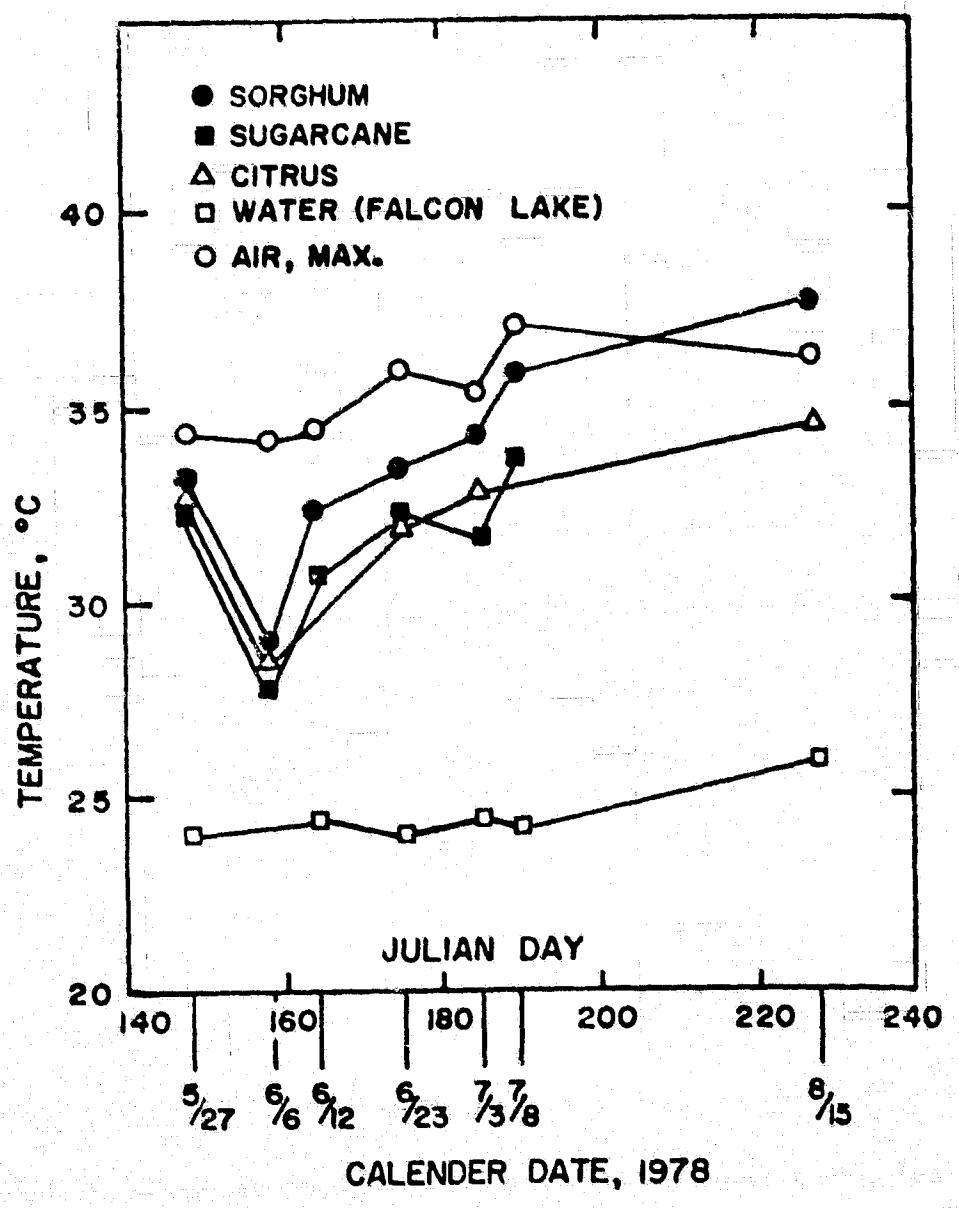

Figure 7.2 Temperatures of sorghum, sugarcane and citrus sites relative to that for Falcon Lake water and air on seven dates (Temperatures were not corrected by radiative transfer model.).

Table 7.1 Linear correlation coefficient matrices among HCMM albedo (R3), HCMM temperature (T3), and plant parameters for mixed crops.

A. Intensive sites (HCMM, Landsat and ground truth(GT) observations)

	R3 (%)	PVI	PVI6	BRT	GVI	PC (%)	PH (cm)	T3 (°C)
		dimensionless						
R	-	-.052	$-.063^{**}$	.062	$-.059^{**}$	.273	.114	$.479^{*}$
PVI		-	$.973^{**}$	-.241	$.987^{**}$	.419	.413	$-.513^{**}$
PVI6			-	-.268	$.996^{**}$	$.406^{*}$	$.347^{**}$	$-.622^{**}$
BRT				-	-.249	$-.501^{*}$	$-.739^{**}$	$.245^{**}$
GVI					-	.339	$.362^{*}$	$-.581^{**}$
PC						-	$.422^{*}$	-.268
PH							-	.023
T3								-
Mean	17.3	13.9	19.0	77.2	22.7	49.2	137.1	31.9
S.D.	1.3	7.6	9.9	9.1	11.2	23.2	111.9	4.5

n = 22 r (0.05) = 0.423 ; r (0.01) = 0.537
Observations of each crop: sorghum, 9; sugarcane, 5; citrus, 4; cotton, 1 and grass, 3

B. Representative and weather station sites (HCMM and Landsat observations)

R	—	.423	$.500^{**}$	$.435^{*}$	$.539^{**}$	No data	No data	.192
PVI		-	$.967^{**}$	.346	$.973^{**}$			$-.302^{*}$
PVI6			-	.355	$.991^{*}$			-.393
BRT				-	.362			.095
GVI					-			-.304
T3								-
Mean	17.2	11.6	15.8	76.4	18.5			31.4
S.D.	2.0	5.5	8.6	11.0	10.0			3.9

n = 30 r (0.05) = 0.361 ; r (0.01) = 0.463
Observations of each crop: sorghum, 4; sugarcane, 1; citrus, 5; mixed crops,12; range, 4; wildlife refuge, 2 and mud flat, 2

C. Above data sets combined

R	-	.221	$.290^{*}$	$.332^{*}$	$.321^{*}$			$.278^{*}$
PVI		-	$.967^{**}$	.084	$.976^{**}$			$-.394^{**}$
PVI6			-	.104	$.993^{**}$			$-.485^{**}$
BRT				-	.122			.156
GVI					-			$-.415^{**}$
T3								-
Mean	17.2	12.6	17.1	76.8	20.3			31.6
S.D.	1.8	6.5	9.2	10.1	10.6			4.1

n = 52 r (0.05) = 0.273 , r (0.01) = 0.354

Table 7.2 Linear correlation coefficient matrix among HCMM albedo, HCMM temperature, and plant parameters for grain sorghum.

	R3	PVI	PVI6	BRT	GVI	PC	PH	T3
	(%)	-------dimensionless-------				(%)	(cm)	(^{o}C)
	r							
R	-	.265	.286	.197	.282	.349	.387	.122
PVI		-	.996**	-.651*	.998*	.740**	.670*	-.719*
PVI6			-	-.632*	-.998**	.750**	.666*	-.718*
BRT				-	-.622*	-.733*	-.704*	.835**
GVI					-	.737**	.653*	-.706*
PC						-	.814**	-.682*
PH							-	-.501
T3								-
Mean	17.2	11.8	16.5	81.7	19.9	31.0	64.2	33.2
S.D.	1.5	6.7	10.1	9.0	11.0	22.2	35.6	3.7

n = 9 r $(0.05)^{*}$ = 0.602 r $(0.01)^{**}$ = 0.735

Table 7.3 Linear correlation coefficient matrix for irrigated sites (part A) and dryland sites (part B). Data are from HCMM, Landsat, and weather observations for JD 163, 168, and 189.

A. Irrigated sites (n = 26)

	IDOP (Ly)	SDEF (mb)	DIST (km)	PVI	PVI6	BRT	GVI	T_{Max} (°C)	DSR (days)	T3 (°C)
				----------dimensionless----------						
R3	0.276	-0.218	0.610**	0.079	0.140	0.161	0.132	0.091	-0.058	0.301
IDOP	-	0.702**	0.580**	-0.342	-0.511**	-0.166	-0.469*	0.876**	0.602**	0.863**
SDEF		-	0.138	-0.163	-0.409*	0.055	-0.345	0.841**	0.580**	0.664**
DIST			-	-0.356	-0.374	-0.104	-0.367	0.387	0.182	0.699**
PVI				-	-0.963**	0.274	0.980**	-0.183	-0.417*	-0.454*
PVI6					-	0.267	0.992**	-0.394*	-0.548**	-0.592**
BRT						-	0.277	-0.023	-0.105	-0.131
GVI							-	-0.340	-0.517**	-0.555**
T_{Max}								-	0.430*	0.722**
DSR									-	0.541**
T3										-
Mean	408	30.6	80.7	14.7	19.9	76.4	23.5	36.1	17.1	31.1
S.D.	53.7	8.9	20.5	6.8	9.1	6.8	10.4	1.5	10.5	4.0

Multiple regression equation for 6 variables:

$$T3 = -5.200 - 0.248(SDEF) + 0.044(DIST) - 0.244(PVI6) + 1.684(Tmax) + 1.396(DSR) - 10.423((DSR)^{1/2})$$

$R^2 = 0.897$;; standard error of the estimate of temperature = 1.5 C.

Table 7.3 cont'd

B. Dryland sites(n=26)

	IDOP	SDEF	DIST	PVI	PVI6	BRT	GVI	Tmax	DSR	T3
R3	0.541**	0.068	0.665**	0.361	0.411*	0.391*	0.470*	0.141	-0.128	0.308
IDOP	–	0.550**	0.527**	-0.184	-0.219	0.321	-0.162	0.327	0.269	0.633**
SDEF		–	0.450*	-0.495*	0.579**	0.319	-0.469*	0.846**	0.943**	0.764**
DIST			–	0.099	0.118	0.417*	0.221	0.508**	0.313	0.708**
PVI				–	0.977**	-0.028	0.975**	-0.229	0.505**	-0.345
PVI6					–	0.000	0.989**	-0.290	-0.591**	-0.378
BRT						–	0.038	0.237	0.160	0.402*
GVI							–	-0.157	-0.487*	-0.274
Tmax								–	0.841**	0 .723**
DSR									–	0.621**
T3										–
Mean	408	28.1	76.6	10.1	14.0	78.6	16.5	35.5	15.7	31.9
S.D.	54.3	8.5	31.9	5.4	8.7	13.2	10.0	1.7	12.4	4.1

$r\ (0.05) = 0.388$, $r\ (0.01) = 0.496$

Multiple regression equation for 6 variables:

$$T3 = 37.58 + 0.055(IDOP) + 0.086(DIST) + 0.231(SDEF) - 1.050(Tmax) - 2.539(DSR)^{\frac{1}{2}} + 0.280(DSR)$$

$R^2 = 0.902$; standard error of the estimate of temperature = 1.4 C.

Table 7.4 Relation between percent cover (PC) and plant height (PH) for four different crops. The data is from ground truth observations corresponding to 8 HCMM overpass dates between 27 May and 15 Aug. 78, for the 22 intensive sites.

Attribute	Crop			
	Sorghum	Sugarcane	Cotton	Citrus
No. of observations:	47	35	28	22
PH Mean (cm):	60.1	169.9	57.6	367.5
PH Stnd. dev. (cm):	33.8	23.3	10.2	57.7
PC Mean (%):	30.2	54.4	52.0	53.4
PC Stnd. dev. (%):	11.9	16.1	17.3	2.4

Crop	Equation	r^2 or R^2	Stnd. error of PC estimate (%)
Sorghum	$PC = 4.375 - 0.302(PH) + 0.009(PH)^2$	0.872^{**}	8.1
Sugarcane	$PC = -50.3 + 0.891(PH)$	0.794^{**}	7.4
Cotton	$PC = -33.2 + 1.478(PH)$	0.764^{**}	8.6
Citrus	$PC = 68.6 - 0.041(PH)$	0.989^{**}	0.04

Table 7.5 Relation between plant cover and temperature among crops. The data are from ground observations corresponding to 8 HCMM overpass dates between 27 May and 15 Aug. 78, for the 22 intensive test sites.

Attribute	Crop			
	Sorghum	Sugarcane	Cotton	Citrus
No. of observations:	33	18	8	16
PC Mean (%):	28.0	56.7	41.0	54.1
PC stnd. dev. (%):	20.2	15.4	14.7	2.0
T3 Mean(^{o}C)	32.7	30.6	29.7	32.2
T3 stnd. dev.	3.8	2.8	2.3	2.4

Crop	Equation	r^2	Stnd. error of T3 estimate
Sorghum	T3= 36.51-0.135(PC)	.522**	2.6
Sugarcane	T3= 29.85+.012(PC)	.005	2.9
Cotton	T3= 28.17+.037(PC)	.058	2.3
Citrus	T3= 3.58+.530(PC)	.192	2.3

Table A.1. Composition of intensive sites by fields, field sizes, and crops within larger sample segments.

Site No.	Typifying field	Hectares	Crop[a]	Sample segment	Hectares	No. of fields
10101	1	76	SR	1010A	392	6
10102	2	99	CO			
30901	1	1538	SR	3090A	1538	1
31001	1	1237	SR	3100	1237	1
31011	1	145	SR	3101	145	1
41341	1	379	SR	4134	379	1
41381	1	312	SR	4138	482	3
41421	2	19	SR	4142	123	8
41422	2	33	SC			6
10194	4	118	SC	1019	395	7
10196	6	73	SC			
30951	1	79	SC	3095	187	6
30955	5	33	CO			
41665	5	125	SC	4166	202	6
51782	2	50	SC	5178	116	3
10381	1,2,6,9	35,40,17,26	CO	1038	290	10
20611	1	231	CO	2061	252	2
20681	11,8	101,15	CT	2068A	282	16
20754	4	82	CT	2075	280	6
31166	6,4,5,7	18,29,9,4	CT	3116	108	10
20612	1	272	GR[b]	2061A	272	1
20651	1	480	GR[b]	2965A	480	1

[a] SR, sorghum; CO, cotton; SC, sugarcane; CT, citrus; GR, grass

[b] 20612, Bermudagrass; 20651, buffelgrass

Table A.2. Ground truth summary for intensive sites for three sampling dates.

Site No.	Julian Date	PH (cm)	PC (%)	DSR (days)	TMAX (°C)	TMIN (°C)	DEPL (mm H_2O)	ET/ETp (-)	DIST (km)	WCAP (cm)
SORGHUM										
10101	163	82	40	5	35.0	22.2	25.4	.58	50.61	17.5
	168	83	40	10	33.9	21.1	41.6	.46		
	189	40	2	31	37.8	21.7	89.2	.17		
30901	163	70	28	3	34.4	23.9	12.7	.52	85.61	15.5
	168	70	28	8	35.6	22.8	27.1	.40		
	189	0(BS)	5	29	37.2	24.4	65.0	.13		
31001	163	95	56	3	34.4	23.9	14.0	.59	99.14	15.5
	168	95	56	8	35.6	22.8	30.8	.46		
	189	10(BS)	5	29	37.2	24.4	75.4	.16		
31011	163	90	56	3	34.4	23.9	14.0	.59	99.59	15.5
	168	90 BS-	57	8	35.6	22.8	30.8	.46		
	189	15(weeds)	10	29	37.2	24.4	75.4	.16		
41341	163	60	21	8	36.1	25.0	25.9	.39	116.51	15.5
	168	61	20	13	36.1	23.3	37.9	.32		
	189	62	18	34	37.8	24.4	64.8	.08		
41381	163	93	65	5	35.0	23.9	28.7	.74	48.4	17.5
	168	93	63	10	35.6	22.2	51.9	.65		
	189	0(BS)	0	31	37.8	23.9	114.2	.24		
41421	163	84	19	5	34.4	23.9	22.4	.52	88.9	15.5
	168	84	18	10	35.6	22.8	36.4	.58		
	189	88	20	31	37.2	24.4	77.7	.14		
SUGARCANE										
10194	163	180	71	4	35.0	22.2	26.7	.94	55.0	17.5
	168	185	75	9	33.9	21.1	57.2	.88		
	189	220	83	17	37.8	21.7	114.2	.82		
10196	163	150	45	4	35.0	22.2	26.5	.92	54.1	17.5
	168	158	49	9	33.9	21.1	56.8	.88		
	189	203	72	19	37.8	21.7	126,1	,82		
30951	163	150	95	5	35.0	23.9	34.7	.96	51.9	17.5
	168	160	95	10	35.6	22.2	66.5	.92		
	189	205	94	10	37.8	23.9	72.7	.91		
41422	163	151	48	0	34.4	23.9	0.0	.89	89.4	15.5
	168	158	51	5	35.6	22.8	32.5	.95		
	189	204	75	11	37.2	24.4	78.2	.87		
41665	163	155	33	4	35.0	22.2	24.2	.84	66.8	19.5
	168	155	35	9	33.9	21.1	51.1	.76		
	189	160	70(weeds) 50%	6	37.8	21.7	45.5	.95		

Table A.2 Continued.

Site No.	Julian Date	PH (cm)	PC (%)	DSR (days)	TMAX (°C)	TMIN (°C)	DEPL (mm H_2O)	ET/ETp (-)	DIST (km)	WCAP (cm)
51782	163	165	47	9	35.0	22.2	53.7	.89	91.3	19.5
	168	170	49	14	33.9	21.1	82.2	.82		
	189	215	72	18	37.8	21.7	90.0	.80		
COTTON										
10102	163	45	26	5	35.0	22.2	30.2	.80	61.0	17.5
	168	45	28	10	33.9	21.1	56.1	.75		
	189	49	38	31	37.8	21.7	145.0	.46		
10381	163	52	62	9	35.0	22.2	51.2	.95	69.9	19.5
	168	58	70	14	33.9	21.1	81.8	.88		
	189	66	81	1	37.8	21.7	6.8	.86		
20611	163	70	64	5	35.0	22.2	30.9	.84	63.2	15.5
	168	70	68	10	33.9	21.1	57.3	.75		
	189	70	66	31	37.8	21.7	111.2	.00		
30955	163	60	50	5	35.0	23.9	33.1	.91	51.8	15.5
	168	62	54	10	35.6	22.2	62.6	.84		
	189	70	62	31	37.8	23.9	133.5	.31		
CITRUS										
20681	163	450	50	5	35.0	22.2	19.5	.41	81.8	17.5
	168	450	50	2	33.9	21.1	8.9	.75		
	189	450	50	18	37.8	21.7	77.8	.41		
20754	163	330	55	19	36.1	25.0	55.0	.43	110.7	15.5
	168	330	55	24	36.1	23.3	69.0	.42		
	189	330	55	14	37.8	24.4	54.1	.45		
31166	163	328	55	9	36.1	25.0	31.8	.40	97.2	17.5
	168	328	55	14	36.1	23.3	44.8	.38		
	189	328	55	17	37.8	24.4	64.2	.43		
BERMUDAGRASS										
20612	163	11	60	5	35.0	22.2	27.2	.74	61.8	15.5
	168	11	60	10	33.9	21.1	51.0	.68		
	189	12	70	31	37.8	21.7	119.6	.17		
BUFFELGRASS										
29651	163	22	75	3	34.4	23.9	14.7	.67	109.7	15.5
	168	22	75	8	35.6	22.8	34.1	.52		
	189	20	70	29	37.2	24.4	48.4	.00		

Table A.3 Landsat digital count sample means and vegetation indexes for two dates.

Site	Landsat Digital Counts				Vegetation Indexes			
	MSS4	MSS5	MSS6	MSS7	PVI	PVI6	BRT	GVI
A, June 15, 1978								
41381	25	54	55	27	15.4	21.5	65.9	25.1
30901	27	29	65	32	18.2	26.2	77.7	30.5
31001	27	28	66	33	19.8	27.7	77.8	32.5
31011	31	35	66	30	14.3	22.2	82.8	25.4
41341	31	39	58	26	9.6	14.5	79.5	17.2
41422	33	34	85	40	23.9	36.9	97.3	41.5
10196	24	21	73	38	27.4	37.6	77.3	43.9
41665	25	24	61	29	17.5	26.4	69.8	29.9
51782	28	27	60	28	16.0	24.0	72.5	27.0
10102	33	37	66	28	12.0	21.4	84.2	23.0
10381	26	25	76	35	23.0	37.0	82.0	41.5
20681	23	25	48	22	10.9	16.8	60.6	19.3
31166	21	21	52	24	14.7	21.7	60.3	25.1
20754	25	28	49	22	9.9	14.8	63.6	17.3
10194	25	24	61	29	17.5	26.4	69.8	30.0
20612	29	35	51	22	7.5	12.0	71.6	13.8
20651	33	43	56	24	5.6	10.5	81.6	11.9

Table A.3 Continued.

Site	Landsat Digital Counts				Vegetation Indexes			
	MSS4	MSS5	MSS6	MSS7	PVI	PVI6	BRT	GVI
B. July 12, 1978								
41381	32	40	42	19	1.9	2.0	69.8	2.4
30901	35	50	54	24	3.2	3.6	85.5	5.8
31001	39	58	64	29	4.6	5.7	99.2	8.5
31011	38	56	66	31	7.2	8.6	99.7	12.4
41341	33	47	60	28	8.0	10.1	87.1	13.6
41421	34	46	52	24	4.8	5.2	81.3	7.5
41422	29	28	68	38	24.2	29.0	80.9	35.2
10194	35	37	72	37	20.0	25.5	91.6	30.1
10196	28	24	70	40	27.4	33.0	80.1	39.7
41665	29	31	52	26	12.0	15.1	70.4	18.1
51782	29.	27	66	36	22.9	28.0	79.1	33.6
30955	30	36	57	28	12.4	15.7	77.0	19.3
10102	32	38	52	24	8.0	10.4	75.9	12.6
20611	28	33	51	26	11.4	13.3	70.7	17.0
10381	24	22	69	37	25.7	34.2	75.4	40.4
20681	28	31	55	28	14.4	17.5	72.3	21.7
31166	25	26	52	27	15.3	18.7	66.1	23.0
20754	27	31	49	25	11.5	13.2	67.4	16.7
20651	33	48	52	23	3.4	3.8	82.4	6.1
20612	30	35	45	22	6.7	7.2	67.8	9.4

Table A.4 Temperatures (T1, T3, T9) and albedos (R1, R3, R9) and their standard deviations for 1x1, 3x3, and 9x9 pixel samples by site number for 12 June 1978 (J.D. 163).[a/]

Site No.	T1	T3	T9	R1	R3	R9
10101	*****	*****	*****	*****	*****	*****
	***	***	***	***	***	***
30901	31.71	31.82	31.39	18.03	17.55	18.37
		0.4	1.6		0.8	1.8
31001	32.34	32.45	32.55	19.21	19.25	19.34
		0.4	0.7		0.6	0.7
31011	33.90	33.03	31.98	18.43	19.08	19.08
		0.9	0.9		0.4	0.8
41341	19.84	23.83	31.16	20.39	17.73	18.27
		4.2	4.9		2.9	2.8
41381	(20.88)	(22.77)	(26.31)	(20.39)	(20.94)	(21.31)
		(2.3)	(2.7)		(2.1)	(1.6)
41421	30.45	30.24	30.40	18.43	18.43	19.30
		0.6	0.9		1.3	1.6
10194	(26.58)	(25.28)	(25.18)	(18.82)	(19.82)	(20.27)
		(2.2)	(1.6)		(1.5)	(1.4)
10196	(25.26)	(23.72)	(25.18)	(20.00)	(21.17)	(20.62)
		(2.3)	(1.7)		(1.4)	(1.4)
30951	(26.91)	(27.51)	(27.28)	(19.60)	(20.61)	(20.61)
		(1.0)	(2.0)		(1.4)	(2.1)
41422	30.77	30.55	30.52	19.21	18.73	19.36
		0.7	0.9		1.0	1.5
41665	(28.21)	(27.14)	(25.81)	(17.25)	(18.87)	(19.08)
		(0.8)	(3.0)		(1.0)	(2.1)
51782	(30.13)	(29.45)	(27.70)	(21.96)	(22.10)	(20.21)
		(1.0)	(2.7)		(1.3)	(2.3)
10102	*****	*****	*****	*****	*****	*****
		***	***	***	***	***
10381	(22.58)	(23.88)	(25.93)	(13.33)	(16.66)	(18.68)
		(3.8)	(3.1)		(1.8)	(2.2)
20611	29.49	29.21	29.34	24.31	20.39	19.11
		1.2	2.7		2.4	2.3
30955	(20.88)	(23.57)	(26.56)	(18.43)	(19.60)	(21.21)
		(2.7)	(2.3)		(1.3)	(2.0)
20681	29.17	29.60	28.75	19.21	18.56	18.74
		0.6	2.3		0.4	1.3
20754	33.28	33.62	33.47	19.60	18.64	18.49
		0.8	0.9		0.7	0.7
31166	31.71	33.17	33.59	17.64	18.16	18.16
		1.0	1.0		0.5	0.8
20612	24.26	25.67	28.36	18.03	19.34	19.60
		3.2	2.7		2.9	2.3
20651	35.44	34.89	34.10	20.00	19.08	19.22
		0.6	1.1		0.7	1.0

[a/] Asterisks denote deleted cloud contaminated data: Parentheses denote sub-visible cirrus contaminated data (also deleted).

Table A.4 continued. Data for 17 June 1978 (J.D. 168).

Site No.	T1	T3	T9	R1	R3	R9
10101	23.93	24.30	24.78	16.86	15.77	16.15
		0.4	0.5		1.0	1.5
30901	29.17	29.03	28.82	16.47	16.07	17.24
		0.5	1.2		1.5	1.7
31001	*****	*****	*****	*****	*****	*****
		***	***		***	***
31011	*****	*****	*****	*****	*****	*****
		***	***		***	***
41341	31.08	30.58	32.89	18.82	17.74	16.65
		2.8	2.4		3.0	2.8
41381	27.23	26.69	26.08	16.07	15.86	16.48
		0.6	0.8		0.6	1.1
41421	*****	*****	*****	*****	*****	*****
		***	***		***	***
10194	25.26	24.71	24.79	14.50	15.64	16.15
		0.4	0.5		1.2	1.1
10196	24.26	24.49	24.67	14.90	15.68	16.33
		0.3	0.5		1.1	1.4
30951	24.26	24.93	25.25	16.86	17.08	16.00
		0.4	0.8		0.9	1.1
41422	*****	*****	*****	*****	*****	*****
		***	***		***	***
41665	(23.60)	(25.00)	(24.97)	(14.50)	(16.07)	(17.52)
		(0.9)	(1.8)		(2.1)	(2.2)
51782	*****	*****	*****	*****	*****	*****
		***	***		***	***
10102	24.26	24.49	24.79	15.68	15.55	15.98
		0.5	0.4		1.4	1.5
10381	(26.25)	(25.70)	(26.55)	(18.43)	(17.47)	(17.72)
		(0.5)	(2.0)		(0.9)	(1.3)
20611	26.25	27.05	26.34	16.86	16.47	15.78
		0.8	1.1		1.3	1.5
30955	24.94	24.97	25.20	15.68	16.12	16.19
		0.3	0.6		0.7	1.1
20681	*****	*****	*****	*****	*****	*****
		***	***		***	***
20754	(34.21)	(32.23)	(29.79)	(16.47)	(17.29)	(17.41)
		(1.2)	(2.3)		(1.3)	(3.5)
31166	*****	*****	*****	*****	*****	*****
		***	***		***	***
20612	25.26	25.59	25.75	17.25	16.64	15.84
		0.5	0.9		1.0	1.3
20651	*****	*****	*****	*****	*****	*****
		***	***		***	***

Table A.4 continued. Data are for 08 July 1978 (J.D. 189).

Site No.	T1	T3	T9	R1	R3	R9
10101	(23.26)	(23.70)	(25.02)	(17.25)	(16.94)	(17.06)
		(1.1)	(3.0)		(0.5)	(0.6)
30901	34.82	35.30	35.89	14.50	15.20	15.91
		1.1	1.0		0.5	1.1
31001	36.35	36.62	36.30	18.43	18.16	18.06
		0.5	0.7	0.3	0.3	0.8
31011	35.44	35.54	35.95	15.29	16.60	17.85
		1.0	1.1		1.1	1.2
41341	38.76	38.49	36.88	18.03	16.03	15.47
		0.7	1.2		1.5	1.1
41381	(27.23)	(27.05)	(26.97)	(16.07)	(17.08)	(17.08)
		(0.8)	(1.3)		(0.6)	(0.9)
41421	36.05	35.22	33.55	18.43	17.90	16.88
		1.7	2.0		0.7	1.3
10194	(26.91)	(25.13)	(25.56)	(16.47)	(16.81)	(17.02)
		(2.7)	(2.7)		(0.8)	(0.8)
10196	25.59	26.35.	26.24	16.07	16.86	16.83
		2.0	2.8		0.9	0.9
30951	*****	*****	*****	*****	*****	*****
		***	***		***	***
41422	36.96	36.01	33.50	18.43	18.30	16.82
		1.1	2.0		0.5	1.3
41665	(31.40)	(31.11)	(30.33).	(15.68)	(15.94)	(16.21)
		(1.5)	(1.7)		(0.8)	(1.1)
51782	29.81	31.28	32.15	18.43	17.82	17.85
		1.9	2.1		0.9	0.9
10102	(22.92)	(23.37)	(25.75)	(18.03)	(17.08)	(17.18)
		(1.1)	(3.5)		(0.6)	(0.9)
10381	(30.45)	(30.41)	(30.10)	(18.43)	(17.64)	(16.99)
		(1.6)	(1.9)		(0.9)	(1.3)
20611	(28.53)	(28.48)	(28.77)	(16.47)	(16.20)	(15.62)
		(2.3)	(2.4)		(0.3)	(0.9)
30955	(27.23)	(27.05)	(26.99)	(18.43)	(17.86)	(17.25)
		(1.2)	(2.1)		(0.6)	(0.9)
20681	(31.40)	(31.78)	(31.61)	(16.47)	(16.38)	(16.31)
		(0.5)	(1.2)		(0.7)	(1.2)
20754	36.96	36.15	35.80	16.07	16.60	16.64
		0.8	1.0		0.9	1.5
31166	36.05	35.53	36.	16.47	16.90	16.89
		1.1	0.9		2.2	1.4
20612	(26.25)	(27.29)	(2	(16.47)	(16.51)	(15.89)
		(2.0)	(2		(0.6)	(1.1)
20651	36.05	36.08	35.65	17.64	17.73	16.98
		0.9	1.7		0.7	1.3

Table A.5 Rainfall summary for 22 intensive sites, mid-May to Mid-July 1978.[a]

Site	Date	Rainfall (mm)
10101	5/22	4
10102	6/1	71
	6/3	54
	6/7	32
	6/19	5
	7/11	11
Source: Site, Monte Alto, Raymondville		
41381	5/22	4
30951	6/3	54
30955	6/7	32
	6/19	5
	7/11	11
Source: Monte Alto, Raymondville		
20611	5/21	5
20612	6/3	36
	6/7	42
Source: Monte Alto		
41665	5/22	3
	6/4	21
	6/27	4
Source: Mercedes(6mi.SSE)		
51782	5/22	7
	6/2	8
	6/3	20
Source: Schuster Farm		
10381		
	6/3	26
	6/7	8
	6/29	6

Site	Date	Rainfall (mm)
30901	5/22	16
31001	6/2	4
31011	6/3	29
41341	6/4	11
	6/8	25
Source: McCook		
41421	5/21	14
41422	6/1	3
20681	6/3	20
	6/7	23
Source: Edinburg		
10194	6/2	57
10196	6/3	29
	6/4	37
	6/7	5
	6/8	17
	6/19	7
	6/29	4
Source: Santa Rosa		
20754	5/22	18
	6/4	15
	6/8	3
	7/24	3
Source: Bates Power		
31166	6/1-3	26
	7/23	7
Source: McAllen		
20651	5/22	18
	6/2-4	29
	6/8	13
Source: Av. Bates Power and McCook		

[a] Amounts less than 2mm not listed.